Estimation of Sea Surface Dynamic Topography, Ocean Tides, and Secular Changes from Topex Altimeter Data

by

Yan Ming Wang

Richard H. Rapp

Report No. 430

Department of Geodetic Science and Surveying
The Ohio State University
Columbus, Ohio 43210-1247

November 1994

FOREWORD

This report was prepared by Dr. Yan Ming Wang, Research Associate and Richard H. Rapp, Professor Emeritus, Department of Geodetic Science and Surveying at The Ohio State University. The research described in this report was supported under NASA's TOPEX Altimeter Research in Ocean Circulation Mission funded through the Jet Propulsion Laboratory under contract 958121, OSURF 720426.

Mr. Dru Smith and Mr. Yuchan Yi, Graduate Research Associates, Department of Geodetic Science and Surveying, aided in selected computations described in this report. Dr. Richard Eanes, Dr. Christian LeProvost and Dr. Richard Ray kindly provided tide information used for the tide gauge comparisons described in Section 3 of this report.

Computer resources were provided by the Academic Computing Services of The Ohio State University and the Ohio Supercomputer Center through Grant pas 160.

ABSTRACT

Sea surface dynamic topography (SSDT) has been determined from the separation of the Topex sea surface height and the geoid undulations implied by the JGM-2/OSU91A merged potential coefficient model. The SSDT was initially analyzed to determine annual and semi-annual variations in the ocean surface, corrections to the M_2, S_2, K_1, O_1 constituents of the Cartwright/Ray tide model, and bias and bias rate terms. All correction terms were represented by spherical series to degree 8 (for most testing purposes) and to degree 15 for final runs. The most complete analysis was done with Topex cycles 4 to 58. From this solution we found that the root mean square annual signal was ±4.5 cm in the Northern Hemisphere and ±3.5 cm in the Southern Hemisphere with an overall amplitude of ±4.0 cm. Large annual signals were associated with features such as the Kurishio Current (±10 cm), Gulf Stream (±7 cm) and the Falkland Current (±6 cm). The tide correction terms were ±2.9 cm (M_2), ±1.5 cm (S_2), ±0.8 cm (O_1), ±1.4 cm (K_1). The improvement in the tide model was proven through comparisons at the 104/95 tide gauge data set provided by C. Le Provost.

The bias rate value was determined at each normal point and then averaged to determine a mean rate of 4.8 mm/yr. After removing an altimeter drift rate of 2.0 mm/yr the net rate is 2.8 mm/yr. This rate could be a combination of sea level change and effects associated with the various correction terms applied to the data.

The second main theme of the report relates to the representation of SSDT in spherical harmonics (SH) and orthonormal (ON) functions. Procedures were implemented to estimate either SH or ON coefficients. It was found that the estimation of SH coefficients was more stable than the ON estimation. For those applications on which spectral information of SSDT is needed a SH model can be transformed into an ON model. It was found that the lower degree SH coefficients are quite sensitive to the bias correction applied to the sea surface height data. This sensitivity does not occur in ON coefficient estimation. For the analysis with data from cycles 4 to 58 a bias term of 55 cm was applied to the data. This value leads to a zero value for the degree zero term in the ON expansion. An SH expansion to degree 24 was computed using a priori degree variance computed from 10 selected cycles of Topex data. The SH expansion was transformed to an ON expansion and both coefficient sets are given in the report. The degree 2,0 coefficient in the SH representation was -37.8 cm quite comparable with other altimeter based solutions.

The analysis of the ON coefficient indicated an rms value of SSDT equal to ±61 cm. The ON power spectrum, in conjunction with the geoid undulation accuracy of the JGM-2 model in the ocean areas, indicated the two values are approximately equal near degree 13. This suggests that SSDT estimates above degree 13 may be unreliable. This statement was consistent with the inconsistency of geostrophic flow patterns implied by the SSDT expansions at the higher degrees. Even at the lower (e.g. 13) degree the flow patterns showed only moderate agreement with known circulation patterns.

1. INTRODUCTION

A fundamental goal of the research with Topex altimeter data has been the determination of the separation between the ocean surface and the geoid. Several studies at Ohio State, funded through the Topex/JPL project, have been carried out prior to this analysis of the Topex data. The first type of analysis was carried out by Denker and Rapp (1990) who used one year of Geosat data to estimate improved (radial direction only) Geosat orbits; potential coefficient parameters and parameters for the spherical harmonic representation, to degree 10, of sea surface dynamic topography. (We recognize that this latter term has numerous designations. In our studies we have used, interchangeably, sea surface topography and dynamic topography.) Maul (1988) suggests "sea surface height anomaly" and Nerem et al. (1994a) use "ocean dynamic topography". A recent paper by Ichikawa and Imawaki (1994) use the terms "sea surface dynamic topography" whose symbol equivalent is SSDT which avoids the conflict when SST is used for sea surface temperature. It is primarily for this reason we have chosen to adopt the term sea surface dynamic topography for this report.) The Denker/Rapp paper showed how altimeter data, even in the presence of substantial orbit error, could be used for the simultaneous study of gravitational field modeling and oceanographic signals. Rapp, Wang and Pavlis (1991) extended the previous study introducing surface gravity data into the solution and carrying out simultaneous and non-simultaneous solutions for the SSDT using spherical harmonic expansions. In both studies, no improvement was sought in the tide information that was put on the altimeter data records. Both studies did point out the problems in the representation of SSDT using spherical harmonic expansions emphasizing that the spectra computed from such expansions could be distorted because SSDT is not defined in land areas although the spherical harmonic expansion represents information on an entire sphere, not just the ocean.

Hwang (1991) carried out a study to evaluate alternate representations of SSDT that would not have the disadvantage of the spherical harmonic representation. Hwang found such a representation through orthonormal functions (ON) and corresponding ON coefficients. These functions were defined for the region in which the data were given, or actually for any region the user chose to work with. This ON expansion process had the potential of removing the problems associated with SH expansions. The solutions of Hwang were directed towards gravitational field improvement, SSDT representation, radial orbit error reduction, etc. No tide modeling improvement was considered.

With the availability of the Topex altimeter data, it was clear that the procedures developed at OSU in the past should be tested. However, it was also realized that it was no longer acceptable to assume the tide model used on the Topex data record was sufficiently accurate for data analysis considering the high accuracy of the radial position. In addition, there are variations (annual and semi-annual) of the ocean surface that were important to take into account. Finally, we wanted to examine the conjecture that the sea surface elevation was changing with time, or that the altimeter measurement was time dependent. The purpose of this report is to analyze the ocean surface using Topex altimeter data with the fundamental goal of determining sea surface dynamic topography, recognizing that other quantities such as tides, seasonal effects, and perhaps, secular effects need to be modeled. Our plan is to build on our past experiences, recognizing the challenge brought on by the very accurate Topex sea surface height measurements, to learn more about the behavior of the ocean surface and corresponding implications for ocean circulation.

2. THEORY: MATHEMATICAL MODEL DEVELOPMENT

2.1 Modeling the Sea Surface Dynamic Topography

The sea surface dynamic topography (SSDT) ς at time t is defined as difference between the sea surface height (SSH) and the geoid undulation N:

$$\varsigma(t,\phi,\lambda)=SSH(t,\phi,\lambda)-N(\phi,\lambda) \qquad (2\text{-}1)$$

where SSH is computed from the TOPEX altimeter data. N can be computed from a potential coefficient model or from such a model and surface gravity data (Rapp and Wang (1994); Rapp and Smith (1994)).

The sea surface height is based on the position of the altimeter satellite in space and the altimeter measurement which must be corrected for environmental and geophysical factors. In addition, the geoid undulation is subject to errors related to our lack of precise knowledge of the Earth's gravitational potential. Consequently, the sea surface dynamic topography represented by eq. (2-1) is contaminated by a number of error sources. In addition, we will postulate that the sea surface may be changing in time in a linear fashion at a specific geographic location. This linear change can not be separated from linear time effects for other correction terms so one will introduce a term $\dot{b}$ calling it the effective sea level secular change rate. One might also consider such a term as a bias rate which implies that there may be a systematic change in the altimeter measurement but in this case, $\dot{b}$ would be independent of position.

Considering the above, we choose to model the following quantities:

$\varsigma_0(\phi,\lambda)$	sea surface dynamic topography at time t_0 (SSDT);
$\Delta\varsigma(t,\phi,\lambda)$	the time varying parts of (SSDT)excluding annual and semi-annual variations;
$c(t,\phi,\lambda)$	tidal corrections to the adopted reference tide model, and annual and semi-annual sea surface height variations;
$\dot{b}(\phi,\lambda)$	effective sea level change rate, or bias rate;
$n(t,\phi,\lambda)$	a noise term representing unmodeled errors in the environmental and geophysical corrections, geoid undulation error, radial orbit error, etc.

One can now write eq. (2-1) in the following form:

$$\varsigma(\tau,\phi,\lambda)=\varsigma_0(\phi,\lambda)+\Delta\varsigma(t,\phi,\lambda)+c(t,\phi,\lambda)+\dot{b}(\phi,\lambda)(t-t_0)+n(t,\phi,\lambda) \qquad (2\text{-}2)$$

In this expression, t_0 is the epoch time chosen for the analysis which is 1^d0 of 1992. In this analysis, the tidal corrections will be to four constituents (M_2, S_2, K_1, 0_1) of the Cartwright/ Ray ocean tide model, values of which are given for each altimeter observation on the Topex GDR (Callahan, 1993).

Averaging (2-2) over a certain time period, e.g., the time of M repeat cycles of TOPEX data, we obtain:

$$\bar{\varsigma}(\phi,\lambda)=\frac{1}{M}\sum_{i=1}^{M}\varsigma(t_i,\phi,\lambda)\equiv\varsigma_0(\phi,\lambda)-b(\phi,\lambda) \qquad (2\text{-}3)$$

where b is the average of the tide correction, time variations of the sea surface height and error of the altimeter data over M cycles of TOPEX data:

$$b(\phi,\lambda)=-\frac{1}{M}\sum_{i=1}^{M}\left[c(t_i,\phi,\lambda)+\dot{b}(\phi,\lambda)(t_i-t_0)+\Delta\varsigma(t_i,\phi,\lambda)+n(t_i,\phi,\lambda)\right] \qquad (2\text{-}4)$$

where the minus sign is for convention. If the average is over one year (about 37 TOPEX cycles), the annual and semi-annual variations average out. The average of the tides over one year should

also be close to zero. However, the average of $\dot{b}(t_i - t_0)$ is not zero so that we can not assume b(ϕ, λ) is zero. We define the residual SSDT as follows:

$$r(t,\phi,\lambda) = \varsigma(t,\phi,\lambda) - \bar{\varsigma}(\phi,\lambda) \tag{2-5}$$

By using equations (2-2) and (2-3), equation (2-5) becomes:

$$r(t,\phi,\lambda) = c(t,\phi,\lambda) + \dot{b}(\phi,\lambda)(t - t_0) + b(\phi,\lambda) + \varepsilon(t,\phi,\lambda) \tag{2-6}$$

with

$$\varepsilon(t,\phi,\lambda) = \Delta\varsigma(t,\phi,\lambda) + n(t,\phi,\lambda) \tag{2-7}$$

where ε is considered an unknown error.

If m observations are given, equation (2-6) represents m observation equations. The parameters of tides c , bias term b and bias rate $\dot{b}$ can be determined by using least squares adjustment in the sense that ε^2 is minimized, provided that the number of the parameters is smaller than m.

The SSDT at a specific location, and at time t_0, can be calculated as

$$\hat{\varsigma}_0(\phi,\lambda) = \bar{\varsigma}(\phi,\lambda) + \hat{b}(\phi,\lambda) \tag{2-8}$$

where the symbol "∧" denotes the estimated quantities. Equation (2-8) enables us to interpret the b(ϕ,λ) value as the difference between the dynamic topography at time t_0 and the mean sea surface dynamic topography over the time period of m cycles as shown in eq. (2-3).

2.2 Spherical Harmonic Expansion of Tides and Sea Level Variations

A component of the four major tides and the annual, semi-annual time variations of the sea surface height, at time t, can be written as (Cartwright and Ray,1990; Knudsen, 1994; Le Provost et al., 1994):

$$Z_k(t,\phi,\lambda) = U_k(\phi,\lambda)\cos(\omega_k t + \chi_k) + V_k(\phi,\lambda)\sin(\omega_k t + \chi_k) \tag{2-9}$$

where k designates a tide constituent, ω_k is the frequency of the tide constituent, χ_k is the astronomic argument, U_k and V_k are two surfaces defined, in our case, by a spherical harmonic series. Note that equation (2-9) is also valid for the annual and semi-annual time variations with the frequencies of 1 cycle/year and 2 cycles/year, $\chi_k = 0$ for the annual and semi-annual terms.

Expand U_k and V_k into spherical harmonic series:

$$U_k(\phi,\lambda) = \sum_{n=1}^{N}\sum_{m=0}^{n}\left(a_{nm}\cos m\lambda + b_{nm}\sin m\lambda\right)\overline{P}_{nm}(\sin\phi) \tag{2-10A}$$

$$V_k(\phi,\lambda) = \sum_{n=1}^{N}\sum_{n=0}^{n}\left(c_{nm}\cos m\lambda + d_{nm}\sin m\lambda\right)\overline{P}_{nm}(\sin\phi) \tag{2-10B}$$

where a_{nm} , b_{nm}, c_{nm} and d_{nm} are fully normalized coefficients, $\overline{P}_{nm}$ is the fully normalized Legendre function, and N is the maximum degree of the expansion. In the same way we can expand the bias term and the bias rate into a spherical harmonic series. Equation (2-6) can be written as:

$$r(t,\phi,\lambda)=\sum_{k=1}^{K}\sum_{n=0}^{N}\sum_{m=0}^{n}(a_{nm}^{k}\cos m\lambda+b_{nm}^{k}\sin m\lambda)\overline{P}_{nm}(\sin\phi)g_k(t)+\varepsilon \qquad (2\text{-}11)$$

where K is the number of sets of coefficients or number of the surfaces, g_k is the cosine, sine functions in equation (2-9) for tide terms and g_k equals $(t-t_0)$ for bias rate and 1 for bias.

For m observations, (2-11) can be written in matrix form:

$$l=AX+e \qquad (2\text{-}12)$$

with

$$l=\begin{bmatrix} r(t_1,\phi_1,\lambda_1) \\ \dots \\ r(t_m,\phi_m,\lambda_m)\end{bmatrix},\quad A=\begin{bmatrix} \overline{R_{00}}(\phi_1,\lambda_1)g_1(t_1) & \overline{R_{10}}(\phi_1,\lambda_1)g_1(t_1) & \dots \\ \dots & \dots & \dots \\ \overline{R_{00}}(\phi_m,\lambda_m)g_1(t_m) & \overline{R_{10}}(\phi_m,\lambda_m)g_1(t_m) & \dots\end{bmatrix},$$
$$X=\begin{bmatrix} a_{00}^{1} \\ \dots \\ b_{nn}^{K}\end{bmatrix},\quad e=\begin{bmatrix} \varepsilon(t_1,\phi_1,\lambda_1) \\ \dots \\ \varepsilon(t_m,\phi_m,\lambda_m)\end{bmatrix} \qquad (2\text{-}13)$$

where $\overline{R}_{00},\overline{R}_{10}$ are the fully normalized spherical harmonics. The solution of (2-13) is:

$$\hat{X}=(A^TPA)^{-1}A^TPl \qquad (2\text{-}14)$$

where P is the weight matrix. If a priori information is used, the solution is then:

$$\hat{X}=(A^TPA+D^{-1})^{-1}A^TPl=N^{-1}U \qquad (2\text{-}15)$$

where $N=A^TPA+D^{-1}$ (the normal matrix) and $U=A^TPl$. The D matrix contains a priori information on the parameters X. Since these X values are, in this case, spherical harmonic coefficients, the D values can be based on degree variance estimates.

2.3 Optimal Weighting for Altimeter Data Analysis

The spatial distribution of the satellite altimeter data is uneven over the ocean. The data density (number of points per square unit) at the higher latitude is greater than it is in the equatorial areas. In the least squares adjustment a weighting scheme has to be used to downweight the dense data at the higher latitudes. Knudesn (1994) empirically used a $\cos^2\phi$ weighting in his analysis. However, we will show that alternatives to $\cos^2\phi$ weighting may be more appropriate.

In the following we will try to find a new optimal weighting procedure. As the first step, we will find the average density of the altimeter data in a latitude band. We divide the Earth's

surface into k latitude bands with band width $\Delta\phi$. For simplicity, we assume the $\Delta\phi$ is not greater than a few degrees. We also assume the center of the band at the equator has latitude zero.

The satellite altimeter ground tracks pass each latitude band $2N_p$ times in which there are N_p ascending and N_p descending tracks, where N_p is the number of revolutions. For Topex the number of revolutions per cycle is 127. The number of points in the latitude band along each track is N_ϕ. This situation is shown in Figure 2.1

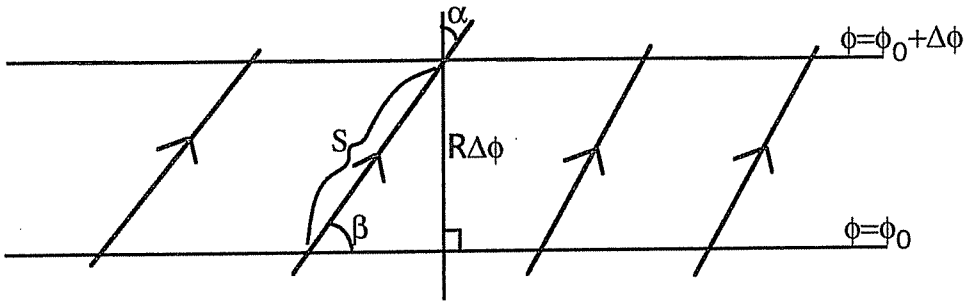

Figure 2.1 Ascending Altimeter Ground Tracks Passing Through the Latitude Band

The value of N_ϕ is given by:

$$N_\phi = (S/\upsilon)\kappa \tag{2-16}$$

where S is the length of an ascending or descending track between latitude ϕ and $\phi + \Delta\phi$, υ is the ground track velocity of the satellite which is assumed constant and κ is the altimeter measurement rate. From Figure 2.1 we have:

$$S = R\Delta\phi/\sin\beta \tag{2-17}$$

where β is the angle between the ground track and the parallel line. The number of points in each latitude band is then:

$$N(\phi) = 2N_p N_\phi = \frac{2N_p \kappa R\Delta\phi}{\upsilon \sin\beta} \tag{2-18}$$

The average point density in the latitude band is defined as:

$$\rho(\phi) = \frac{N(\phi)}{\text{area of latitude band}} = \frac{N(\phi)}{2\pi\cos\phi R\Delta\phi} = \frac{\kappa N_p}{\pi\cos\phi\upsilon\sin\beta} \tag{2-19}$$

In a unit area at the equator the number of the altimeter data points is:

$$n_0 = \rho(\phi = 0)\cdot 1 = \frac{\kappa N_p}{\pi\upsilon\sin\beta(\phi = 0)} \tag{2-20}$$

and at the latitude ϕ the number of data points in a unit area is:

$$n = \rho(\phi) \cdot 1 = \frac{\kappa N_p}{\pi \cos\phi \upsilon \sin\beta} \tag{2-21}$$

The ratio of the number of points in the areas at the equator and latitude ϕ is then:

$$r = \frac{n_0}{n} = \frac{\sin\beta(\phi)}{\sin\beta(\phi = 0)} \cos\phi \tag{2-22}$$

Now we derive the formula for $\sin\beta$. Because $\Delta\phi$ is assumed to be small, the planar approximation is appropriate. We let:

$$\beta = \frac{\pi}{2} - \gamma \tag{2-23}$$

where γ is an angle defined in Parke et al. (1987) and given by (ibid., p. 11,696):

$$\gamma = \tan^{-1}\left|\frac{V_S \sin\alpha \mp V_E \cos\phi}{V_S \cos\alpha}\right| \tag{2-24}$$

with

$$\sin\alpha = \left|\frac{\cos i}{\cos\phi}\right| \tag{2-25}$$

where we take the minus sign in (2-24) for inclinations less than 90°. V_S is the along track velocity of the satellite, V_E is the velocity of the Earth's rotation at the equator, and i (in eq. (2-25)) is the satellite inclination. We then have from eq. (2-24) and (2-25):

$$\sin\beta = \cos\gamma = \cos\left[\tan^{-1}\left|\frac{V_S \sin\alpha \mp V_E \cos\phi}{V_S \cos\alpha}\right|\right] \tag{2-26}$$

We next consider the impact of the point density variations on weighting in a least squares adjustment. The n data points contribute to the normal matrix in the following general way:

$$\begin{aligned} I_1 = [paa] &= \sum_{i=1}^{n} P_i \ldots (\text{assume } a = 1) \\ &= np \ldots (\text{assume } P_1 = P_2 = \ldots P) \end{aligned} \tag{2-27}$$

where I_1 is the diagonal element of the normal equations. The standard case is that there are n_0 points in the unit area at latitude ϕ. The contribution of these n_0 points to the normal matrix is:

$$I_2 = [\bar{p}aa] = \sum_{i=1}^{n_0} \overline{P_i} \qquad (\text{assume } a = 1)$$
$$= n_0 \overline{P} \qquad \left(\text{assume } \overline{P}_1 = \overline{P}_2 = \ldots \overline{P}\right) \tag{2-28}$$

We chose P in such a way that $I_1 = I_2$. By using eq. (2-27) and (2-28) we have:

$$P = \frac{n_0}{n} \overline{P} = \frac{\sin\beta(\phi)}{\sin\beta(\phi = 0)} \cos\phi \overline{P} \tag{2-29}$$

As a numerical check of eq. (2-22) an area of 36 x 10^4 km^2 centered at longitude 220° was chosen for analysis (Smith, 1994, private communication). The length of the area in latitude is 6° while the length in longitude changes for different latitudes based on the cosϕ variation. The number of the altimeter data on the Topex reference track (Rapp and Yi, 1994) that fell into the equal areas were counted and compared with the number of points in the area at the equator. Let N be the values in the equal area cell and RATIO the ratio of the number in the cell centered at the equator to the number in the cell centered at a specified latitude. The value of RATIO would be an approximation to a weight designed to reduce the impact of greater data density as latitude increases in absolute value. Values of N and RATIO are given in Table 2.1. The value of r computed from eq. (2-22) is given with the percentage difference (D3) between RATIO and r. One sees that the maximum difference is about 7% and there is no systematic difference which indicates eq. (2-22) is a good approximation.

This discussion has developed analytic expressions that represent the latitude dependent data density variations along the altimeter ground track. In addition, we point out the need to consider this variation in the formation of the normal equations from the altimeter observations. This requirement is needed so that the denser altimeter values at higher latitudes do not dominate the solution. Consequently, for most (but not all) our analysis, we adopt the following weight for an observation at latitude ϕ having a standard deviation m:

$$[P] = \frac{1}{m_i^2} \frac{\sin\beta(\phi)}{\sin\beta(\phi = 0)} \cos\phi \tag{2-30}$$

Some authors have used a cosϕ or a $\cos^2\phi$ weighting to compensate for the increase data density. These values are shown in Table 2.1 with percentage differences with respect to RATIO. Note that both cosϕ and $\cos^2\phi$ approximate RATIO (and r) well up to approximately 30° after which the % error generally increases with cosϕ giving very poor results at the higher latitude. A plot of r, cosϕ, and $\cos^2\phi$ is shown in Figure 2.2 where it becomes clear cosϕ allows too much weight with respect to r, and $\cos^2\phi$ gives too little weight (to ϕ = 64°) with respect to r.

Table 2.1

Data Density Ratios Computed Using $\cos\phi$, $\cos^2\phi$ and Eq. (2-22) for r with Comparison to "RATIO" Computed Using Data Points on the Reference Track

ϕ°	N	RATIO	r	D3(%)	$\cos\phi$	D1(%)	$\cos^2\phi$	D2(%)
0.	417	1.00	1.00	0.00	1.00	0.00	1.00	0.00
2.	448	0.93	1.00	7.35	1.00	7.37	1.00	7.30
4.	418	1.00	1.00	-0.07	1.00	0.00	1.00	-0.25
6.	400	1.04	0.99	-4.74	0.99	-4.60	0.99	-5.12
8.	424	0.98	0.99	0.43	0.99	0.69	0.98	-0.29
10.	449	0.93	0.98	5.61	0.98	6.04	0.97	4.43
12.	422	0.99	0.97	-1.59	0.98	-1.01	0.96	-3.18
14.	421	0.99	0.96	-2.83	0.97	-2.04	0.94	-4.95
16.	450	0.93	0.95	2.63	0.96	3.73	0.92	-0.29
18.	458	0.91	0.94	3.04	0.95	4.46	0.90	-0.66
20.	447	0.93	0.92	-0.98	0.94	0.73	0.88	-5.35
22.	455	0.92	0.91	-0.94	0.93	1.17	0.86	6.20
24.	469	0.89	0.89	0.16	0.91	2.75	0.83	-6.14
26.	479	0.87	0.87	0.15	0.90	3.24	0.81	-7.21
28.	490	0.85	0.85	0.07	0.88	3.75	0.78	-8.39
30.	501	0.83	0.83	-0.28	0.87	4.05	0.75	-9.89
32.	515	0.81	0.81	-0.33	0.85	4.73	0.72	-11.18
34.	536	0.78	0.78	0.59	0.83	6.56	0.69	-11.66
36.	546	0.76	0.76	-0.91	0.81	5.93	0.65	-14.30
38.	570	0.73	0.73	-0.28	0.79	7.71	0.62	-15.12
40.	595	0.70	0.70	0.00	0.77	9.30	0.59	-16.27
42.	621	0.67	0.67	-0.12	0.74	10.67	0.55	-17.76
44.	645	0.65	0.64	-1.15	0.72	11.26	0.52	-19.96
46.	683	0.61	0.61	-0.75	0.69	13.78	0.48	-20.96
48.	726	0.57	0.57	-0.56	0.67	16.50	0.45	-22.05
50.	791	0.53	0.53	1.41	0.64	21.93	0.41	-21.63
52.	839	0.50	0.50	-0.18	0.62	23.87	0.38	-23.74
54.	908	0.46	0.46	-0.84	0.59	27.99	0.35	-24.77
56.	1007	0.41	0.41	-0.51	0.56	35.04	0.31	-24.49
58.	1152	0.36	0.37	0.88	0.53	46.40	0.28	-22.42
60.	1344	0.31	0.31	1.08	0.50	61.15	0.25	-19.42
62.	1739	0.24	0.25	6.23	0.47	95.78	0.22	-8.09

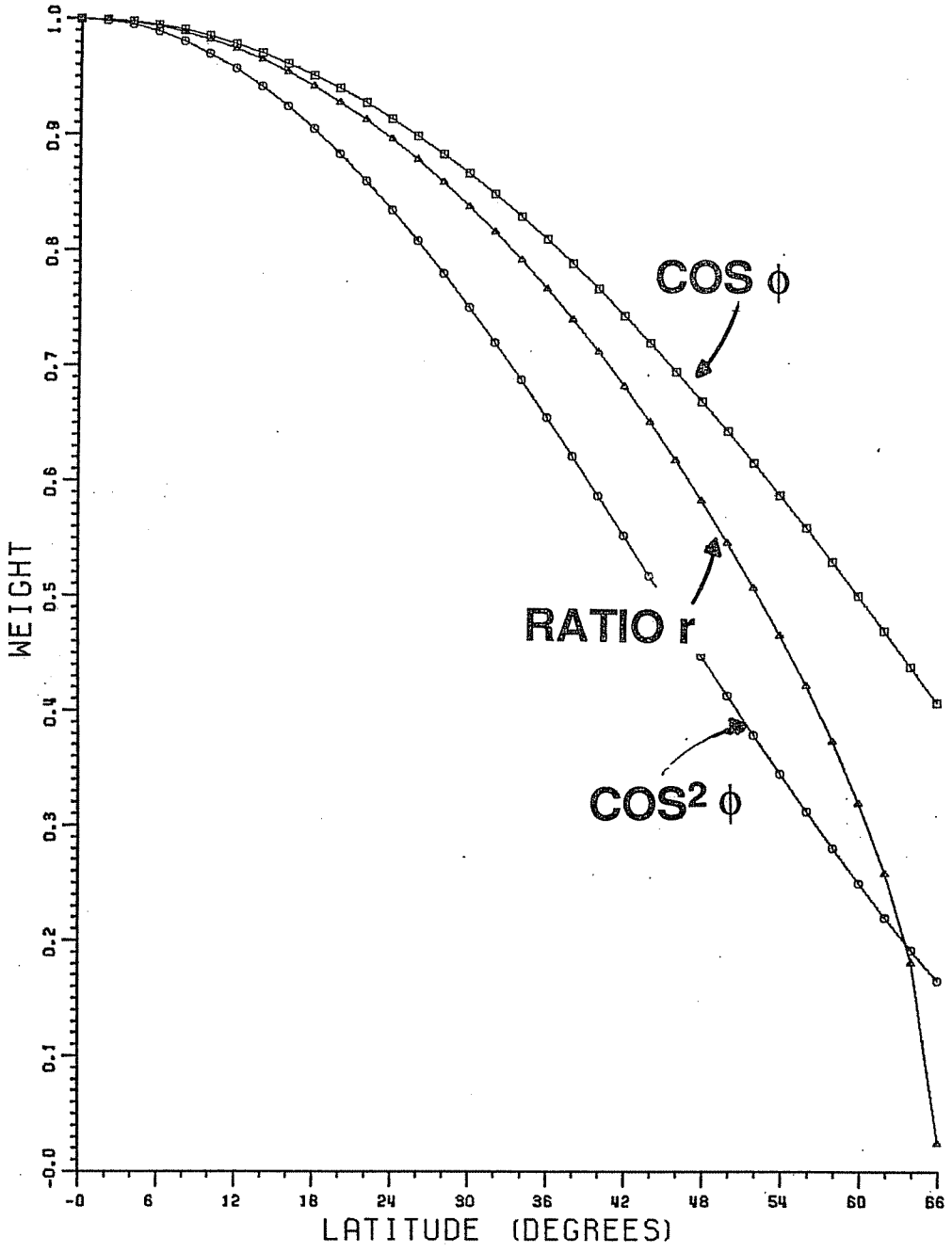

Figure 2.2 Plot Showing Altimeter Data Weighting Factors of $\cos\phi$, $\cos^2\phi$, and r. Given by Eq.2-22

3. TIDE, ANNUAL, SEMI-ANNUAL VARIATIONS, BIAS AND BIAS RATE ESTIMATES

3.1 Data Editing and Normal Point Computation

This analysis is based on the Topex altimeter geophysical data records distributed by the Jet Propulsion Laboratory. The data was edited by the OSU editing procedure described by Rapp, Yi, and Wang (1994) with the additional condition that only OSU edited data with a valid Cartwright/ Ray valid tide was used. In order to eliminate inaccurate points not yet deleted, data with absolute values of sea surface dynamic topography, SSDT, (see below) greater than 3m were deleted. The OSU editing generally allows 10% more data for analysis than the somewhat more conservative editing (JPL) suggested by Callahan (1993). The main difference is that data in shallow water is retained by the OSU editing procedure. The edited data is reduced to a reference Topex ground track using the procedures described in Rapp and Yi (1994) to take into account the geoid gradient problem. All standard environmental and geophysical corrections described in the GDR Users Handbook (Callahan, 1993) were applied with one exception. In this case, the inverted barometer correction was applied using a reference pressure corresponding to the mean pressure on the cycle instead of a constant (1013.3 mb) pressure. The rational for this procedure is described in Rapp, Yi, and Wang (1994).

For each cycle the SSDT was computed by using eq. (2-1):

$$\varsigma_i = h_i - N \tag{3-1}$$

where h_i is the sea surface height at the point i calculated from TOPEX altimeter measurements. N is the geoid undulation in the mean tide system computed by:

$$N = N_Z + P_c \tag{3-2}$$

where N_Z is the "zero tide" geoid undulation computed from the augmented JGM2/91A coefficients model (JGM2 (Nerem et al., 1994b), to degree 70; OSU91A, degree 71 to 360) by subtracting $9.3324 \times 10^{-9} / \sqrt{5}$ from coefficient C_{20} . P_c is the permanent tide correction given by (Rapp et al., 1991):

$$P_c = -0.198(1.5\sin^2\phi - 0.5)m \tag{3-3}$$

The undulation from JGM2/91A, in the mean tide system, was gridded into a global $0.25° \times 0.25°$ grid, and then interpolated to the point i using a cubic-spline interpolation procedure using a 5 X 5 point interpolation window. The gridded undulation file is called \$TS0548.UNDUZERO.JGM2.OSU91A.TO360.QUARTER. Despite the implications in the naming of this file, the values are given in the tide free system.

The altimeter data on the reference track is given at one second time interval. This data is denser than needed in the least squares adjustment for this report. Some procedures have to be taken to smooth and thin the data. In consideration of the change of SSDT over several hundred kilometers the SSDT is calculated at every 20th second (~130 km) by using a straight line fitting procedure. The points at which the sea surface dynamic topography are computed are called normal points.

After the data editing a normal point was computed in following way:

a. Select all points in the time interval of 20 seconds. If the number of the data points was less than 16 (80%), no normal point was computed.

b. Fit a straight line to the selected data by a least squares fitting process. Compute the misfit for every point. If the misfit was greater than 3 times the RMS value of the misfit, the point was eliminated.

c. Fit a straight line to the remaining data points. The SSDT was computed at the time center of the line. The RMS value of the misfit was recalculated.

The program to calculate the normal points is $TS0548.LIB.HWANG#SSTNP20. The location of the normal points from cycle 17 is shown in Figure 3.1. A typical cycle will contain 25,000 normal points. For example, cycle 17 has 27,651 points with the standard deviation of SSDT equal to ±82 cm. This value is affected by errors in tides, geoid undulations, etc.

3.2 Tests and Preliminary Results

In initial test computations the two components of the annual , semi-annual and four residual tides (M2, S2, 01, and K1) are represented by two spherical harmonic series from degree 1 to 8. There are 80 coefficients for each series. The bias and bias rate terms are also expanded into spherical harmonic series from degree 0 to 8. There are 81 coefficients for bias or bias rate. Together we have 14 sets of coefficients (or 14 surfaces) to estimate. The total number of coefficients is 1122. Because the degree of the spherical harmonic expansion is low, no a priori information was needed in these test solutions. For these and other solutions, the mean SSDT, defined by eq. (2-3) was computed by averaging over Topex cycles 17 to 53 which covers approximately one year. Future solutions can average over larger time periods but this should be in multiples of a year to average out the annual and semi-annual effects.

Various corrections have been applied to the altimeter measurements. More detailed descriptions about the corrections can be found in Rapp, Yi, and Wang (1994) in the section "Data Correction". Callahan (1993, p. 310) pointed out that the Topex attitude pointing was a problem with cycles 1 to 8. Based on tests not described here it was felt that only the sea surface heights from cycles 1 to 3 were questionable. Therefore, solutions described in this paper use data starting from cycle 4. For the test solutions of this section, data from Topex cycles 4 to 54 were used so that at each point on the reference track there is a maximum of 48 observations of sea surface dynamic topography.

Due to changes in data coverage in a cycle, the number of observations at a normal point could vary from 1 to the maximum of 48. To avoid non-representative normal points, a minimum number of observations at the normal point on the reference track is required. In order to see the impact of the minimum number on the solutions we set the minimum number at 5 and at 28. In addition, we wanted to see how the editing criteria effected the solution. The OSU and JPL edit were also used. Every 4th normal point was used in the solution to save computation time. Many different solutions were run as the tests progressed. In Table 3.1, statistical information is given for some test solutions of interest where the values are based on the evaluation of the specific quantity, or correction term, at each normal point observation. The final term in the table is based on the sum of the individual corrections at a specific observation normal point.

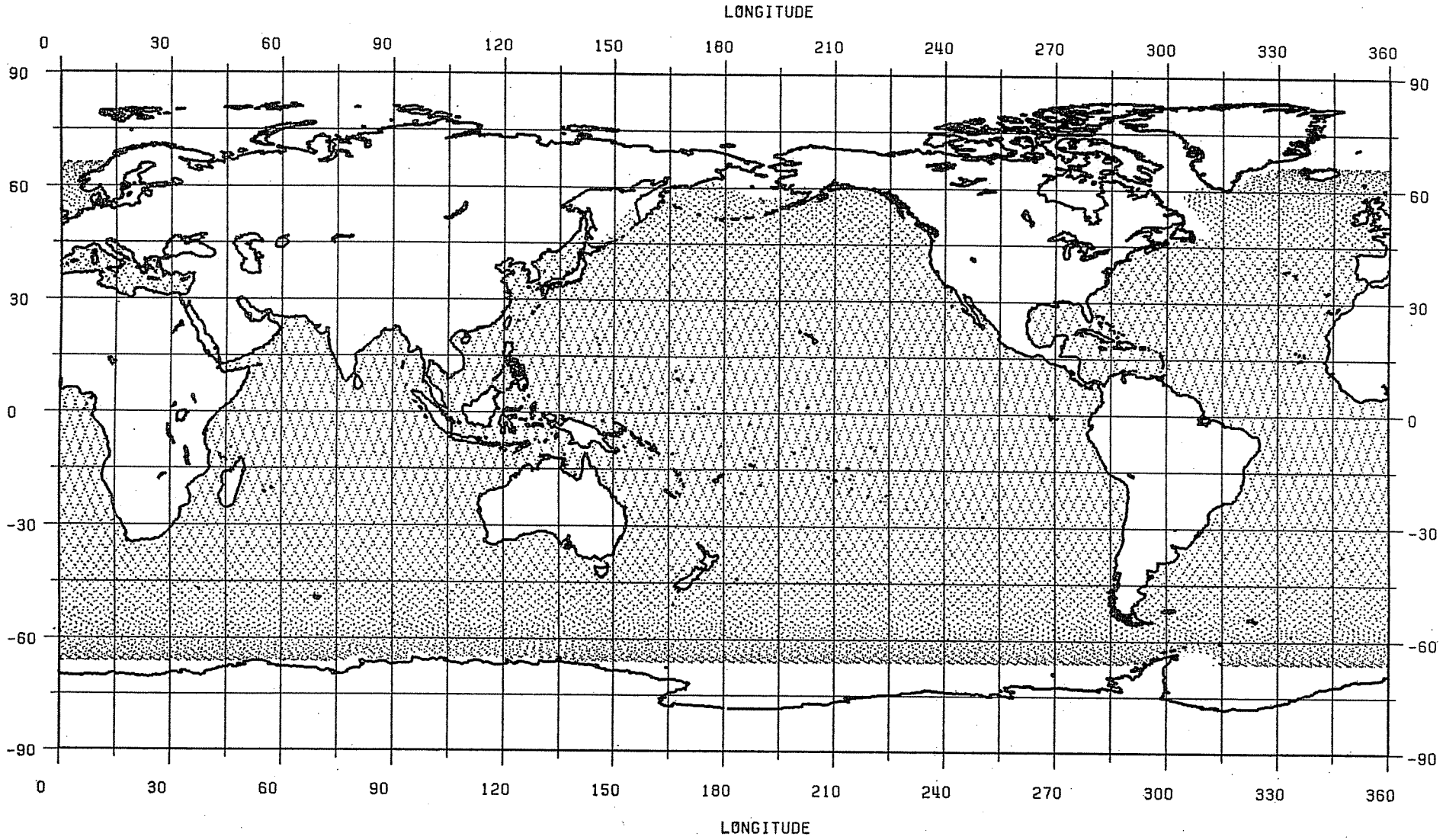

Figure 3.1 Location of 27,651 Normal Points from Topex Cycle 17

Table 3.1
Magnitudes of Parameters from Normal Point Evaluations for Four Degree 8 Solutions Based on Cycles 4 to 54

	N15	N14	N16	N13
EDIT PROC.	OSU	OSU	JPL	JPL
Min. No.	5	28	5	28
No. of Obser.	252770	240391	249455	236476
	AnnualVariation (Units are cm)			
Mean	0.07	0.03	0.05	0.02
RMS	2.69	2.74	2.66	2.72
Min.	-10.28	-10.67	-9.99	-12.34
Max.	10.31	10.77	10.19	12.33
	Semi-annual Variation (Units are cm)			
Mean	0.01	0.01	0.01	0.00
RMS	0.99	0.95	0.96	1.00
Min.	-6.17	-6.02	-6.10	-6.90
Max.	6.14	6.01	6.16	6.89
	M2 Tide Correction (Units are cm)			
Mean	0.00	0.00	0.00	0.00
RMS	2.75	2.79	2.76	2.81
Min.	-9.23	-9.63	-8.52	-9.54
Max.	9.19	9.61	8.55	9.58
	S2 Tide Correction (Units are cm)			
Mean	-0.01	-0.01	-0.01	-0.01
RMS	1.36	1.36	1.36	1.35
Min.	-6.26	-6.56	-5.59	-7.33
Max.	6.26	6.62	5.62	7.36
	01 Tide Correction (Units are cm)			
Mean	0.00	0.00	0.00	0.00
RMS	0.74	0.78	0.75	0.76
Min.	-2.48	-2.46	-3.02	-2.49
Max.	2.48	2.45	3.03	2.49
	K1 Tide Correction (Units are cm)			
Mean	0.00	0.01	0.00	0.01
RMS	1.55	1.49	1.53	1.49
Min.	-6.76	-5.76	-5.33	-6.46
Max.	6.78	5.79	5.32	6.45
	Bias (Units are cm)			
Mean	-0.39	-0.19	-0.35	-0.20
RMS	1.36	1.32	1.33	1.28
Min.	-3.87	-4.50	-5.26	-4.42
Max.	3.25	4.12	3.31	3.31
	Bias Rate (Units are cm/year)			
Mean	0.24	0.07	0.22	0.11
RMS	1.85	1.87	1.86	1.81
Min.	-6.60	-6.27	-8.08	-7.34
Max.	5.99	5.78	7.17	5.48
	Sum of corrections (Units are cm)			
Mean	-0.09	-0.11	-0.09	-0.10
RMS	4.55	4.61	4.54	4.59
Min.	-23.46	-25.33	-25.47	-25.86
Max.	27.06	28.25	28.45	27.37

Table 3.1 shows that the impact of the edit criteria and minimum point numbers to the solutions is small. The RMS values change at the mm level if different edit and minimum number criteria are used. Even the changes of the extreme values (maximum and minimum values) are less than 2 cm. A relatively large change in the mean value of bias rate can be seen by comparing solution N15 with N14. However, this change is small (in mm/yr level) in an absolute sense. The corrections are small, but they can not be ignored. The maximum total correction can reach 28 cm. The RMS value of the total correction is about ±4.6 cm which is not small in comparison with sea surface height variability which is 10 ~ 13 cm (Wang and Rapp, 1993).

In order to validate our solutions we compare our estimated tides with the tide constituents on 104 tide gauge stations developed by LeProvost (April 1994, private communication). Because our residual tides are with respect to the Cartwright/Ray model we needed the Cartwright/Ray tide values at the 104 tide gauge stations in order to make comparisons. Eanes (April, 1994) made available, via ftp, his tide model and the comparison at the 104 tide gauge stations. The tide difference file named "104gage_diff2" was obtained and used for our comparisons. In Eanes' comparisons, the altimeter tides and the Cartwright/Ray model were multiplied by 1.060 and 1.047 for diurnal and semi-diurnal constituents, respectively, to eliminate the ocean tide loading effect. In the file "104gage_diff2" the tide differences between the Cartwright/Ray model and ground truth were listed for each station. That is:

$$di = (C/R)_i - (GT)_i \tag{3-4}$$

where the subscript i denotes one of the tide constituents, C/R is the Cartwright/Ray model and GT is the ground truth. In our calculations we have:

$$\tilde{d}_i = (C/R)_i + Z_i - (GT)_i = d_i + Z_i \tag{3-5}$$

where Z_i is the residual tide defined by (2-9). Note that the U_K and V_K are called in-phase and quadrature component of tides (Cartwright and Ray, 1990, p. 3076). The tide difference in-phase and quadrature component of $\tilde{d}_i$ were computed and the RMS value of the tide differences was computed by:

$$RMS(d) = \sqrt{\sum_{i=1}^{M}\left[(dh_1)_i^2 + (dh_2)_i^2\right]} \tag{3-6}$$

where $(dh_1)_i$ and $(dh_2)_i$ are the in-phase and quadrature component of $\tilde{d}_i$ and M is the number of stations used in the comparison. The results of these comparisons are shown for several tide models in Table 3.2.

Table 3.2
RMS Values of the Differences Between Tide Test Models and Ground Truth at 104 Tide Gauge Stations. Units are in cm

Model	C/R	UT	N15	N14	N16	N13
M_2	3.61	2.47	2.71	2.71	2.71	2.73
S_2	2.39	1.66	1.66	1.67	1.67	1.68
0_1	1.27	1.19	1.15	1.13	1.14	1.13
K_1	1.98	1.77	1.47	1.50	1.46	1.50

C/R, in the table, is the difference between Cartwright/Ray tide model and ground truth. C/R values were taken from Eanes file 104gage_test2. UT is the difference between the University of Texas' model and ground truth. Note that in the comparisons for solutions N13 to N16 no loading factors (1.06 or 1.047) were applied to the tide correction values. This incorrect procedure effects the results given in Table 3.2 on the order of ±0.02 cm.

We first see that in all cases, the new models give better agreement than found with the original Cartwright/Ray model. This improvement is most significant for the M_2 and S_2 constituents and least significant for the 0_1 component. The differences between the four OSU solutions are minor. The UT solution shows better agreement for the M_2 component and poorer agreement for the K_1 component. These solutions remain preliminary since the expansion degree is only 8 and only data through Topex cycle 54 has been used. Based on the test solutions we

decided to use the OSU edit with a minimum number of 5 observations at a normal point on the reference track.

It is also useful to look at the degree variances of the solutions. This will provide a priori information to be used in later solutions. In Table 3.3, we give the square root of the degree variances of solution N15 for the annual (A), semi-annual (SA), tidal, and bias related terms. These degree variances are computed as the sum of the squares of the spherical harmonic coefficients for each quantity represented. These degree variances can be misleading, especially at higher degrees, because the number represents variations not only over the ocean, but also over the land where no data has been used. In such areas, the spherical harmonic models generally imply large values of the quantities, especially in the case when no a priori information was used in the estimation of the coefficients.

Table 3.3
Square Root of Degree Variances of Solution N15. Units are in cm*

Degree	1	2	3	4	5	6	7	8	Cumulative
A	3.2	1.9	2.4	1.8	2.3	2.5	2.3	1.4	6.5
SA	0.6	1.2	1.6	1.5	1.5	1.2	1.0	0.8	3.4
M_2	2.7	1.7	2.9	1.8	2.1	1.7	1.4	0.9	5.7
S_2	0.8	0.9	1.5	1.0	1.4	1.0	1.0	0.8	3.0
0_1	0.5	0.3	0.7	0.5	0.3	0.4	0.3	0.3	1.3
K_1	1.0	1.3	1.4	0.8	1.2	0.9	0.7	0.6	2.9
b	2.1	2.2	2.1	1.9	1.6	1.3	1.1	0.7	4.9
$\dot{b}$	2.5	2.7	3.0	2.7	2.4	2.1	1.7	1.3	6.7

*The unit of $\dot{b}$ is cm/year.

3.3 Solution N34 with Data from Cycles 4 to 58

The least squares adjustment solutions are very time consuming. A solution up to spherical harmonic degree 24 could take approximately 20 hours of CPU time on the CRAY Y-MP8 at The Ohio State University. To reduce computer costs, but also go to a higher degree than 8 to obtain higher frequency tide information, we chose the next solution to be to degree and order 15. The number of coefficients to estimate is 3572. The solution, to degree 15, now including data from cycles 56, 57, and 58 takes approximately 5.5 hours of CRAY time. The incremental time by adding a cycle is small (100 secs) as all normal equation information is saved. 98% of CPU time in the solution is used to form the normal matrix. Therefore, it will be beneficial, if the normal matrix can be formed in a faster way, such as the method Hwang (1993a) used.

In order to stabilize the solution at the higher degree of this next solution, a priori degree variances are needed. The D matrix in eq. (2-15) is set diagonal and its elements are given by:

$$[D] = \frac{\delta_\ell^2}{2\ell+1}, \quad \ell = 1,2,\ldots 15 \tag{3-7}$$

with

$$\delta_\ell = \frac{c}{\ell} \tag{3-8}$$

Eq. (3-8) has been used by Knudsen (1994) as a priori information in his solution. Based on the degree variances of the test solution (Table 3.3), we chose c=4 cm in our analysis. In the case of b, c was taken as 4 cm/yr.

The P matrix in eq. (2-15) is also set to be diagonal and its elements are given by eq. (2-30). (The test solutions described earlier used a $\cos^2\phi$ weighting as the more rigorous equation had not been derived at the time the test solutions were carried out.) The standard deviation of the observation is computed by:

$$m_i^2 = R_i^2 + 0.1^2 (m^2) \tag{3-9}$$

where R_i is the RMS value of the misfit of the normal points. The value of R_i is around 2-5 cm. The constant 10 cm is added to R_i to bring up the m_i to a realistic level taking into account unmodeled error sources.

Together there were 321302 normal points from cycles 4 to 58 used to estimate 3572 harmonic coefficients to yield the solution designated N34. In the following sections we will discuss the solution, designated N34, in detail.

3.3.1 Annual and Semi-annual Variations of the Sea Surface Dynamic Topography

Annual and semi-annual variations of the SSDT or equivalently, in this case, the sea surface height have been studied by using GEOSAT and TOPEX altimeter data (Koblinsky et al., 1992; Jacobs et al., 1992; Nerem et al., 1994a) These variations are described in terms of an amplitude and phase. To calculate such terms we write eq. (2-9) in the following form:

$$Z_k(t,\phi,\lambda) = U_k(\phi,\lambda)\cos\omega_k(t-t_0) + V_k(\phi,\lambda)\sin\omega_k(t-t_0) \tag{3-10}$$

where t_0 has been chosen as the beginning of 1992. Eq. (3-8) can also be written as:

$$Z_k(t,\phi,\lambda) = A_k(\phi,\lambda)\cos\left[\omega_k(t-t_0) - \Psi_k\right] \tag{3-11}$$

with

$$A_k(\phi,\lambda) = \sqrt{U_k^2 + V_k^2}$$
$$\Psi_k(\phi,\lambda) = \tan^{-1}\frac{V_k}{U_k} \tag{3-12}$$

where A_k and Ψ_k are the amplitude and phase of the k component. Annual variations correspond to an $\omega_k = 1$ cycle/year and the semi-annual variation corresponds to $\omega_k = 2$ cycles/year. There is a direct link between the phase and the time. For the annual variation, one cycle (360°) is completed once a year. Therefore, a phase of 180° corresponds to a time of a half year. Similarly, 90° in phase corresponds to 3 months time. Because the time origin is at the start of the year, the phase can also be measured from here so that, for example, a phase of 90° corresponds to April 1. Figures 3.2 and 3.3 show the amplitude and phase of the annual variation based on Topex cycles 4 to 58. Figure 3.2 shows large amplitudes of the annual variation associated with the major current systems. Some of the largest amplitudes are: ±10 cm (Kurishio Current); ±7 cm (Gulf Stream); and ±6 cm (Falkland Current). The patterns in Figure 3.2 are similar to these found by Nerem et al. (1994a) but with less detail since the Nerem solution uses discrete 1°x1° grids using a 3° averaging radius. Higher variations, in our results, north of Australia, in the South China Sea,

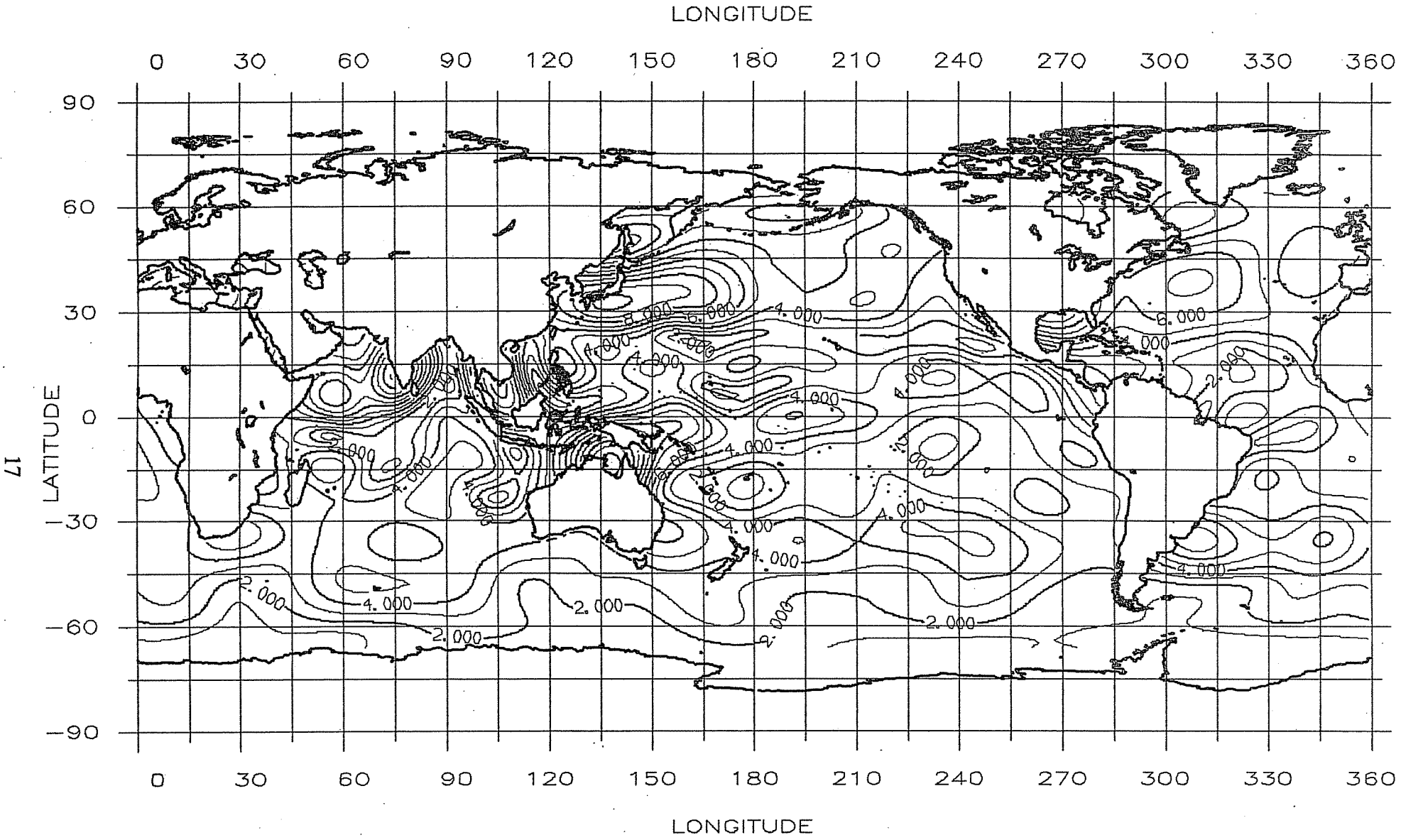

Figure 3.2 Annual Amplitude of Ocean Surface Based on Degree 15 Solution Using Topex Normal Point Data from Cycles 4 to 58. Contour interval is 1 cm.

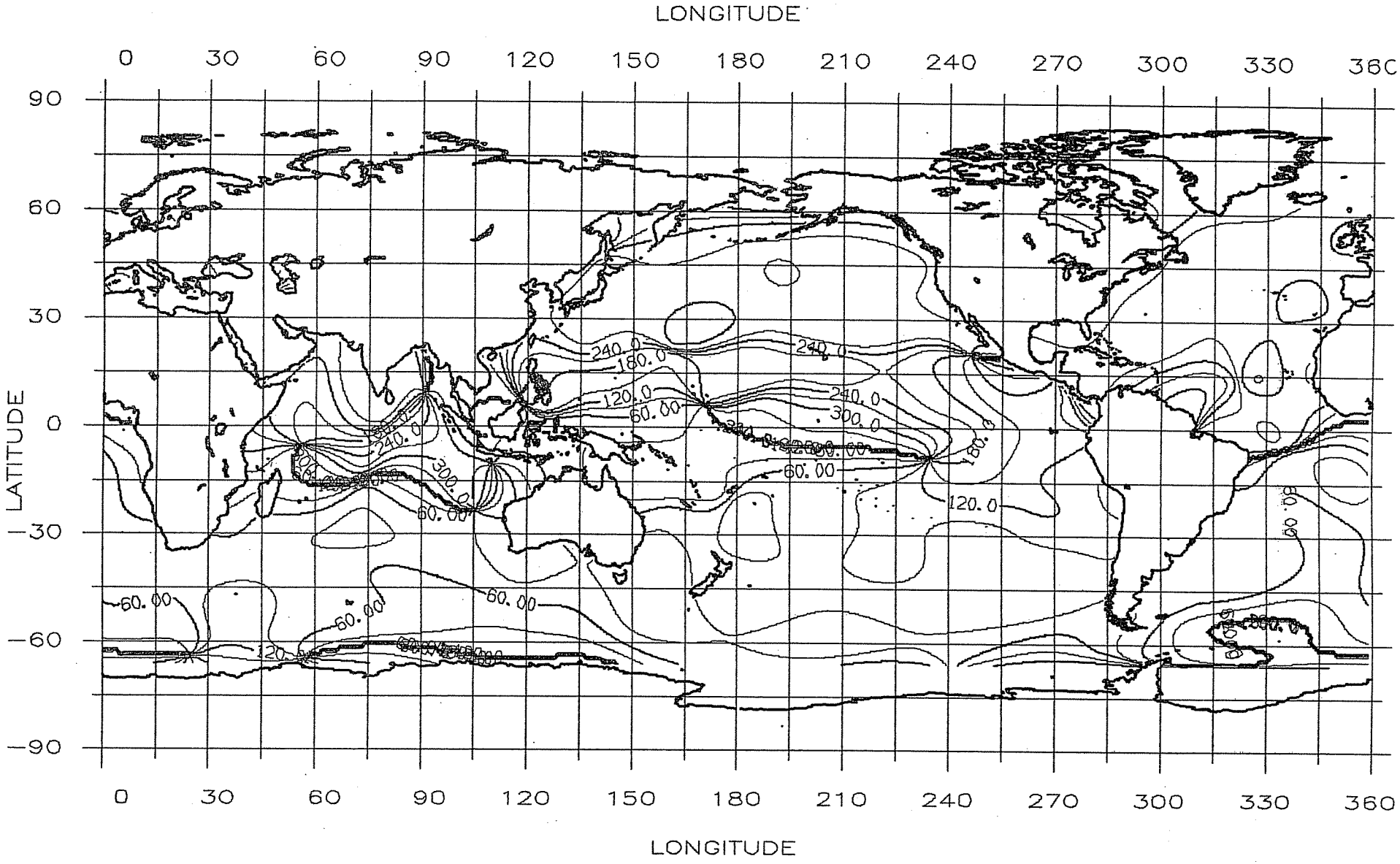

Figure 3.3 Phase of Annual Variation Based on Degree 15 Solution Using Topex Normal Point Data from Cycles 4 to 58. Contour interval is 20°.

etc., are probably unreal and can be associated with unmodeled (or high frequency) residual tide errors and other time dependent quantities. One can also see the areas of the ocean which have small (<2 cm) annual signal. The root mean square amplitude of the annual signal based on the degree 15 expression is, ±4.54 cm in the Northern Hemisphere; ±3.54 cm in Southern Hemisphere; and ±3.97 cm for all oceans. The values have been computed deleting amplitudes in shallow (d<1000m) water areas to avoid contamination from other error sources. From these values, one sees that the magnitude of the annual signal is almost 22% smaller in the Southern Hemisphere than the Northern Hemisphere.

We note that the phase shown in Figure 3.3 represents the time (in degrees from the start of the year) of maximum annual amplitude. In the mid-latitudes in the Pacific Ocean, the phase is 300° (ϕ=30°, λ=170°) indicating the maximum annual amplitude is reached 0.8 years (10 months (October)) from the start of January. In the north Atlantic Ocean the phase in the vicinity (ϕ=43°, λ=290°) of the Gulf Stream is 270° corresponding to the end of September. The general pattern is reversed in the Southern Hemisphere where at ϕ = -30°, λ = 170°, the phase is 80° indicating the maximum amplitude is reached 0.2 years (2.7 months (March)) from the start of the year. The phase difference between the corresponding point in the Northern Hemisphere is 220° or 7.3 months. Comparisons at other points show no precise 6 month (180°) difference in the time of maximum amplitude between the Northern and Southern Hemispheres.

An independent check of an annual amplitude is found in Perigaud and Delecluse (1992) who describe such variations in the Southern Tropical Indian Oceans (STIO). Based on Geosat data and simulations involving observed winds, they found that the maximum annual amplitude is on the order of 12 cm located near 12°S and 90°E. At this location, their analysis indicates the maximum sea level rise is in November. Considering Figures 3.2 and 3.3 (and more detailed plots not given here) the amplitude and phase at this location, from our analysis of the Topex data, are 5 cm and 340°. This amplitude is somewhat more than half that found by Perigaud and Delecluse (ibid.) while the phase angle implies the maximum occurs 11.3 months (November) from the start of the year, agreeing with the Periguad and Delecluse estimate. The amplitude disagreement may relate to the use of the lower degree expansion in the representation of the annual amplitude.

Estimates of annual and semi annual amplitudes and phases has been described by Tsimplis and Woodworth (1994) using tide gauge data. These results are marginally comparable to the altimeter results since the tide gauge data are generally representative of shallow or coastal waters. Despite this reservation there are reasonable similarities between the different estimates of the annual signal. For example large amplitudes in the Gulf of Carpentaria are seen in both the altimeter(14cm) ant the tide gauge solution. Along the east coast of the United States the altimeter amplitudes are on the order of 6 cm which is similar to that found from the tide gauge analysis.

One also sees several areas of the ocean where there are rapid phase changes in a region. The clear example is the Indian Ocean where high phase gradients are seen. The value of the annual amplitude also shows complex changes in this area. Which is consistent with the results of Tsimplis and Woodworth.

The amplitude and phase of the semi-annual variation is shown in Figures 3.4 and 3.5, respectively. The root mean square amplitude of the semi-annual signal is ±1.36 cm in the Southern Hemisphere and ±1.42 cm for the whole ocean. The semi-annual amplitude is again smaller in the Southern Hemisphere but not by as large amount as found in the annual signal. The semi-annual amplitude does reach 4 to 5 cm in a few locations (e.g. Kurishio Current and the Gulf Stream). As would be expected of this higher frequency phenomenon, the phase map in Figure 3.5 is more complex than the phase map of the annual variations (Figure 3.3).

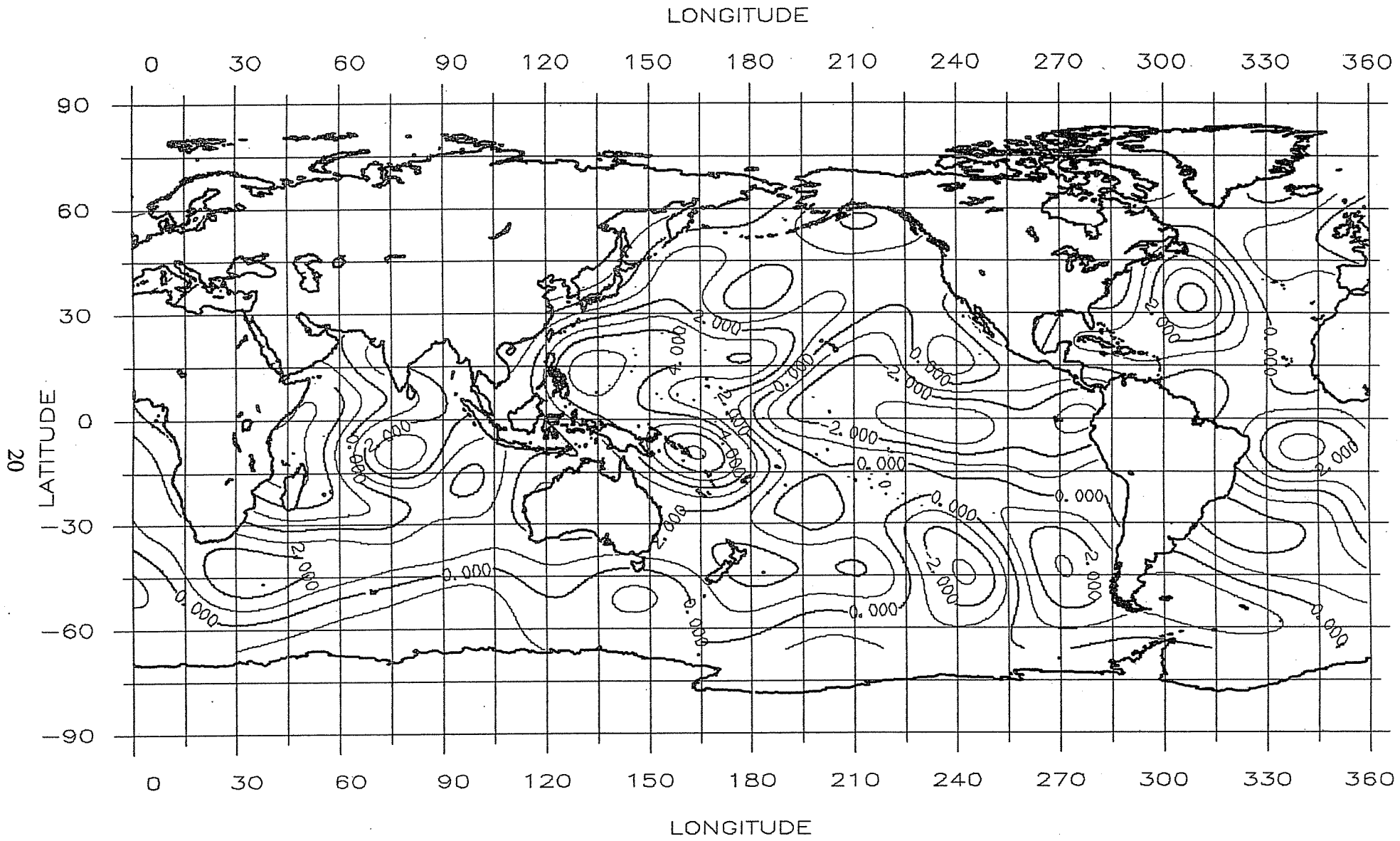

Figure 3.4 Semi-Annual Amplitude of Ocean Surface Based on Degree 15 Solution Using Topex Normal Point Data from Cycles 4 to 58. Contour interval is 1 cm.

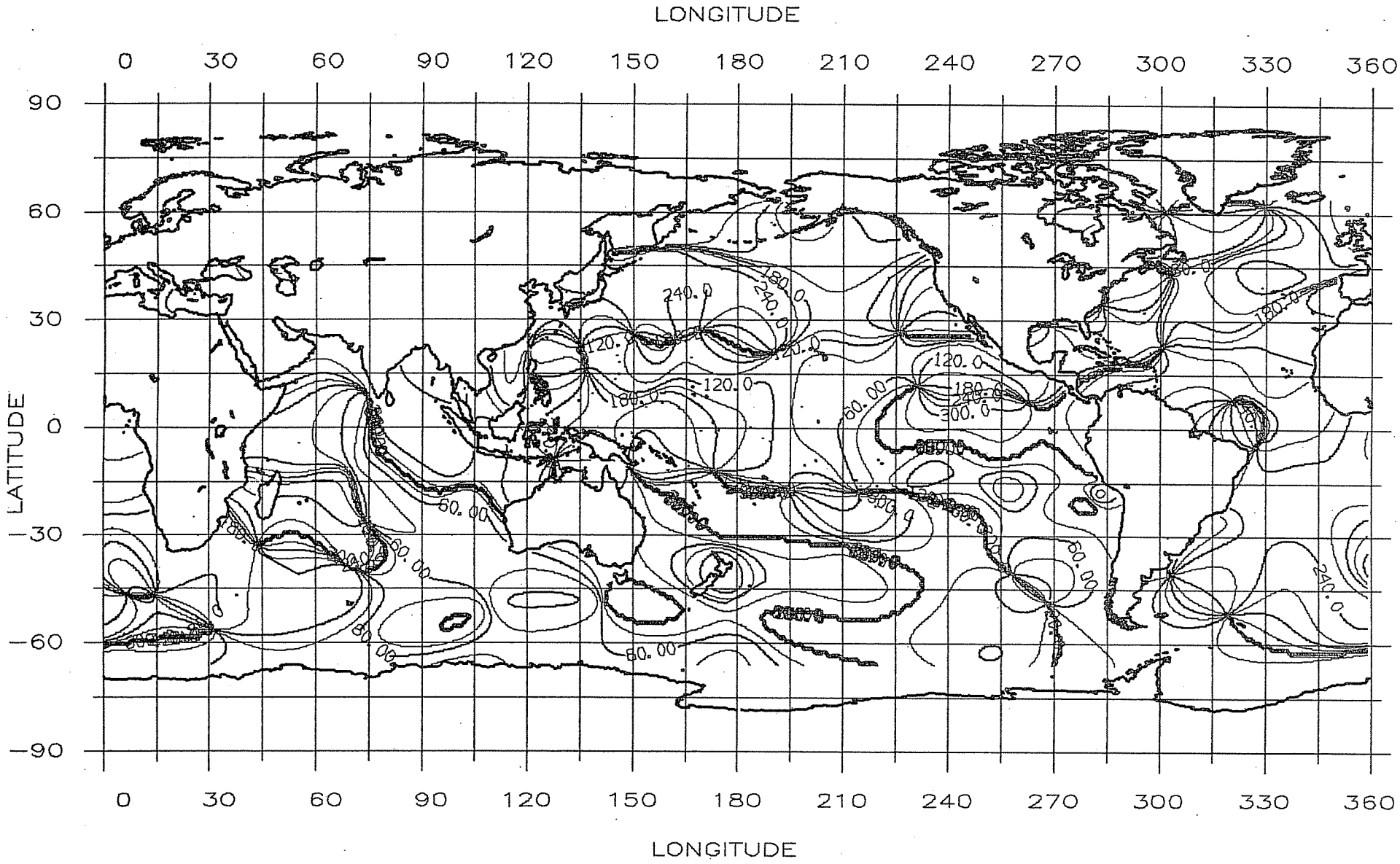

Figure 3.5 Phase of Semi-Annual Amplitude Based on Degree 15 Solution Using Topex Normal Point Data from Cycles 4 to 58. Contour interval is 20°.

3.3.2 Estimated Residual Tides of the N34 Solution

The residual tides for the M_2, S_2, 0_1, and K_1 constituents were estimated with respect to the Cartwright/Ray model given on the Topex GDRs. The constituents were represented by a degree 15 spherical harmonic expansion as discussed in Section 2.2. The amplitude and phase of these corrections can be computed using eq. (3-12). As an example, the amplitude of the M_2, S_2, K_1 and 0_1 tide correction is given in Figures 3.6, 3.7, 3.8, and 3.9, respectively. Statistical information on the value of the tide correction, over all normal points, of the solution are given in Table 3.4.

Table 3.4
Statistics of Residual Tides Based on the Degree 15 Solution N34 Using Topex Data From Cycles 4 to 58. Units are in cm.

	M_2	S_2	0_1	K_1
No. of Samples	321302	321302	321302	321302
Mean	0.00	-0.01	0.00	0.01
Std.	2.93	1.51	0.78	1.41
RMS	2.93	1.51	0.78	1.41
Min.	-12.06	-9.57	-2.59	-4.77
Max.	11.84	9.64	2.58	4.79

The statistical information given in Table 3.4 has been computed using the weighting procedure described in Section 2.3. This assures the statistics are not skewed towards the latitudes having the greater data density. If x_i is the residual and w_i is the weight (r in eq. (2-22)) the mean and standard deviation are defined by the following:

$$\bar{x} = \frac{\sum_i x_i w_i}{\sum_i w_i} \tag{3-13}$$

$$Std = \sqrt{\frac{\sum_i (x_i - x)^2 w_i}{\sum_i w_i}} \tag{3-14}$$

where $w_i = \frac{\sin\beta_i}{\sin\beta_0}\cos\phi_i$. (3-15)

From Table 3.4 one can see that the residual tides vary (in RMS value) from 0.8 to 2.9 cm. The maximum residual tide is M_2 with an RMS value of ±2.9 cm. The residual M_2 tide has an extreme value of 12 cm.

We next use these tide corrections to carry out the comparisons between predicted and ground truth at the Le Provost station set. The initial comparisons were carried out using the 104 station set and the same procedures followed in the construction of Table 3.2. In this case, the RMS differences are: 2.64 cm (M_2); 1.56 cm (S_2); 1.10 cm (0_1); and 1.36 cm (K_1). The results are slightly (5%) better than the N15 solution given in Table 3.2 and primarily reflects the influence of the higher degree (15) representation of the tides.

Another comparison was made with the 95 station subset used by Andersen, Woodworth, and Flather (1994). For these comparisons, the ocean tide grids obtained from R. Ray (April 1994) were used for the base representation of the Cartwright/Ray model. The correction values were scaled using the same values used by Earnes' (1.047 for M_2 and S_2; 1.06 for K_1 and 0_1). These values are based on Table 1 of the Ray and Sanchez (1989). The RMS differences for the C/R model and the N34 model are given in Table 3.5 as computed by Y. Yi (1994, private communication).

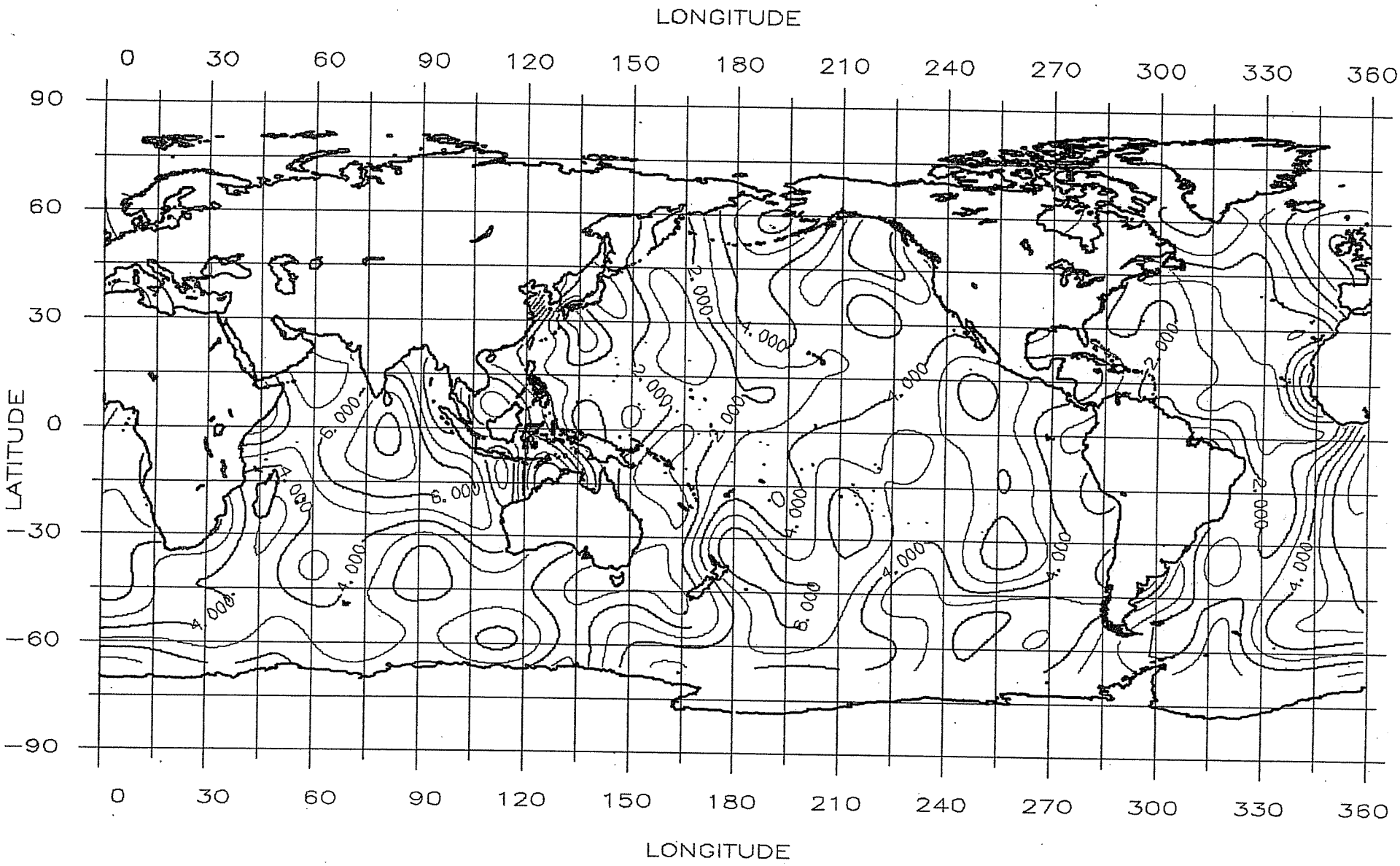

Figure 3.6 Amplitude of M_2 Tide Correction to Cartwright/Ray Topex GDR Model Based on Cycles 4 to 58 of Topex Data. Contour interval is 1 cm.

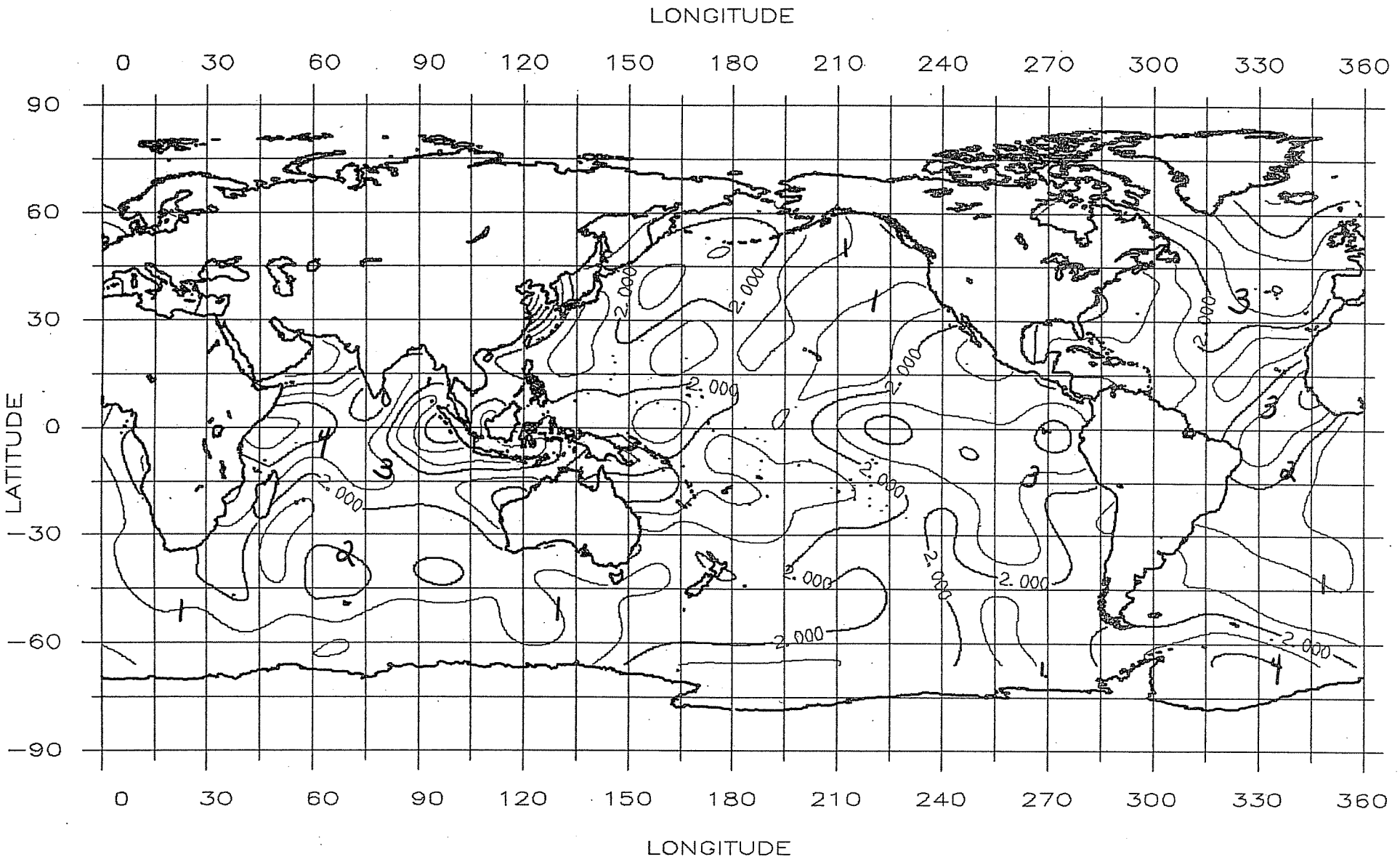

Figure 3.7 Amplitude of S_2 Tide Correction to Cartwright/Ray Topex GDR Model Based on Cycles 4 to 58 of Topex Data. Contour interval is 1 cm.

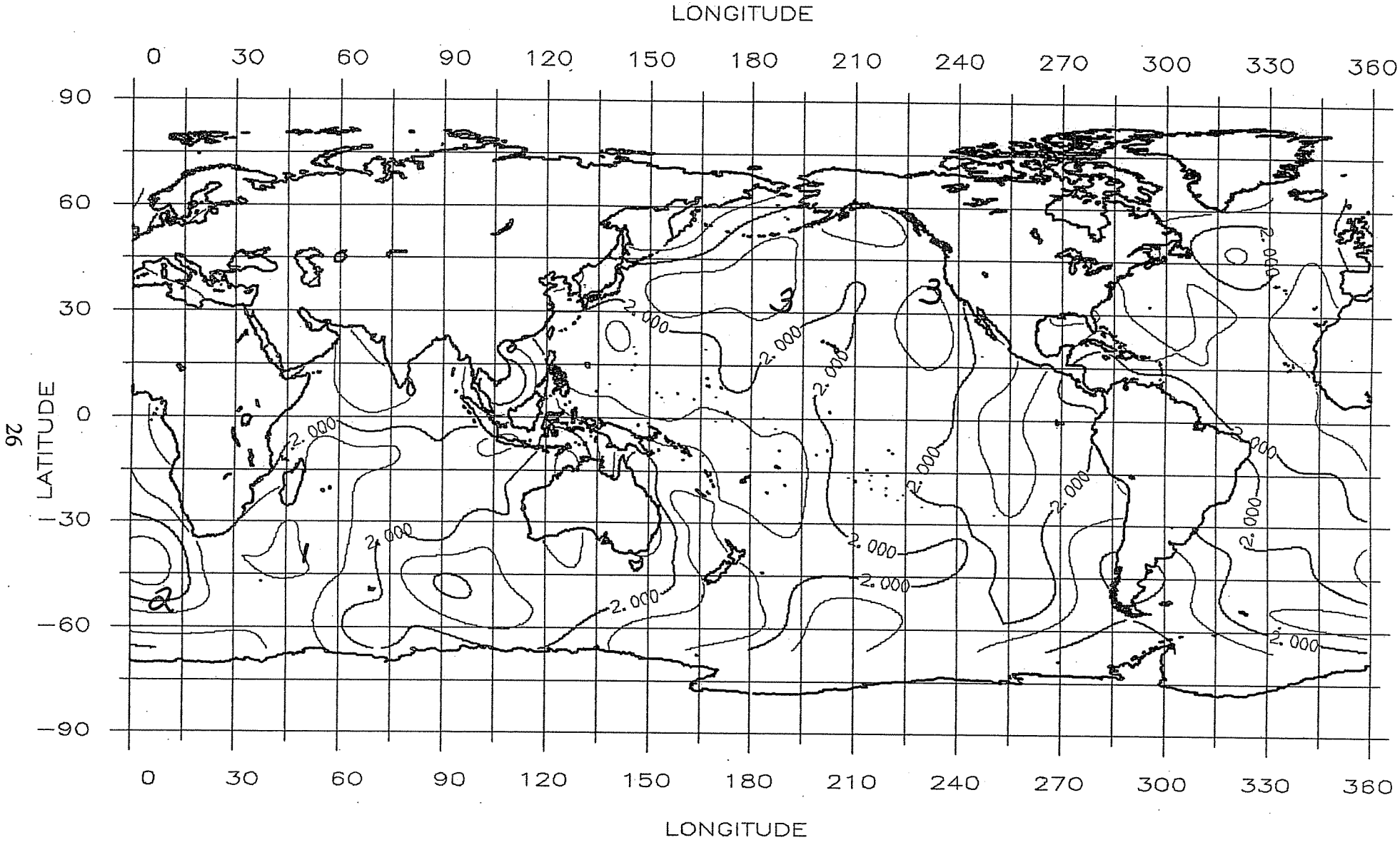

Figure 3.8 Amplitude of K_1 Tide Correction to Cartwright/Ray Topex GDR Model Based on Cycles 4 to 58 of Topex Data. Contour interval is 1 cm.

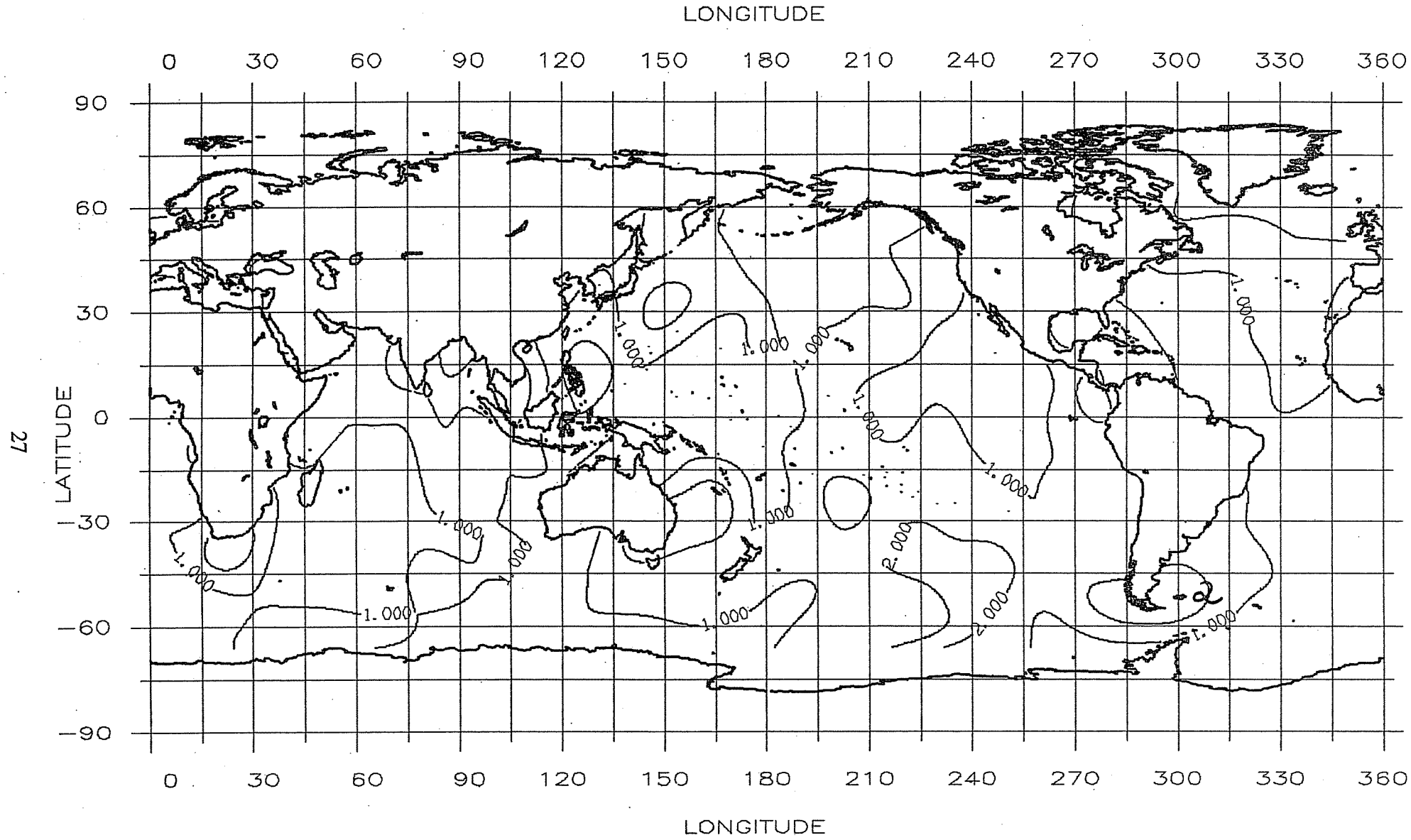

Figure 3.9 Amplitude of O_1 Tide Correction to Cartwright/Ray Topex GDR Model Based on Cycles 4 to 58 of Topex Data. Contour interval is 1 cm.

Table 3.5

RMS Values of Four Tide Constant Differences Based on the C/R Ocean Tide Model and the N34 Ocean Tide Model at 95 Tide Gauge Stations

Tide	C/R	N34
M_2	±3.26 cm	±2.19 cm
S_2	2.29	1.38
0_1	1.28	1.10
K_1	1.99	1.35

It is clear that a significant improvement of the C/R model has taken place in this analysis. The application of the loading factors to the tide correction terms makes no significant impact on the values given for the N34 solution.

Andersen et al (1994) summed the rms differences over the M_2, S_2, K_1 and O_1 components to determine a total tide gauge error measure. This value for several models is as follows: Cartright/Ray (8.8 cm); N34 of this paper (6.0 cm); Knudsen (via Andersen, 6.6 cm); Schrama and Ray (via Andersen, 5.3 cm). These comparisons indicate the tide model estimated here is measurably better that the original C/R model, somewhat better that the Knudsen model, and somewhat poorer than the Schrama/Ray model, as judged by the 95 station gauge comparison.

The development of an improved tidal model was not an original goal of our research. Our original emphasis was on the development of sea surface dynamic topography models. However, it was clear that the development of such models could not rely on the tide models provided on the Topex GDR. This led to our tide improvement activities. The model we have done has not been undertaken with the idea of producing the best tidal model with improvements to all tidal constituents. Instead, we selected the four constituents which were reasonable to improve and such improvement has been achieved as evidenced by the reduction in altimeter residuals and the tide gauge comparisons. In addition, this study solved for these model parameters taking into account a possible drift in the altimeter or sea level rise which can introduce some (but small) error in the tidal analysis. Other studies can clearly develop better tide models than given in this paper. However, the model we have adopted should be sufficient for most sea surface dynamic topography studies. An important exception will be geographic regions where high frequency tidal variations can not be modeled by a degree 15 spherical harmonic representation.

3.3.3 Bias and Bias Rate Estimates from Solution N34

The solution carried out for this study estimates a bias (b) and bias rate ($\dot{b}$) model in terms of a spherical harmonic representation. The values of b and ($\dot{b}$) can be computed at each normal point (a total of 7082) on the reference track and statistical information determined. Such information is given in Table 3.6 where two solutions of different data spans have been carried out. (Solution N33 uses data from cycles 4 to 54.)

Recall from the previous discussion that b is the difference between the mean dynamic topography at time t_0, and the mean dynamic topography based on the Topex data on cycles 17 to 53. The ($\dot{b}$) value infers a secular rate of many possible things including sea level change, altimeter bias change, secular changes in correction terms, etc. Although this method represents variations over the entire ocean, the most meaningful results are probably the ocean wide averages.

Table 3.6
Statistics of Bias and Bias Rate Estimates

Solution	N33		N34	
Parameter	b (cm)	$\dot{b}$ (cm/yr)	b (cm)	$\dot{b}$ (cm/yr)
No. of samples	7082	7082	7085	7085
Mean	-0.26	0.24	-0.34	0.48
Std.	1.59	1.70	1.68	1.85
RMS	1.61	1.72	1.71	1.91
Min.	-5.95	-3.96	-6.13	-3.88
Max.	4.15	6.55	5.07	7.11
Cycles Used	4 to 54		4 to 58	

The mean b value for solution N33 is -2.6 mm and -3.4 mm for N34. These small values reflect the consistency of the two sets of sea surface dynamic topography. One also sees that the b values can reach 6.0 cm in some regions. The ($\dot{b}$) value is 2.4 mm/yr for solution N33 increasing to 4.8 mm/yr when just three cycles of data were added. The sensitivity of $\dot{b}$ to data time span was also noted by Rapp, Wang, and Yi (1994). Note that the $\dot{b}$ for solution N33 is the same as that of solution N15 (to degree 8) shown in Table 3.1. This indicates the insensitivity of ($\dot{b}$) to the maximum degree of the harmonic expansion (8 or 15). This implies that ($\dot{b}$) values can be studied through degree 8 expansions which are much less expensive, in terms of computer resources, to carry out.

Hayne (private communication, 25 Oct. 1994) has provided information that suggests the altimeter measurement has a small drift. Based on the data for cycles 4 to 58 the drift is estimated to be 0.20 cm/yr. The net change in the sea surface (and/or other quantities of interest) is (4.8-2.0) = 2.8 mm/yr. This value appears high with respect to expected values of sea level rise. Longer time series are needed to monitor this slope.

Figures 3.10 and 3.11 show the bias and bias rate values over the ocean. Both figures reflect the extreme values shown in Table 3.5. Substantial variations of b and ($\dot{b}$) are seen over the ocean. The ($\dot{b}$) values vary from -4 cm/yr to 7 cm/yr which seems unrealistic although the average value of 0.48 cm/yr is reasonable, considering the altimeter drift noted in the previous paragraph. In comparing Figures 3.10 and 3.11 one can see a very strong common contour pattern. The magnitude of the contours are opposite in sign so that one can conclude that the global estimates of b and ($\dot{b}$) have a high negative correlation. This suggests that b and ($\dot{b}$) may not be well (if at all) separable with only 54 cycles (540 days) of data. Additional studies are needed to examine this clear correlation of the bias and bias rate estimates.

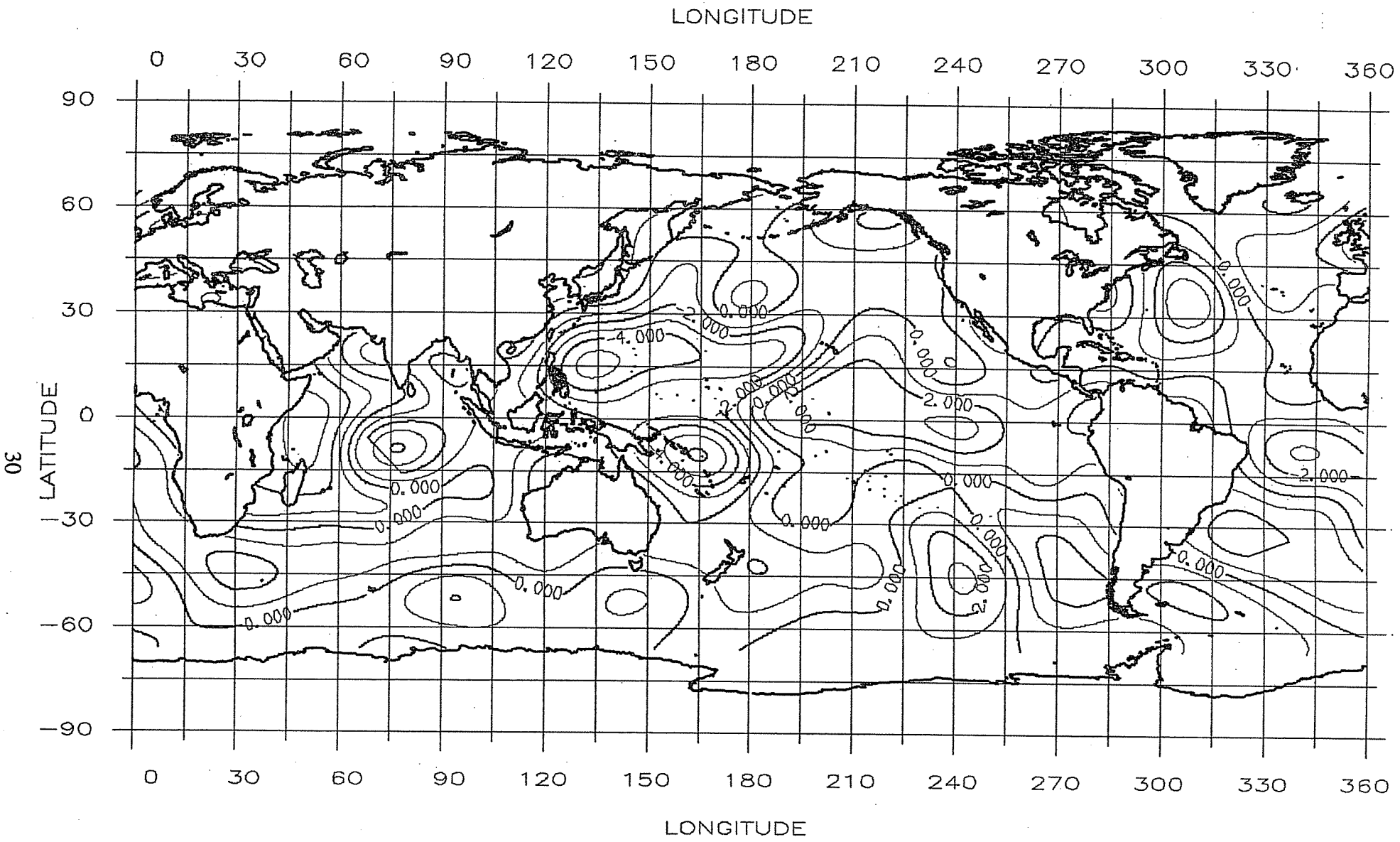

Figure 3.10 Bias Values Based on Degree 15 Solution Using Topex Cycles 4 to 58.
Units are in cm.

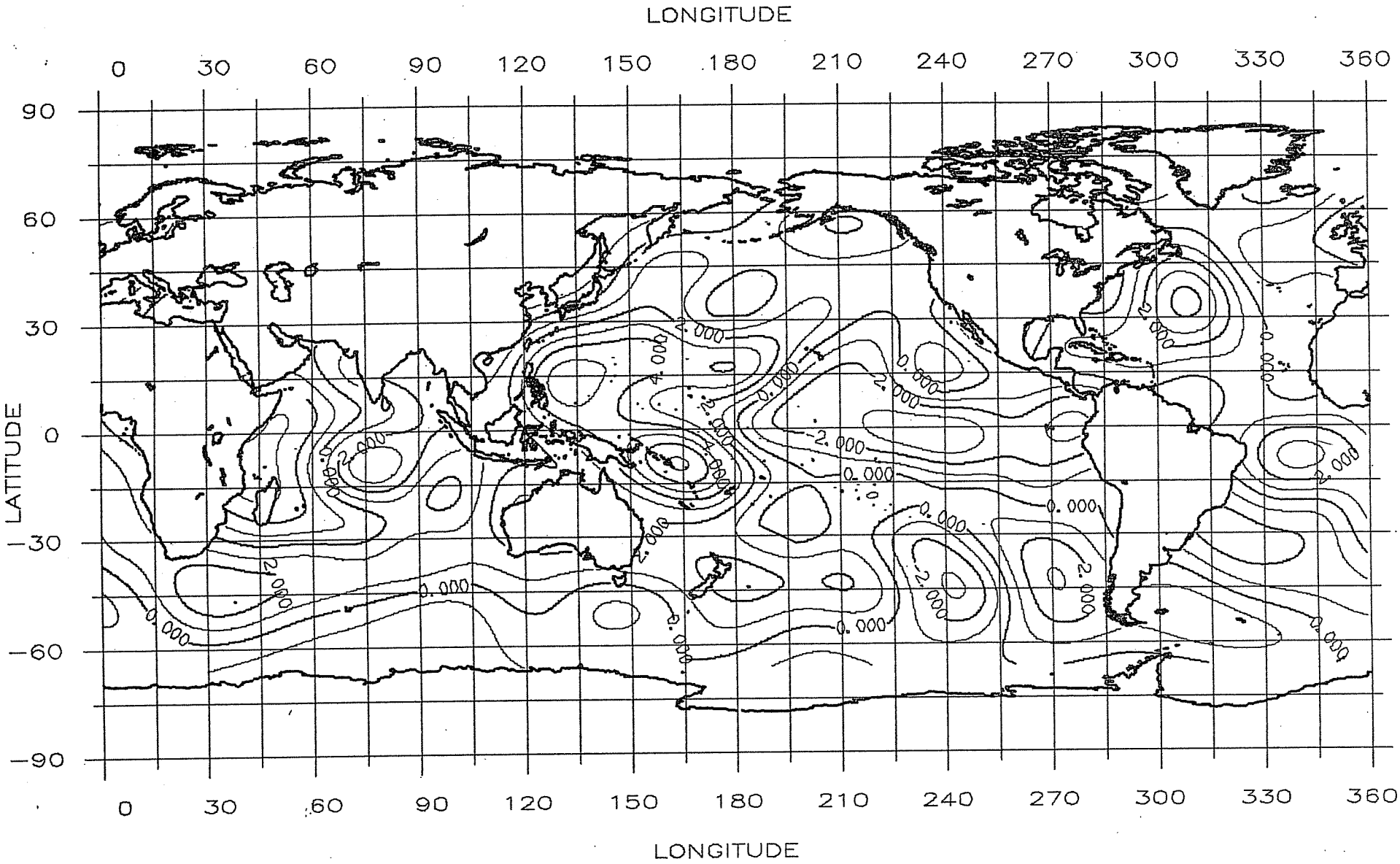

Figure 3.11 Bias Rate Values Based on Degree 15 Solution Using Topex Cycles 4 to 58.
Units are cm/yr.

3.3.4 The Degree Variances of Primary Solution N34

In Section 3.2, we examined the degree variances of the harmonic representations of the tide constituent correction terms, annual and semi-annual terms, and the bias and bias rate quantities. At this stage, only test solutions to degree 8 were available. In this section, we report the degree variances of the final solution of this report which was carried to degree 15. In the case of the residual tidal parameters and the annual/semi-annual variations, there are two components defined by the U_k and V_k series (eq. (2-10)). We then have for the n degree component of the k term:

$$(\delta_n)_k^2 = \sum_{m=0}^{n}\left[\left(a_{nm}^2 + b_{mn}^2\right) + \left(c_{nm}^2 + d_{mn}^2\right)\right]_k \tag{3-16}$$

The bias and bias rate are represented by a single set of spherical harmonic coefficients, respectively. Their degree variances were computed simply by:

$$(\delta_n)_k^2 = \sum_{m=0}^{n}\left[\left(a_{nm}^k\right)^2 + \left(b_{mn}^k\right)^2\right], \tag{3-17}$$

where a_{nm}^k and b_{nm}^k are the coefficients of the spherical harmonics for bias or bias rate. Table 3.7 gives the square root of the degree variances computed from our final solution.

Table 3.7
Square Root of Degree Variances of the Spherical Harmonic Solution N34
(All units are cm except for $\dot{b}$ which is cm/yr.)

	Quantity							
deg	A	SA	M_2	S_2	K_1	O_1	b	$\dot{b}$
0							0.33	0.13
1	2.46	0.49	2.49	0.65	0.89	0.49	0.86	0.65
2	1.67	0.91	1.44	0.81	1.10	0.23	1.07	0.87
3	1.77	0.51	2.25	1.14	1.24	0.84	0.82	0.52
4	1.09	0.50	0.89	0.74	0.71	0.26	0.56	0.65
5	1.35	0.38	1.28	0.88	0.56	0.35	0.50	0.55
6	1.05	0.49	0.71	0.41	0.35	0.23	0.55	0.47
7	1.14	0.41	0.81	0.54	0.39	0.23	0.29	0.33
8	0.79	0.41	0.54	0.53	0.27	0.22	0.38	0.37
9	0.75	0.43	0.65	0.44	0.26	0.18	0.35	0.33
10	0.65	0.34	0.47	0.39	0.30	0.15	0.24	0.29
11	0.64	0.33	0.49	0.34	0.24	0.13	0.27	0.27
12	0.62	0.27	0.38	0.34	0.24	0.15	0.32	0.25
13	0.52	0.20	0.34	0.30	0.23	0.15	0.21	0.22
14	0.49	0.26	0.34	0.30	0.19	0.13	0.20	0.19
15	0.47	0.24	0.34	0.28	0.18	0.13	0.17	0.13
acum.	4.53	1.72	4.31	2.30	2.26	1.22	2.05	1.75

From Table 3.7 one can see that the power (square root of the degree variance) of the corrections (annual, semi-annual, residual tides, bias and bias dot) typically decrease as the degree increases. Note the values in Table 3.7 were computed from the coefficients of the spherical harmonics which can be misleading as this power also represents the magnitude of the function in land areas for which no data was used in the solution.

We transformed the coefficients of the corrections into orthonormal functions (see discussion in Section 4) and recalculated the degree variances of the corrections in orthonormal coefficients using eqs. (3-16) and (3-17). Table 3.8 gives the square root of the degree variances of the corrections in the orthonormal function representation.

Table 3.8
Square Root of Degree Variances of Solution N34 in Orthonormal Function
(All units are cm except for $\dot{b}$ which is cm/yr.)

	Quantity							
deg	A	SA	M_2	S_2	K_1	0_1	b	$\dot{b}$
0	0.72	0.05	0.64	0.26	0.67	0.29	0.34	0.47
1	2.42	0.50	2.30	0.84	0.70	0.46	0.56	0.72
2	1.21	0.56	1.24	0.53	0.85	0.22	0.78	0.90
3	1.22	0.39	2.29	1.13	1.20	0.77	0.51	0.62
4	0.85	0.38	0.95	0.54	0.62	0.28	0.52	0.58
5	1.38	0.40	0.95	0.78	0.42	0.31	0.59	0.58
6	1.17	0.55	0.64	0.45	0.37	0.20	0.50	0.51
7	1.01	0.38	0.75	0.39	0.39	0.24	0.40	0.40
8	0.75	0.40	0.57	0.51	0.26	0.22	0.35	0.38
9	0.76	0.38	0.55	0.41	0.31	0.17	0.41	0.43
10	0.69	0.35	0.50	0.42	0.29	0.17	0.25	0.27
11	0.60	0.28	0.37	0.31	0.22	0.12	0.24	0.25
12	0.60	0.23	0.34	0.31	0.25	0.16	0.32	0.29
13	0.53	0.21	0.31	0.27	0.22	0.14	0.20	0.18
14	0.39	0.21	0.27	0.21	0.17	0.12	0.13	0.13
15	0.28	0.17	0.23	0.18	0.12	0.09	0.08	0.07
acum.	4.15	1.47	4.07	2.13	2.10	1.18	1.70	1.91

Note the square root of the degree variances of degree 0 is the absolute value of the mean values of the corrections. They are generally small (less than 1 cm). But they still seem to violate the water conservation law which requires the mean values of the corrections to be zero. However, this is not considered as critical because we even do not know what is the mean value of the tide constituents which might not be centered (Cartwright et al., 1991). Here we see the advantage of using the orthonormal function in analyzing the altimeter data. By using the orthonormal function, we can force the mean to be zero by forcing the coefficient of zero degree to be zero. Note this is not true for the spherical harmonics. Even if we force the coefficient of the zero degree spherical harmonics to zero, the average value of the expanded quantity in spherical harmonic will not be zero.

The values in Table 3.8 diminish faster than the values based on spherical harmonic expansion. The square root of the accumulative degree variances are smaller than the values of the spherical harmonics with the exception of the bias rate. Note that the mean value of the bias rate is 0.47 cm/yr. from Table 3.8 in good agreement with 0.48 cm/yr given in Table 3.5. The 0.13 cm/yr, given from the spherical harmonic expansion in Table 3.7, is clearly contaminated by the land representation of the function.

4. SEA SURFACE DYNAMIC TOPOGRAPHY EXPANSIONS USING ORTHONORMAL FUNCTIONS AND SPHERICAL HARMONICS

In geodesy and oceanography some quantities, such as sea surface dynamic topography, the sea surface height and the ocean tides etc., are only defined over the ocean. The usual way to represent these quantities is through a spherical harmonic series. However, the spherical harmonic functions are defined globally. If we expand the dynamic topography, for example, into spherical harmonics, we have the problem to interpret the coefficients because there is no direct relationship between the "true" power spectrum and the coefficients of the spherical harmonic expansion. An alternative way is to find a set of functions which are orthonormal over the ocean. They are called orthonormal functions and can be used to expand quantities defined only in ocean areas. Because the functions are orthonormal over the ocean, it is easy to interpret the coefficients. In the following we will estimate orthonormal function coefficients and make comparisons between the orthonormal and spherical harmonic expansion of the SSDT. The basic theoretical development followed here is from Hwang (1991, 1993b).

4.1. Definition of Ocean and Generation of the Orthonormal Functions

Before the orthonormal function is formed, the ocean has to be defined. For different purposes the ocean has been defined differently (Sanchez and Morrow, 1993, p. 38; Hwang, 1991, p. 88). By using the 1°x1° mean elevation file (Kim and Rapp, 1990) we define the ocean as an area between latitude ±70° and the depth of the ocean is greater than zero meters. This definition is consistent with the availability of Topex/Poseidon data between ±66° latitude. This area is denoted as domain 1 and plotted in Figure 4.1. Note that isolated islands, such as Bermuda and Kerguelen, were excluded. The Caspian Sea and the Black Sea were also excluded from the definition of the ocean. Even after these simplifications the ocean boundaries are still very complicated.

The orthonormal function over the ocean can be computed in two ways. One way is to solve a differential equation with given boundary values (Sanchez and Morrow, 1993). Another way is to use the Gram-Schmidt orthonormalizing process to form the orthonormal functions from the spherical harmonic functions (Hwang, 1991,1993). The difference between the orthonormal functions from the two approachs is that the orthonormal function of the first approach satisfies the boundary conditions and the orthonormal function from the second approach is free from any boundary condition. In other words, the orthonormal function from the second approach is not restricted to any boundary value.

It is worthwhile to point out that the orthonormal functions might have unfavorable numerical properties as the degree of expansion increases goes higher. This is possibly caused by the complexity of the boundary of the domain. Rigorously speaking, it is not clear if there is a solution for the differential equation, such as the eq. (1) in Sanchez and Morrow (1993) with a very complicated boundary.

In the following we will describe briefly the procedure used to form the orthonormal function by using the well-known Gram-Schmidt process. More detailed discussion can be found in Hwang(1991).

Given a set of linearly independent base functions $X^T = (x_1, x_2, \ldots)$ over the ocean, where the superscript T denotes the transpose, the orthonormal function $Y^T = (y_1, y_2, \ldots)$ can be computed by (Hwang 1991, p. 11):

$$h_1 = x_1, \qquad y_1 = h_1 / \|h_1\|$$

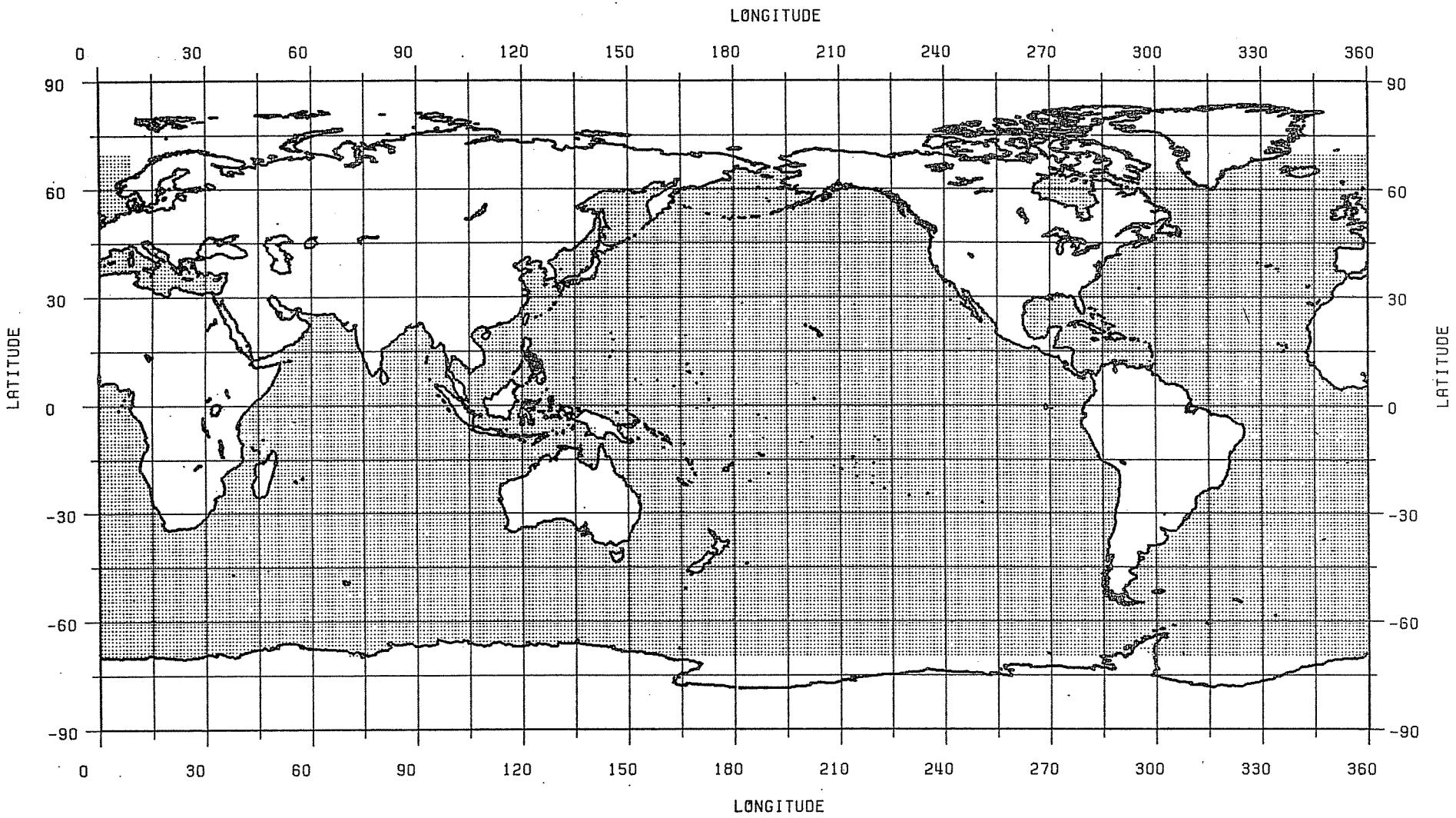

Figure 4.1 Ocean Domain for Orthonormal Function Definition

$$h_2 = x_2 - (x_2, y_1)y_1, \qquad y_2 = h_2 / \|h_2\|, \tag{4-1}$$

$$h_n = x_n - \sum_{k=1}^{n-1}(x_n, y_k)y_k, \qquad y_n = h_n / \|h_n\|,$$

where $\| \ \|$ is the norm of the function, and the inner product of two base functions is defined as:

$$(f_k, f_n) = \iint_{d_1} f_k f_n d\sigma \tag{4-2}$$

where $d\sigma$ is an element of the unit sphere σ and d_1 is the part of the unit sphere where ocean is defined. Obviously, if d_1 is the unit sphere, the inner product of (4-2) becomes 0 as $k \neq n$ and 1 as $k = n$, and the orthonormal functions become spherical harmonic functions. In general the orthonormal function y_n can be written as:

$$y_n = \sum_{j=1}^{n} c_{nj} x_j; \quad n = 1,2,...$$

The orthonormal function is a linear combination of the base functions (spherical harmonic functions). In matrix notation the above equation can be written as (Hwang, 1991, p. 12):

$$Y = CX \tag{4-3}$$

where C is the combination matrix and defined in (ibid., eq. (3.6)). Since C^{-1} exists, eq. (4-3) can also be used to calculate X given Y (Hwang, 1993, eq. (44)).

4.2. Estimation of the Coefficients of the Spherical Harmonic and Orthonormal Expansions of the Sea Surface Dynamic Topography

The sea surface dynamic topography (SSDT), ς, can be expanded into spherical harmonics and orthonormal functions as follows:

$$\varsigma = \sum_{n=0}^{k} \sum_{m=0}^{n} (c_{nm}\overline{R}_{nm} + s_{nm}\overline{S}_{nm}) \tag{4-4}$$

$$\varsigma = \sum_{n=0}^{k} \sum_{m=0}^{n} (a_{nm}O_{nm} + b_{nm}Q_{nm}) \tag{4-5}$$

where $\overline{R}_{nm}, \overline{S}_{nm}$ are the fully normalized spherical harmonics and c_{nm}, s_{nm} are the SH coefficients; in the same way O_{nm} and Q_{nm} are the orthonormal functions and a_{nm} and b_{nm} are the ON coefficients. In numerical computations it is convenient to order the orthonormal functions (as well as spherical harmonic functions) and the corresponding coefficients in a one dimensional vector by

degree. Equation (4-4) may be written as:

$$\varsigma = \sum_{i=1}^{N} \beta_i x_i = \beta X \tag{4-6}$$

where $X^T = (\overline{R}_{00}, \overline{R}_{10}\overline{R}_{11}, \overline{S}_{11}, ...)$ is the vector of the spherical harmonics, and $\beta = (c_{00}, c_{10}, c_{11}, s_{11}, ...) = (\beta_0, \beta_1, ...\beta_N)$ is the coefficient vector of the spherical harmonics. N is the number of the coefficients (N =625 for m, n up to degree 24). In the same way, eq. (4-5) may be written as:

$$\varsigma = \sum_{i=1}^{N} \alpha_i y_i = \alpha Y \tag{4-7}$$

where $Y^T = (O_{00}, O_{10}, O_{11}, Q_{11}, ..)$ is the vector of orthonormal functions , $\alpha = (\alpha_0, \alpha_1, ... \alpha_N)$ is the coefficient vector.

For discrete observations equations (4-6) and (4-7) may be written as the following observation equation:

$$l = A\,\alpha^T + \varepsilon \tag{4-8}$$

$$l = A_S \beta^T + \varepsilon_S \tag{4-9}$$

where

$$\mathrm{A} = \begin{pmatrix} \mathrm{y}_1(\phi_1,\lambda_1) & \mathrm{y}_2(\phi_1,\lambda_1) & . & . & . \\ \mathrm{y}_1(\phi_2,\lambda_2) & \mathrm{y}_2(\phi_2,\lambda_2) & . & . & . \\ . & . & . & . & . \\ . & . & . & . & . \\ . & . & . & . & . \end{pmatrix}, \mathrm{l} = \begin{pmatrix} \varsigma_1 \\ \varsigma_2 \\ . \\ . \\ . \end{pmatrix} \text{ and } \varepsilon = \begin{pmatrix} \varepsilon_1 \\ \varepsilon_2 \\ . \\ . \\ . \end{pmatrix} \tag{4-10}$$

and

$$\mathrm{A_S} = \begin{pmatrix} \mathrm{x}_1(\phi_1,\lambda_1) & \mathrm{x}_2(\phi_1,\lambda_1) & . & . & . \\ \mathrm{x}_1(\phi_2,\lambda_2) & \mathrm{x}_2(\phi_2,\lambda_2) & . & . & . \\ . & . & . & . & . \\ . & . & . & . & . \\ . & . & . & . & . \end{pmatrix}, \text{ and } \varepsilon = \begin{pmatrix} \varepsilon_1 \\ \varepsilon_2 \\ . \\ . \\ . \end{pmatrix} \tag{4-11}$$

where ε and ε_S are the misfits or residuals of the orthonormal and spherical harmonic expansions.

The least squares solutions of equations (4-8) and (4-9) are:

$$\alpha^T = -(A^T P A)^{-1} A^T P l = -N^{-1} A^T P l \tag{4-12}$$

and

$$\beta^T = -(A_S^T P A_S)^{-1} A_S^T P l = -N_S^{-1} A_S^T P l. \tag{4-13}$$

where P is the weight matrix and $N = A^T PA$ and $N_S = A_S^T PA_S$. Using equation (4-3) and the definition of matrices A and A_S we have:

$$A^T = \left[Y(\phi_1,\lambda_1)\, Y(\phi_2,\lambda_2)...\right] = \left[CX(\phi_1,\lambda_1)\, CX(\phi_2,\lambda_2)...\right] = C\left[X(\phi_1,\lambda_1)\, X(\phi_2,\lambda_2)...\right]$$

$$A^T = CA_S^T \tag{4-14}$$

The relationship between the normal equation matrices N and N_S is then:

$$N = CA_S^T PA_S C^T = CN_S C^T \tag{4-15}$$

By using with (4-15) with (4-12) and (4-11) we have:

$$\alpha^T = (C^T)^{-1} N_S A_S^T Pl = (C^T)^{-1} \beta^T \tag{4-16}$$

Note that β^T is the estimated spherical harmonic coefficients by using the least squares adjustment. Equation (4-16) gives the relationship between the estimated orthonormal coefficients (α) and the spherical harmonic coefficients. If there is no a priori information used, there is no difference between the estimation of the orthonormal coefficients using equation (4-12), and estimated spherical harmonic coefficients which are transformed into coefficients of the orthonormal functions through (equation (4-16)).

If a priori information such as the degree variances of the (for example) Levitus' SSDT is used, the solution of (4-8) is then:

$$\alpha^T = -(CN_S C^T + D^{-1})^{-1} CA_S^T Pl, \tag{4-17}$$

where D is a diagonal matrix with elements of the degree variances of the Levitus' sea surface dynamic topography in the orthonormal function.

Noting that

$$(CN_S C^T + D^{-1})^{-1} C = (N_S C^T + C^{-1} D^{-1})^{-1} = (C^T)^{-1}[N_S + (C^T DC)^{-1}]^{-1}, \tag{4-18}$$

equation (4-17) may be written as

$$\alpha^T = -(C^T)^{-1}[N_S + (C^T DC)^{-1}]^{-1} A_S^T Pl = (C^T)^{-1} \beta_a^T \tag{4-19}$$

where

$$\beta_a^T = -[N_S + (C^T DC)^{-1}]^{-1} A_S^T Pl \tag{4-20}$$

The matrix $(C^T DC)^{-1}$ is a symmetric positive definite matrix.

4.3. Boundary Constraints

Sea surface dynamic topography can be used to infer geostrophic flow vectors (both magnitude and direction). Near a shore line, special consideration may be needed because sea surface dynamic topography is not defined on land but remains defined to the land/water interface. Without these considerations, one can have the unrealistic case of water flowing into land. Two special conditions were considered for testing when sea surface dynamic topography is estimated from satellite altimetry and geoid undulations.

For the first case consider the velocity of the geostrophic flow $\underline{v}$ calculated from the sea surface dynamic topography by (Hwang, 1991, p. 126):

$$\underline{v} = \frac{g}{2R\omega \sin\phi}\left(-\frac{\partial \varsigma}{\partial \phi}\hat{e}_E + \frac{\partial \varsigma}{\partial \lambda}\hat{e}_N\right) \tag{4-21}$$

where $\hat{e}_N$ and $\hat{e}_E$ are unit vectors in the north and east directions, respectively; ω is the angular velocity of the Earth's rotation; R is the mean radius of the earth. On the shore there should be no currents flowing into land so that the SSDT must satisfy the following condition:

$$\underline{v}.\underline{n} = 0 \tag{4-22}$$

where n is the normal to the shore line. Assuming the angle between the tangent of the shore line and the parallel of latitude is α, the normal to the shore line can be written as:

$$\underline{n} = \cos\alpha\hat{e}_N - \sin\alpha\hat{e}_E \tag{4-23}$$

By using (4-21) and (4-23) the condition (4-22) becomes:

$$\frac{\partial \varsigma}{\partial \phi}\sin\alpha - \frac{1}{\cos\phi}\frac{\partial \varsigma}{\partial \lambda}\cos\alpha = 0 \tag{4-24}$$

Preliminary numerical tests of the above constraint concept was carried out using Topex data from cycle 17 with JPL editing. Every normal point was used. In this analysis, orthonormal normal coefficients to degree 24 were estimated. An a priori degree variance model was used. In the test involving eq. (4-24) the land ocean boundary was defined by a 1°x1° mean elevation file. Equation (4-24) was used to form a set of pseudo-observation equations which were evaluated along the coast line from Alaska to southern Chile on a 1°x1° grid. Plots were made of the SSDT and the corresponding geostrophic flow vectors (see Section 5.5) to degrees 10, 13, 15, and 24. No significant improvements were seen in the SSDT plots or the flow vector plots in comparison to corresponding solutions in which the constraint was not applied. Consequently, no further testing of this type of constraint was carried out.

The second type of condition was tested by using pseudo-observations of SSDT equal to zero in "land" areas near the land/ocean interface. This type of condition is the same as the boundary condition used by Sanchez and Morrow (1993, eq. (11)) for creating normal modes of the global ocean. In the test solutions, the SSDT values, on a 1°x1° grid, were set to zero in cells where $0 < h < 100$m. This simple boundary condition is efficient to force no currents on shore. But it causes high gradients of dynamic topography along the shore. However, this problem can be solved by introducing different constants along the shore in different areas, but the question remains what should be the right values which do not effect the sea surface dynamic topography near shore?

4.4. Test Expansions of SSDT

In order to make comparisons between the spherical harmonic and orthonormal expansion of the sea surface dynamic topography, a number of test expansions have been made to degree 24, seven of which are described in Table 4.1. Solution A, for example, is an orthonormal expansion with the OSU edit procedure. All solutions described here used Topex cycle 17 data.

Table 4.1
Definition of the Test Expansions Using Topex Cycle 17 Data

Solution	A	B	C	D	E	F	G
OSU Edit	x		x				
JPL Edit		x		x	x	x	x
ON	x	x			x		x
SH			x	x		x	

The counterpart of solution A, in the spherical harmonic estimation is solution C. For both solutions a priori degree variances were used. For solution A, the Levitus' degree variances from orthonormal harmonics as given by Hwang (1991, Table 6.4) were used to stabilize the solution. For solution C (SH), the degree variances of a spherical harmonic expansion of a global sea surface dynamic topography file, with zero values on land (Hwang, 1991, private communication) were used to stabilize the spherical harmonic expansion. The coefficients of solution A were next transformed to SH coefficients and the values of SSDT implied by these coefficients computed are shown in Figure 4.2. The SSDT values computed by the directly estimated SH coefficients are shown in Figure 4.3. In comparing these 2 figures, one sees no visual differences in the open ocean areas. However, solution A (Figure 4.2) shows high gradients along some coastal areas which are not seen in solution C.

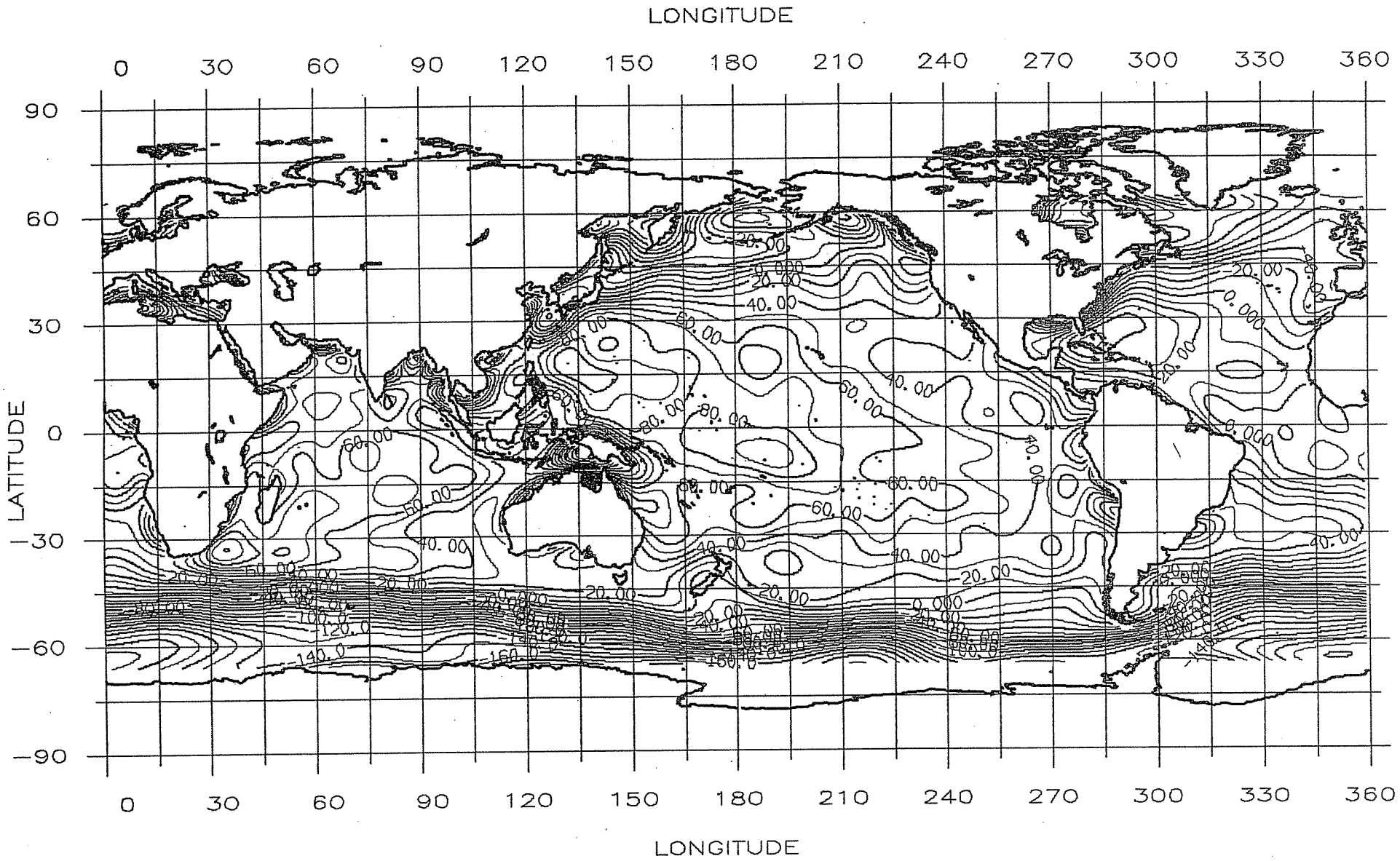

Figure 4.2 SSDT from Test Solution A with ON Coefficients to Degree 24.
Contour interval is 10 cm.

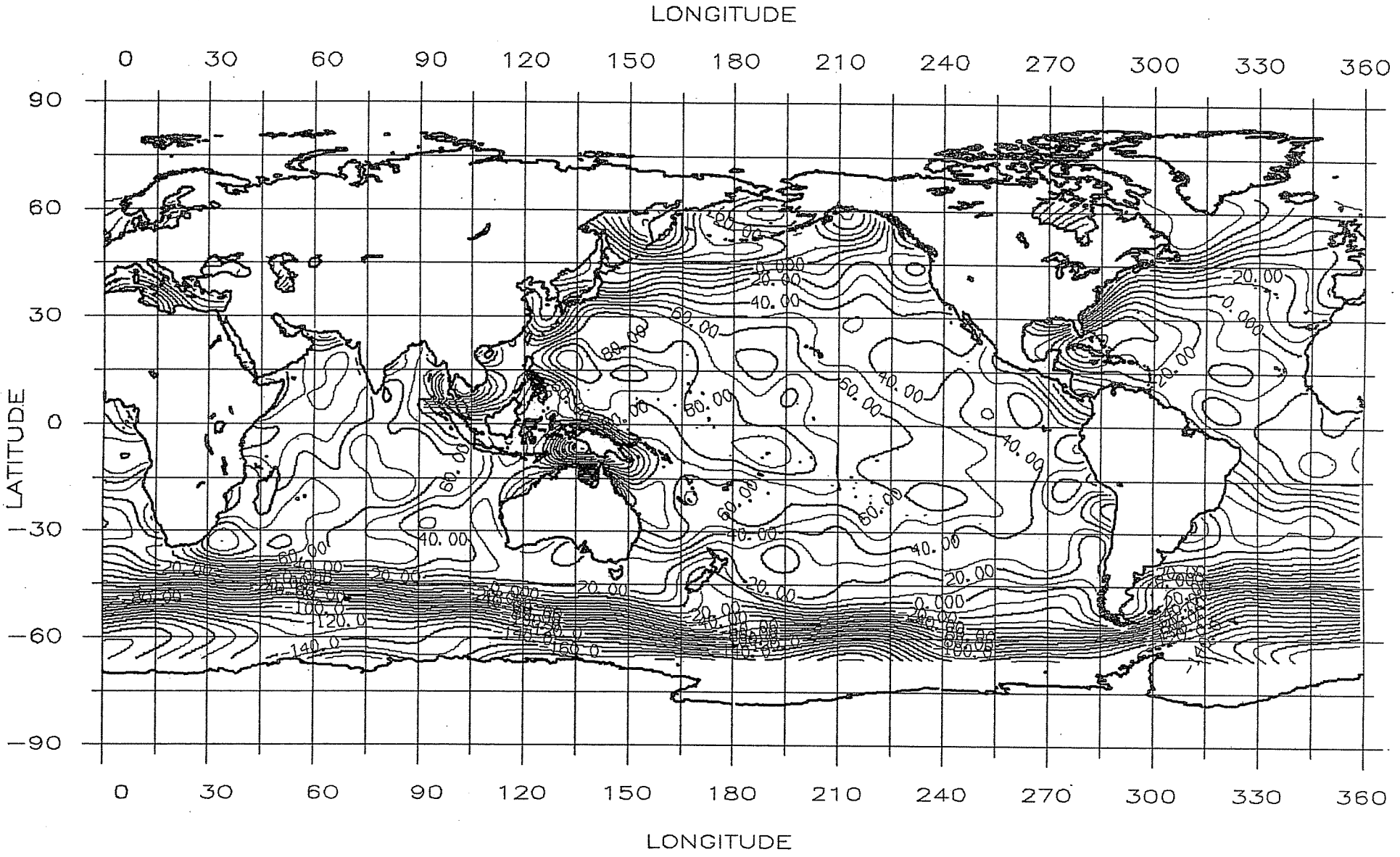

Figure 4.3 SSDT from Test Solution C with SH Coefficients to Degree 24.
Contour interval is 10 cm.

The coefficients of solution A (ON) and solution B (SH) are given in Table 4.2 to degree 3. Also given are the equivalent coefficients in the alternative representation. For example, under solution A a column SH gives the spherical harmonic coefficients transformed from the ON coefficients.

Table 4.2
Coefficients of Sea Surface Dynamic Height to Degree 3 of Test Solutions A and C.
Units are in meters.

	Solution					
	A		C		A-C	
	ON	SH†	ON*	SH	ON	SH
c_{00}	0.127	7.276	0.131	0.001	-0.004	7.275
c_{10}	0.193	10.234	0.196	0.070	-0.003	10.164
c_{11}	-0.190	2.758	-0.189	-0.168	-0.001	2.926
s_{11}	0.063	21.548	0.063	0.027	0.000	21.521
c_{20}	-0.461	6.855	-0.459	-0.543	-0.002	7.398
c_{21}	-0.025	4.847	-0.025	-0.036	0.000	4.883
s_{21}	0.031	37.325	0.031	0.003	0.000	37.322
c_{22}	-0.013	-12.969	-0.014	0.006	0.001	-12.975
s_{22}	0.035	3.997	0.035	0.015	0.000	3.982
c_{30}	0.151	1.619	0.154	0.173	-0.002	1.446
c_{31}	-0.027	4.912	-0.028	-0.010	0.001	4.921
s_{31}	-0.059	40.946	-0.056	-0.087	-0.003	41.033
c_{32}	0.029	-26.701	0.027	0.048	0.002	-26.749
s_{32}	-0.050	7.676	-0.050	-0.009	0.000	7.685
c_{33}	-0.051	-3.322	-0.052	-0.026	0.001	-3.296
s_{33}	0.001	-7.130	0.001	-0.004	0.000	-7.126

†transformed from ON
*transformed from SH

From Table 4.2, one can see that the uniform magnitude of the orthonormal coefficients of solution A indicates the solution is stable. However, if the orthonormal coefficients are transformed into spherical harmonic coefficients, the coefficients become abnormally large with respect to the magnitude of SSDT. The spherical harmonic coefficient s31 even reaches 41 meters. The combination of the spherical harmonic coefficients gives correct SSDT over the ocean areas as can be seen from Figure 4.2. The directly estimated spherical harmonic coefficients and the orthonormal coefficients transformed from spherical harmonic coefficients are similar in magnitude. A very surprising fact is that the coefficients of both solutions are almost identical in orthonormal functions but totally different in spherical harmonics. This can be explained as the spherical harmonic functions represent a global function while the orthonormal function represent a function value in the oceans only. In spherical harmonic expansions through least squares adjustment, the solution is stabilized by a priori information which somewhat reduces large magnitudes of sea surface dynamic topography values, in land areas, computed from the estimated coefficients. In contrast, the orthonormal function represents a function over ocean only (or the domain in which the orthonormal functions are defined). Recall that the spherical harmonic coefficients are computed from the orthonormal coefficients by (cf. eq. (4-19)):

$$\beta_\alpha^T = C^T \alpha^T \tag{4-25}$$

By inspecting Table 4-2, one can see that the differences between the orthonormal coefficients of Solutions A and C are very small. If these small differences between the orthonormal coefficients

are transformed into the coefficients of the spherical harmonics, the differences between the spherical harmonic coefficients become very large. Equation (4-25) means then that a small change in the orthonormal coefficients α^T (in mm level), there is a large change in the spherical harmonic coefficients β_α^T. Therefore, the combination matrix C^T is ill-conditioning. Note that the ill-conditioned does not mean that the orthonormal coefficients can not be transformed into the spherical harmonic coefficients by using the combination matrix. As long as the combination matrix is not singular, the orthonormal coefficient can be transformed into spherical harmonic coefficients and vice versa since the transformation is unique.

The following tables gives the square root of the degree variances of the solution A and C:

Table 4.3
Square Root of Degree Variances for SSDT of Solutions A and C
(Units are in meters)

	Solution					
	A		C		A-C	
Deg.	ON	SH†	ON*	SH	ON	SH
0	0.127	7.276	0.131	0.001	0.004	7.275
1	0.278	24.014	0.280	0.184	0.003	23.980
2	0.464	40.593	0.462	0.544	0.002	40.690
3	0.182	50.369	0.183	0.202	0.005	50.460
4	0.179	52.394	0.178	0.111	0.005	52.373
5	0.088	50.268	0.086	0.067	0.006	50.283
6	0.084	49.832	0.083	0.128	0.007	49.819
7	0.006	50.268	0.064	0.123	0.007	50.605
8	0.081	48.712	0.083	0.095	0.007	48.679
9	0.043	43.199	0.040	0.082	0.007	43.202
10	0.033	36.302	0.035	0.028	0.009	36.309
11	0.041	30.726	0.043	0.045	0.007	30.730
12	0.045	26.513	0.044	0.063	0.007	26.502
13	0.035	22.077	0.033	0.059	0.007	22.092
14	0.047	17.162	0.045	0.058	0.008	17.160
15	0.047	12.448	0.041	0.051	0.009	12.441
16	0.034	8.653	0.028	0.041	0.011	8.647
17	0.029	5.859	0.027	0.042	0.009	5.850
18	0.028	3.817	0.024	0.031	0.010	3.817
19	0.031	2.282	0.024	0.032	0.012	2.294
20	0.025	1.259	0.022	0.033	0.013	1.261
21	0.029	0.641	0.022	0.029	0.019	0.639
22	0.027	0.305	0.020	0.032	0.017	0.296
23	0.021	0.125	0.019	0.028	0.013	0.124
24	0.011	0.042	0.013	0.027	0.013	0.048
Accum	0.647	152.985	0.645	0.679	0.048	153.014

†transformed from ON
*transformed from SH

As we can see, both solutions are very close in the orthonormal system, or over the oceans. The square root of the accumulative degree variances of solutions A and C are 64.7 and 64.5 cm, respectively. Their accumulative difference is about ±4.8 cm. In the spherical harmonic system, the square root of degree variances of the differences is ±153m. This large difference must come from the differences on land, because the differences of solution A and C, or the orthonormal system, is only ±4.8 cm.

Comparison of Fig. 4.2 and 4.3 indicates good agreement between the two representations of the dynamic topography in open ocean areas. In a few shoreline regions (north end of the Arabian Sea, off the Indochina peninsula in the South China Sea, off the northwest coast of Australia, etc.) the dynamic topography gradients for the orthonormal expansion are larger than in the spherical harmonic representation. This undesirable feature may relate to the domain definition and the altimeter data available in a specific region. We conclude that the spherical harmonic solution gives a more reasonable representation of dynamic topography than the orthonormal normal function.

The next test is the use of the edit criteria. The JPL edit was used for solutions B (ON) and D (SH). The sea surface dynamic topography computed from both solutions are plotted in Figures 4.4 and 4.5. By comparing Figures 4.2 and 4.4, one finds that the gradients of dynamic topography in north Australia and in the South China Sea area are reduced. This indicates that the OSU edit might accept some data with large SSDT variations in the areas. Because the OSU edit takes more data than the JPL edit does, we decided to use the OSU edit with some modifications. Detailed information on the modified OSU edit will be given in Section 5. The modified edit was only used for solutions to be described in later sections. Tables 4.4 and 4.5 give the coefficients, to degree 3, and the degree variance comparisons between solutions B and D. We have the same conclusions as the comparisons between solutions A and C discussed above. The ON expansion when transformed to a SH expansion yields coefficients and degree variances that are unreasonable in magnitude. The direct SH expansion and its transformation to the ON expansion gives coefficients of reasonable magnitude. In fact, the difference between the directly estimated ON coefficients and the ON coefficients from the SH expansion is less than 1 mm up to degree 6 showing the excellent consistency in the procedure.

Table 4.4
Coefficients of Sea Surface Dynamic Height to Degree 3 of Test Solutions B and D with Topex Cycle 17 Data and JPL Edit. Units are in meters.

	Solution					
	B		D		B-D	
	ON	SH†	ON*	SH	ON	SH
c00	0.117	10.510	0.125	-0.002	-0.008	10.512
c10	0.183	15.113	0.189	0.065	0.006	15.048
c11	-0.192	6.222	-0.191	-0.154	-0.001	6.376
s11	0.062	28.143	0.064	0.039	-0.002	28.104
c20	-0.474	11.711	-0.471	-0.551	-0.003	12.262
c21	-0.024	11.395	-0.023	-0.039	-0.001	11.434
s21	0.023	50.006	0.023	0.025	0.000	49.981
c22	-0.010	-15.225	-0.013	-0.005	0.003	-15.220
s22	0.038	7.907	0.036	0.029	0.002	7.878
c30	0.139	4.935	0.143	0.149	-0.004	4.786
c31	-0.026	12.973	-0.026	-0.009	0.000	12.982
s31	-0.056	57.769	-0.057	-0.046	0.001	57.815
c32	0.034	-31.515	0.029	0.022	0.005	-31.537
s32	-0.055	15.995	-0.054	-0.033	-0.001	16.028
c33	-0.051	-6.545	-0.049	-0.037	-0.002	-6.508
s33	0.002	-7.107	0.003	-0.008	-0.001	-7.099

†transformed from ON expansion
*transformed from SH expansion

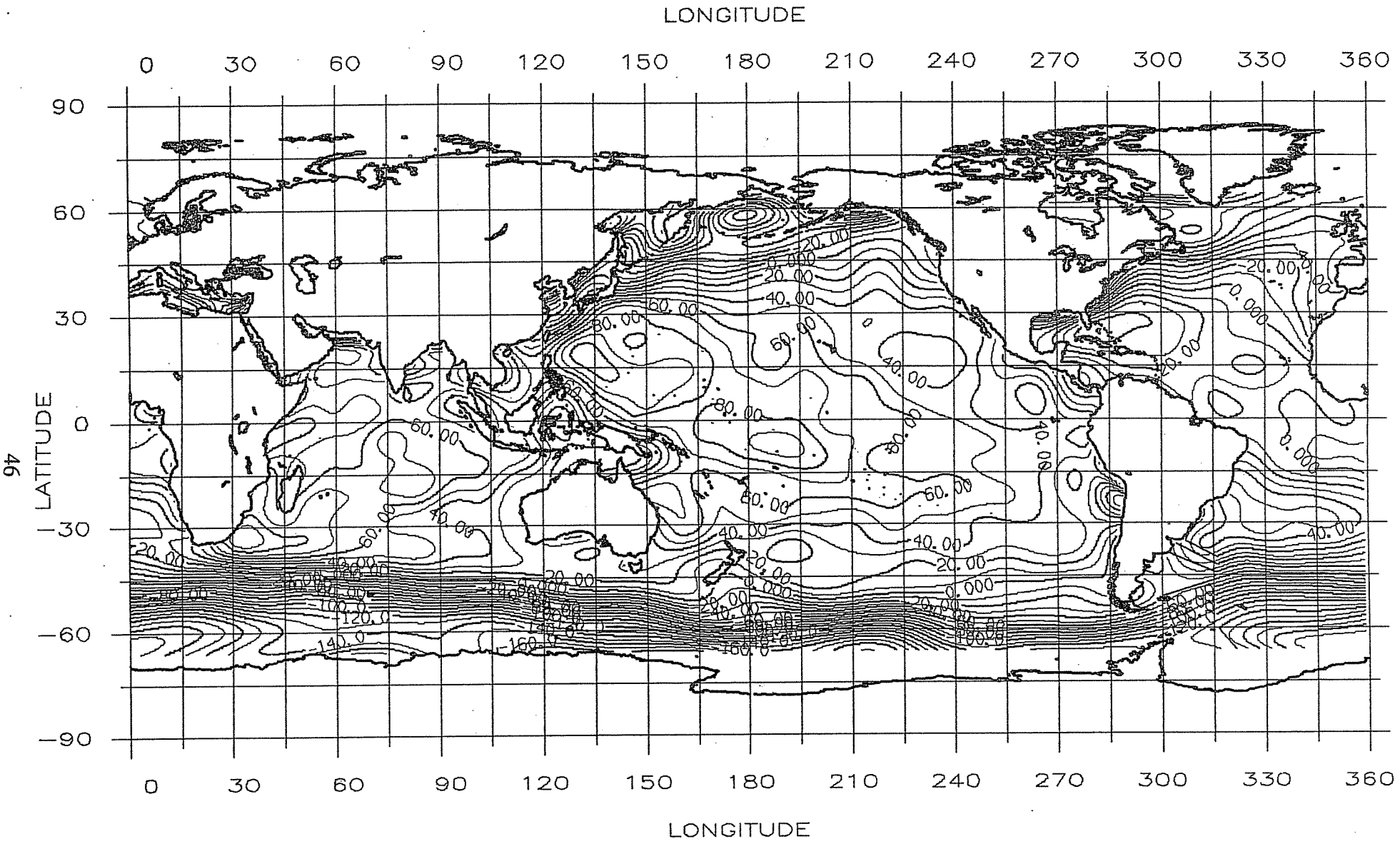

Figure 4.4 SSDT from Test Solution B with ON Coefficients and JPL Data Editing.
Contour interval is 10 cm.

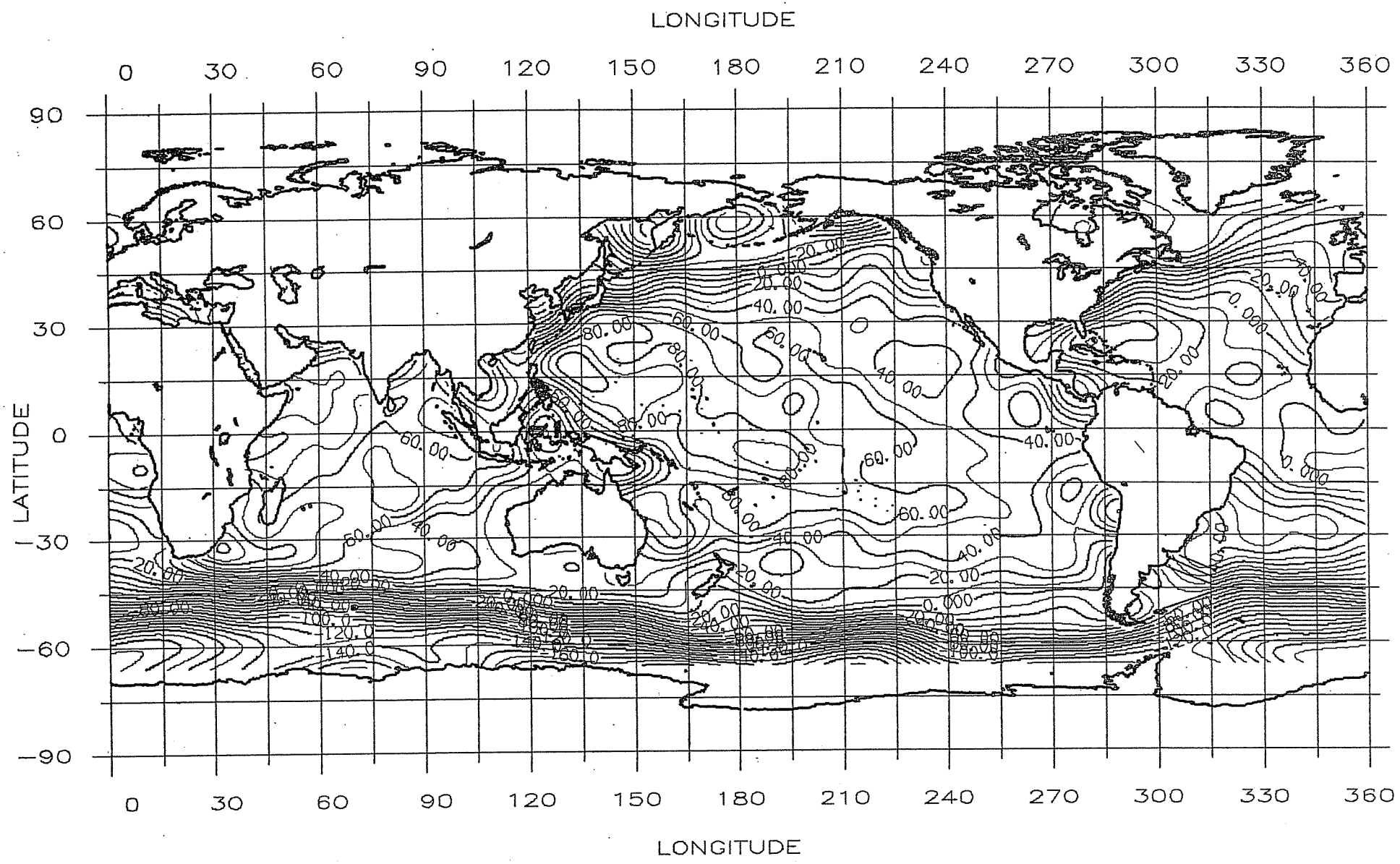

Figure 4.5 SSDT from Test Solution D with SH Coefficients and JPL Data Editing.
Contour interval is 10 cm.

Table 4.5
Square Root of Degree Variances of Solution B and D.
Units are in meters.

	Solution					
	B		D		B-D	
Deg.	ON	SH†	ON*	SH	ON	SH
0	0.117	10.510	0.125	0.002	0.008	10.512
1	0.272	32.544	0.276	0.172	0.006	32.511
2	0.477	55.335	0.473	0.554	0.005	55.433
3	0.173	69.802	0.175	0.166	0.007	69.844
4	0.188	72.992	0.182	0.106	0.009	72.954
5	0.083	68.509	0.080	0.063	0.008	68.503
6	0.080	63.645	0.078	0.137	0.010	63.609
7	0.072	60.783	0.069	0.100	0.007	60.768
8	0.075	56.851	0.079	0.091	0.011	56.828
9	0.041	49.455	0.038	0.050	0.011	49.463
10	0.032	40.205	0.033	0.028	0.011	40.207
11	0.038	31.714	0.038	0.025	0.011	31.716
12	0.042	25.250	0.040	0.039	0.008	25.243
13	0.027	20.000	0.028	0.044	0.009	20.019
14	0.037	14.970	0.039	0.040	0.009	14.965
15	0.028	10.521	0.026	0.035	0.008	10.512
16	0.021	7.135	0.019	0.019	0.008	7.136
17	0.021	4.781	0.021	0.026	0.007	4.788
18	0.017	3.150	0.013	0.016	0.009	3.147
19	0.022	1.910	0.019	0.014	0.008	1.909
20	0.016	1.051	0.015	0.020	0.008	1.051
21	0.016	0.511	0.014	0.017	0.011	0.512
22	0.015	0.233	0.014	0.018	0.010	0.235
23	0.012	0.090	0.012	0.017	0.009	0.090
24	0.008	0.035	0.008	0.017	0.007	0.034
Accum	0.645	191.394	0.643	0.655	0.044	191.395

†transformed from ON expansion
*transformed from SH expansion

In an attempt to have more meaningful SH coefficients derived from the ON coefficients it was decided to add additional "data" to the ON estimation procedure. This "data" consisted of sea surface dynamic topography values, in near shore land areas, computed from the spherical harmonic coefficients of solution D. The values were estimated on a 1°x1° grid and used in areas where the elevation is greater than zero but less than 100m. This "data", as well as Topex data from cycle 17, were used to determine another ON expansion (Solution E) and a SH expansion (Solution F).

The SSDT from the two solutions are plotted in Figure 4.6 and 4.7. In comparing the two maps, one can see that two solutions are visually almost identical, except in the Mediterranean Sea and the Black Sea where solution E (ON) has larger gradients than solution F (SH). The comparison of the coefficients and degree variances are given in Tables 4.6 and 4.7.

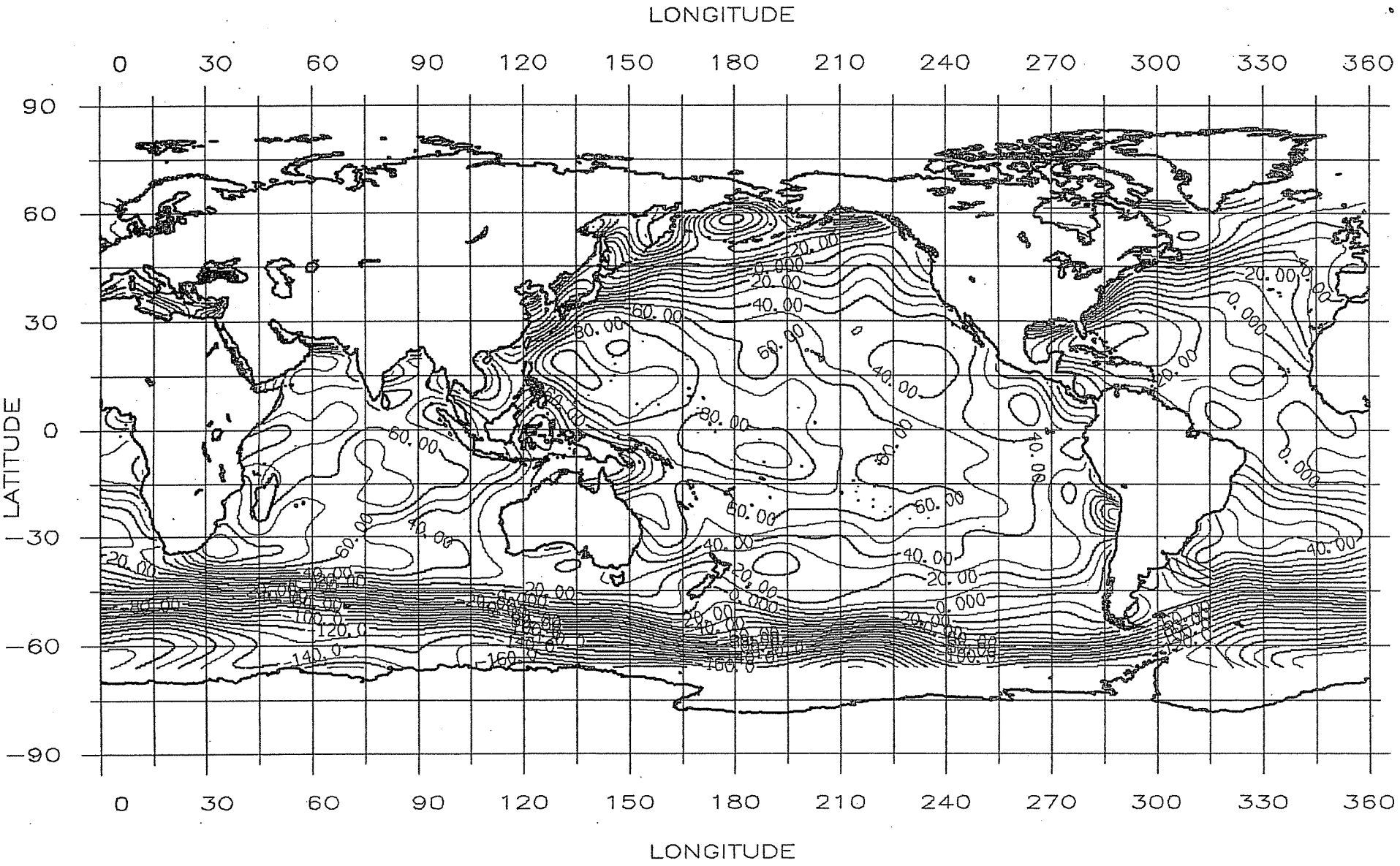

Figure 4.6 SSDT from Test Solution E with ON Coefficients and an Augmented Data Set. Contour interval is 10 cm.

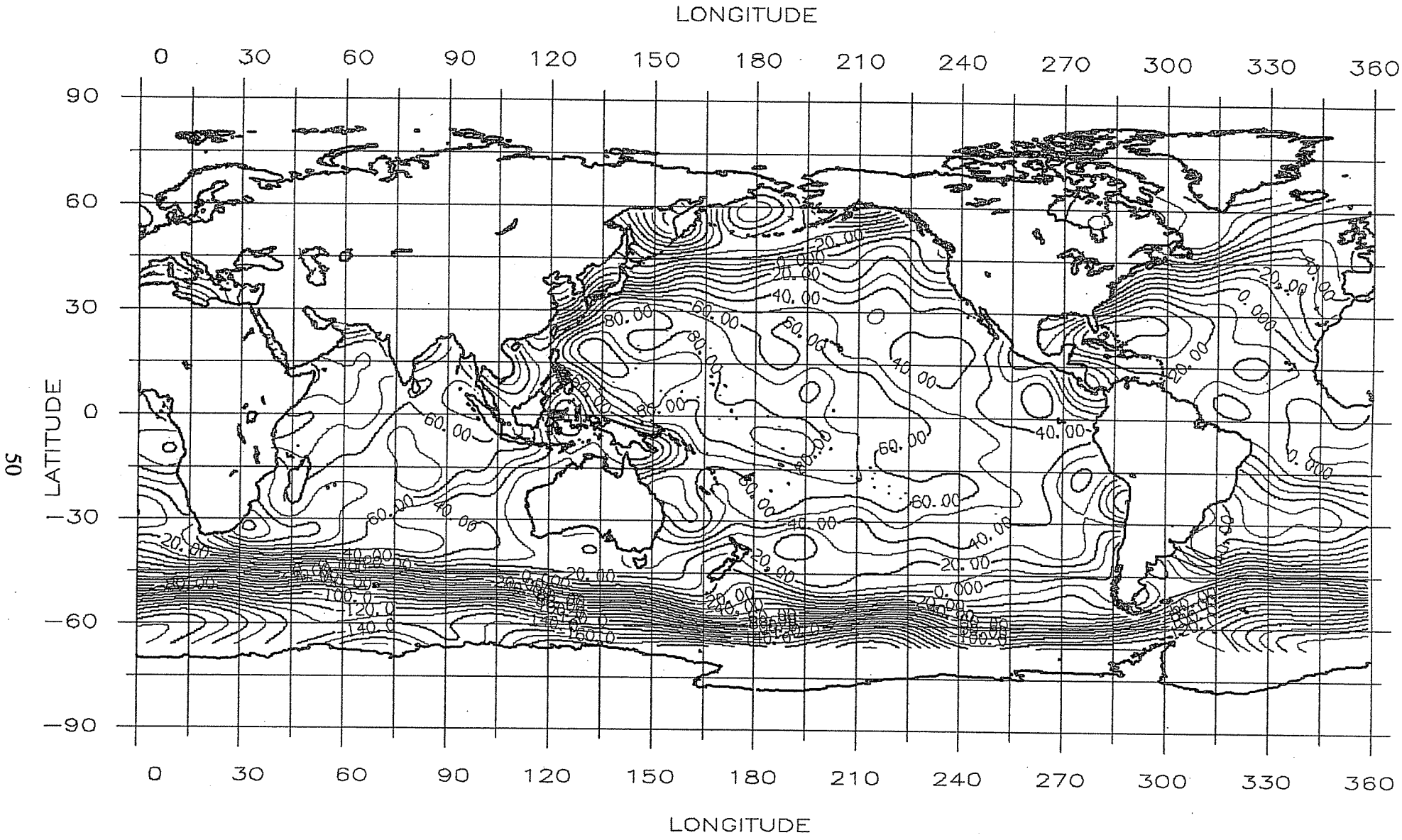

Figure 4.7 SSDT from Test Solution F with SH Coefficients and an Augmented Data Set. Contour interval is 10 cm.

Table 4.6
Coefficients of Sea Surface Dynamic Height to Degree 3 of Test Solutions E and F.
Units are in meters.

	Solution					
	E		F		E-F	
	ON	SH†	ON*	SH	ON	SH
c_{00}	0.119	0.155	0.125	-0.002	-0.006	0.157
c_{10}	0.185	0.553	0.189	0.065	0.004	0.488
c_{11}	-0.192	-0.266	-0.191	-0.154	-0.001	-0.112
s_{11}	0.064	0.142	0.064	0.039	0.000	0.103
c_{20}	-0.474	0.168	-0.471	-0.550	-0.003	0.718
c_{21}	-0.024	-0.200	-0.023	-0.039	-0.001	-0.161
s_{21}	0.024	0.244	0.023	0.025	0.001	0.219
c_{22}	-0.011	-0.044	-0.013	-0.005	0.002	-0.039
s_{22}	0.036	-0.002	0.036	0.029	0.000	-0.031
c_{30}	0.140	0.807	0.143	0.149	-0.003	0.658
c_{31}	-0.026	-0.234	-0.026	-0.009	0.000	-0.225
s_{31}	-0.055	0.266	-0.057	-0.046	0.002	0.312
c_{32}	0.032	-0.027	0.029	0.022	0.003	-0.049
s_{32}	-0.054	-0.059	-0.054	-0.033	-0.000	-0.026
c_{33}	-0.049	-0.070	-0.049	-0.037	0.000	-0.033
s_{33}	0.001	-0.063	0.003	-0.008	-0.002	-0.055

†transformed from ON expansion
*transformed from SH expansion

Table 4.7
Square Root of Degree Variances for SSDT of Solution E and F.
Units are in meters.

	Solution					
	E		F		E-F	
Deg.	ON	SH†	ON*	SH	ON	SH
0	0.119	0.155	0.125	0.002	0.006	0.157
1	0.274	0.630	0.276	0.172	0.004	0.511
2	0.477	0.360	0.473	0.553	0.004	0.770
3	0.172	0.889	0.175	0.165	0.005	0.767
4	0.186	0.605	0.182	0.106	0.007	0.647
5	0.080	0.962	0.080	0.063	0.007	0.925
6	0.078	0.791	0.079	0.137	0.008	0.692
7	0.069	0.979	0.069	0.100	0.006	1.058
8	0.077	0.848	0.079	0.091	0.007	0.803
9	0.039	0.930	0.038	0.050	0.006	0.946
10	0.031	0.726	0.033	0.028	0.008	0.727
11	0.039	0.823	0.038	0.025	0.007	0.823
12	0.044	0.653	0.040	0.039	0.007	0.660
13	0.027	0.659	0.028	0.044	0.007	0.640
14	0.038	0.479	0.039	0.040	0.008	0.483
15	0.029	0.452	0.025	0.035	0.008	0.451
16	0.021	0.365	0.019	0.019	0.007	0.364
17	0.022	0.310	0.021	0.026	0.006	0.314
18	0.015	0.244	0.013	0.016	0.006	0.238
19	0.019	0.188	0.019	0.014	0.005	0.188
20	0.015	0.160	0.015	0.020	0.006	0.154
21	0.013	0.109	0.014	0.017	0.007	0.109
22	0.014	0.079	0.014	0.018	0.006	0.077
23	0.011	0.044	0.012	0.017	0.007	0.039
24	0.007	0.023	0.008	0.017	0.006	0.020
Accum	0.644	2.944	0.643	0.655	0.033	2.955

†transformed from ON expansion
*transformed from SH expansion

The transformed ON to SH coefficients of Solution E have a more reasonable magnitude than found earlier (Table 4.4) with Solution B. For Solution B the largest SH coefficient (to degree 3) was 57m while the largest SH (from ON) coefficient for Solution E is 0.8m. In addition, the root mean square (rms) difference of ±4.4 cm (Table 4.5) between the ON (direct) and ON (from SH) is reduced to ±3.3 cm (Table 4.7) in the E/F solutions. In comparing the transformed SH (from ON) to SH (direct) the rms difference was ±191m (Table 4.5) with solutions B/D and ±2.9m (Table 4.7) with solutions E/F. These results indicate the improvement in the estimate of the SH coefficients from the ON coefficients when "data" is added in low elevation land areas. One should also note that the addition of this data has minor impact on the direct (or indirect) ON expansion. For example, the cumulative power for solution B (ON) is 64.5 cm^2 while it is 64.4 cm^2 for solution E (ON). Similar comparisons are seen for the direct SH expansions (D vs F).

Although the addition of the special data has helped the ON to SH transformation no improvement is seen (or needed) when the SH to ON transformation is made. Consequently this type of solution, where artificial data is added to the solution, is not thought to be reasonable, especially considering the additional computation effort needed. These results do imply that it is

better to estimate the SH coefficients to represent the sea surface dynamic topography and then convert the SH coefficients to ON coefficients where spectral studies are of interest.

4.5 Expansion Conclusions

Based on the various expansions described in Section 4.4, the following conclusions can be made:

1. The RMS difference between a direct ON expansion and a SH to ON expansion, to degree 24, is slightly less than ±5 cm (Table 4.3 and 4.5). Larger differences can occur in the shoreline regions with the ON representation having some anomalous gradients in a few near shoreline regions.

2. The direct spherical harmonic expansion appears consistent between different solution when a priori degree variances are used. The direct ON expansion yields transformed SH expansion that are very sensitive to the data sets used.

3. It is only meaningful to compare and analyze the orthonormal coefficients. Two totally different sets of spherical harmonic coefficients may give very close values over the oceans. But the differences between individual coefficients can be 40 or 50 meters.

Based on the results of these tests, we recommend that the sea surface dynamic topography be represented by a direct estimation of spherical harmonic coefficients, and that for the spectral analysis of SSDT, the orthonormal expansion (either direct or transformed SH expansion) be used.

5. SEA SURFACE DYNAMIC TOPOGRAPHY DETERMINATION AND SPECTRAL ANALYSIS FROM MULTIPLE TOPEX CYCLES

The annual, semi-annual sea surface height variations, four tide constituents, bias and bias rate were solved in a simultaneous solution as discussed previously in Section 3.3. The sea surface dynamic topography computed by using eq. (2-1) was corrected for the residual tides and expanded into a spherical harmonic expansion from degree zero to 24. In this section, we will describe the final analysis procedures for SSDT estimation based on the experiences and test solutions described in the previous sections.

5.1 Data Editing and Spherical Harmonic Expansion

After the residual tide corrections, the SSDT in some geographic areas may be contaminated by geoid undulation error and residual, high frequency tide error. Additional editing is needed to eliminate data thay may have such errors. Several tests were carried out that led to the deletion of SSDT values exceeding 1m, in absolute value, in two geographic regions: a) $0° \le \phi \le 15°$, $90° \le \lambda \le 127°$, and b) $-30° \le \phi \le 0°$, $105° \le \lambda \le 155°$. This edit criterion is called a modified OSU edit. In comparison with the JPL edit, this procedure accepts somewhat more data points.

Another consideration in the spherical harmonic expansion of the SSDT is the use of a priori information. Two different degree variance sets were used for the test solutions. One set is the Levitus degree variances computed from coefficients of spherical harmonic expansion of Levitus dynamic topography (set 3, Engelis, 1987). Another set was based on a set of harmonic coefficients formed by averaging ten sets of harmonic coefficients found for Topex cycles 9, 12, 15,...36. Test solutions for SSDT, to spherical harmonic degree 24, were made using the tide corrected normal points for Topex cycle 17. The degree variances of the two solutions (one with Levitus degree variances and the other with mean coefficient degree variances) are given in Table 5.1.

Table 5.1
Square Root of A Priori and Solution Degree Variances of Dynamic Topography Based on Topex Cycle 17 Using a Spherical Harmonic Expansion to Degree 24. Units are in cm.

	A Priori Values		Test Solution	
Degree	Levitus	Average	Levitus (ap)	Average (ap)
0	0.00	0.19	0.40	0.03
1	18.19	23.65	19.74	20.74
2	22.20	44.29	51.74	52.86
3	9.45	18.87	22.82	24.26
4	7.15	14.55	9.38	11.16
5	7.18	8.10	8.47	9.77
6	13.75	10.18	14.66	13.56
7	10.92	11.29	12.89	11.91
8	7.64	9.67	12.57	13.39
9	6.09	5.59	9.37	9.06
10	3.04	2.82	4.38	3.91
11	3.59	3.02	5.34	4.58
12	5.13	4.37	6.26	6.10
13	4.29	4.42	6.71	6.90
14	4.44	3.74	7.25	6.93
15	2.97	3.19	6.29	6.38
16	2.93	1.85	5.23	3.93
17	2.93	2.98	5.92	5.74
18	2.18	2.06	4.20	4.01
19	2.07	2.00	4.31	4.16
20	2.55	2.00	4.41	3.81
21	2.37	2.00	3.48	3.09
22	2.48	2.00	4.17	3.63
23	2.20	2.00	3.67	3.33
24	2.09	2.00	3.16	3.07
Cumulative			70.50	69.06

From this table one first notes the fairly good agreement between the Levitus degree variances and the average degree variance above degree 4. At and below degree 4, the square root of the degree variances for the Levitus data are substantially smaller than the average set. For degrees 2, 3, and 4, the Levitus values are half the average based values. Also note that the degree variances for the average set were set to be $(2.0 \text{ cm})^2$ from degree 18 to 24 so one can see that the solution is not sensitive to a priori information. For example, at degree 2, the square root of degree variances of two solutions using different a priori degree variances (22.20 cm vs 44.29 cm) are almost the same (51.74 and 52.86 cm). The same phenomenon happened for degree 3 and 4. In our later analysis we will use the degree variances computed from the average solution as a priori information since they should be representative of the current properties of sea surfacedynamic topography.

After the calculations for Table 5.1 were completed it was found that a small error had been made in referencing the dynamic topography to the correct tide system. To correct this error, a correction of 5.9 $(1.5 \sin^2\phi - 0.5)$ cm should have been added to the initial value of ζ. The dominant effect of this error would be to increase the c_{20} spherical harmonic coefficient by approximately 2 cm with much smaller changes for the other coefficients. There would also be an impact on the values given in Table 5.1 under column average. The primary effect would be in the degree 2 term where the corrected value would be approximately 42 cm. Since these values were

used only for apriori weighting it was decided not to redo the tests as the final results were fairly insensitive to the apriori values.

5.2 Correlation Between Bias in SSDT and Low Degree Coefficients On Cycle 17

Because of the bias of the altimeter (Christensen et al., 1994) and the uncertainty of the equatorial radius of the best reference ellipsoid adopted for the Topex project, there is a bias in the estimated sea surface dynamic topography estimates. As we will see in the following, this bias is strongly correlated with the coefficients of the low degree spherical harmonic coefficients of SSDT. As a test, we used the altimeter data of cycle 17. Two constants, 44 cm and 60.1 cm, were removed from the sea surface dynamic topography at the normal points. Table 5.2 lists the low degree ($n \leq 2$) coefficients of the spherical harmonic expansions. As a comparison, we also list the low degree ($n \leq 2$) coefficients from several different solutions previously published. The OSU solutions are based on a spherical harmonic expansion to degree 24 with the improved weighting procedure described in Section 2.2. The a priori degree variances were based on the 10 cycle average given in Table 5.1. For solution OSU1, OSU3, and OSU4, the a priori degree variance at degree zero was set to $(0.001\text{m})^2$. For solution OSU2, the a priori values was $(0.3\text{m})^2$ which allowed the zero degree term more flexibility to change. The modified OSU editing if ($|\zeta| > 1$ m, in specified areas, data deleted) was used for OSU1, 2, 3 while the JPL edit was used for OSU4.

Table 5.2
Effect of Mean Removal on Low Degree Coefficients of Spherical Harmonic Expansions of Sea Surface Dynamic Topography Based on Cycle 17 Data and Comparison with Previous Estimates. Units are cm.

Sol.	Mean Removed	c_{00}	c_{10}	c_{11}	s_{11}	c_{20}	c_{21}	s_{21}	c_{22}	s_{22}
OSU91 (10)†			13.0	-15.5	-9.8	-49.3	-6.3	3.7	1.1	3.2
OSU91 (15)†			13.0	-15.4	-9.1	-51.7	-5.9	2.1	1.6	3.0
Levitus*		-4.1	13.0	-17.7	3.6	-28.0	-4.5	1.0	2.6	0.9
Nerem et al. (1994a)			14.5	-18.7	3.3	-41.6	-7.7	4.7	0.1	2.9
OSU1	44	0.0	12.5	-17.4	3.9	-53.8	-5.1	1.8	-0.6	0.7
OSU2	44	-6.5	4.6	-18.3	1.1	-61.7	-5.7	-2.8	0.9	-0.2
OSU3	60.1+	0.0	31.9	-15.4	10.9	-34.1	-3.5	13.3	-4.5	2.8
OSU4	44	0.0	13.0	-16.1	6.1	-54.3	-4.1	5.3	-1.4	2.2

*from Engelis, 1987, ocean solution to degree 10 (Table 1)
†from Rapp, Wang and Pavlis (1991)
+based on weighting using eq. (2-22)

Table 5.2 reveals the following information:

1. The solutions OSU1 and OSU3 are the same, in terms of data used, except that different biases (44 cm and 60.1 cm) were removed from the data. This 16 cm bias difference caused c_{10} to change from 12. 5 cm to 31.9 cm. However c_{00} remains the same. Since forcing the degree zero term to zero may be inappropriate when high correlations exist between the estimated coefficients, we relaxed the 0.001 meter a priori value to 0.3 meter for solution OSU2. The major changes again happened in the coefficients c_{10} and c_{20} while c_{00} changed from 0.0 cm to -6.5 cm. But the question remains as to the meaning of the c_{00} term.

2. Comparing OSU4 (JPL edit) with OSU1 (OSU edit) there is no significant difference between the coefficients. The coefficients of low degree are insensitive to the editing criteria.

3. In comparing the coefficients from different models, we see the coefficients change significantly from model to model. Because the degree 0 coefficient is strongly correlated with other low degree coefficients, the estimate of such coefficients is significantly impacted by the bias removed from the data.

It is interesting to transform the spherical harmonic coefficients into orthonormal functions and then compare them. Table 5.3 gives the coefficients of the orthonormal expansion.

Table 5.3
Effect of Mean Removal on Low Degree Coefficients of Orthonormal Expansion, Transformed from the Spherical Harmonic Coefficients, of Sea Surface Dynamic Topography Based on Cycle 17 Data, and Comparison with Previous Estimates. Units are in cm.

Sol.	Mean Removed	c_{00}	c_{10}	c_{11}	s_{11}	c_{20}	c_{21}	s_{21}	c_{22}	s_{22}
Levitus**		1.0	18.3	-17.9	4.9	-30.3	-1.6	2.8	-0.2	2.7
OSU91 (10)		12.7	24.5	-17.8	-8.1	-44.5	-3.7	3.4	-0.3	3.8
OSU91 (15)		13.3	24.5	-17.4	-7.2	-44.5	-3.4	2.8	-1.7	4.1
Diff.		-0.6	0.0	-0.4	-0.9	0.0	-0.3	0.6	1.4	-0.3
OSU1	44	11.3	20.3	-19.0	5.9	-46.3	-2.5	2.6	-1.4	3.6
OSU3	60.1+	-4.3	21.0	-18.9	5.9	-45.3	-2.4	2.5	-1.6	3.6
Diff. (OSU1 - OSU3		15.6	-0.7	-0.1	0.0	-1.0	-0.1	0.1	0.2	0.0
OSU4	44	11.1	19.7	-19.2	6.0	-47.3	-2.3	1.9	-1.2	3.5

**computed using data set: $ts5788.sst.harmin.to24.nobeta
(global solution, program used is $ts0548.lib.hwang1#f419sst.)

Table 5.2 shows that the on coefficients of lower degree are significantly decorrelated from the bias terms. The c_{00} of the orthonormal function expansion can be well determined. This is very important for the estimation of the equatorial radius of the reference ellipsoid. The difference between the biases removed in solutions OSU1 and OSU3 is 16.1 cm, and this difference is almost the difference between c_{00} of two solutions in orthonormal function systems. Even so we see up to 20 cm differences between the spherical harmonic coefficients of solution OSU1 and OSU3 although the differences are now below 1 cm level in orthonormal functions (excluding c_{00} term). Therefore, the coefficients of the sea surface dynamic topography expansion should be compared in the orthonormal function system, instead of through the spherical harmonic coefficients which may not have a unique meaning for individual coefficients. However, as we showed earlier, the spherical harmonic expansion can represent the SSDT as well as the orthonormal function, but if we do the spectral analysis the orthonormal function has to be used.

5.3 The Equatorial Radius and the Zero Degree Term of Sea Surface Dynamic Topography

In this section we will discuss the relationship between the c_{00} (orthonormal) or global mean sea surface dynamic topography and the equatorial radius of the best fitting ellipsoid. The orthonormal functions are orthonormal over the ocean. The c_{00} equals the average value of the sea surface dynamic topography over the ocean. It is plausible to define the "ideal" ellipsoid so that the average value of SSDT is zero (Engelis (1985)). In the altimeter analysis the SSDT is computed by:

$$\zeta = SSH(t, \phi, \lambda) - N(\phi, \lambda)$$

The oceanwide average of ζ is then

$$\bar{\bar{\zeta}} = \overline{\overline{SSH}} - \bar{N} \tag{5-1}$$

with

$$\overline{\overline{SSH}} = \frac{1}{|\sigma_0| T} \int_0^T \iint_{\sigma_0} SSH(t,\phi,\lambda)\, dt\, d\sigma$$

$$\bar{N} = \frac{1}{|\sigma_0|} \iint_{\sigma_0} N(\phi,\lambda)\, d\sigma \tag{5-2}$$

where σ_0 in the ocean and $|\sigma_0|$ is the area of the ocean, T is an appropriate averaging time. If the equatorial radius of the reference ellipsoid increases Δ meter, the SSH(t, ϕ, λ) decreases Δ meter under the spherical approximation. The change of the geoid undulation computed from the potential coefficient model, due to the change of the equatorial radius of the reference ellipsoid, is under mm level and can be ignored. Therefore, the SSDT also decreases Δ meter. By changing the equatorial radius of the reference ellipsoid the average value of SSDT can be forced to zero. In other words, by analyzing the SSDT computed from the altimeter data, we can find a equatorial radius of the ellipsoid which makes the average value of the SSDT zero. This equatorial radius will be considered as the "ideal" equatorial radius of the reference ellipsoid for this discussion.

Based on previous analysis, we know there is a bias in the sea surface dynamic topography estimated with the Topex altimeter data and the parameters of the Topex reference ellipsoid. This bias can be uniquely determined by using the orthonormal function expansion. In order to estimate the bias, we analyzed one year of TOPEX altimeter data (cycle 17 to 53). The SSDT was averaged at the normal points and then expanded into spherical harmonics from degree zero to 24. The sinβ weighting (eq. (2-30)) was used with constant 10 cm for m_i. As a test, we also removed two different biases from the dynamic topography before the spherical harmonic expansions and the solutions were designated by A and B. Table 5.4 gives the coefficients of the solutions in spherical harmonics and orthonormal functions.

Table 5.4
Low Degree Spherical Harmonic and Orthonormal Coefficients of One Year Mean Dynamic Topography Based on Topex Cycles 17 to 53. Units are in cm.

Spherical Harmonic Coefficients										
Sol.	Mean removed	c_{00}	c_{10}	c_{11}	s_{11}	c_{20}	c_{21}	s_{21}	c_{22}	s_{22}
A	44	0.0	17.4	-18.8	5.1	-48.4	-7.3	4.9	-0.6	0.1
B	55	-0.1	29.9	-17.3	10.5	-36.9	-5.9	13.5	-4.0	2.1
Orthonormal Coefficients Transformed from Spherical Harmonics										
Sol.	Mean removed	c_{00}	c_{10}	c_{11}	s_{11}	c_{20}	c_{21}	s_{21}	c_{22}	s_{22}
A	44	10.4	22.1	-19.4	5.6	-43.0	-2.7	3.1	-1.1	3.3
B	55	-0.1	22.4	-19.5	5.8	-42.7	-2.6	3.2	-1.3	3.1

Table 5.4 implies that the zero degree term of the orthonormal expansion, is effectively zero when the 55 cm bias value is removed from the Topex data. This value is based on the analysis of one year (cycle 17 to 53) of Topex data. Christensen et al. (1994) have reported a Topex altimeter bias of -14.5 cm so that the ideal equatorial radius, for this type of study, would be 6378136.30m (the Topex ellipsoid "a") + 0.55m - 0.14m which equals 6378136.71m. This radius is 11 cm larger than implied by other analysis described in Rapp, Yi, and Wang (1994). The difference may be related to the different definitions used in defining the equatorial radius. For solutions to be described in the next section, the 55 cm bias has been removed.

5.4 MEAN SEA SURFACE DYNAMIC TOPOGRAPHY AND ITS SPECTRAL ANALYSIS

Based on the experiences described in the previous sections it was decided to estimate sea surface dynamic topography (SSDT) for each Topex cycle from 4 to 58. The normal points were corrected for the residual tide corrections based on the N34 solution described in Section 3.3. In addition, the 55 cm mean bias described in the previous section was subtracted from the SSDT value. Values were deleted if the magnitude exceeded 1m in the selected geographic regions noted earlier. This data was then used to estimate the spherical harmonic coefficients from degree 0 to 24 using the a priori degree variances based on 10 cycles of Topex data as described in Section 5.1 and Table 5.1. A total of 51 harmonic coefficient sets were determined. These sets represent a time series of variations in the ocean surface. A mean set of SH coefficients were determined by averaging the individual sets. These coefficients are given in Table 5.5. The $c_{2,0}$ value is now -37.8 cm in contrast to -36.9 cm given in Table 5.4 using data from cycles 17 to 53, a one year (approximately) time period. For referencing purposes the data set containing the one year dynamic topography coefficients is TS0548.SST.COEF.AVER.FCYC17.T053.B55. This set was created through the use of program TS0548.LIB.SSTEXPAN(SSTADJ). The data set with the average of 51 solutions is TS0548.SST.COEF.AVER.FCYC4.T058.SHONSTD.

Each SH solution was transformed into a ON solution. These 51 solutions were then averaged to determine a mean ON coefficient set for SSDT. These ON coefficients are also listed in Table 5.5. Equivalent values could have been obtained by transforming the mean SH coefficients. The standard deviation of each ON coefficient, about the mean value, was computed and is given in Table 5.5. The c_{00} coefficient, in the ON system, is 0.2 mm indicating a mean of 55.02 cm should have been removed from the data instead of 55.00 cm. However, this value is likely to change as additional cycles are studied. The c_{20} coefficient of the ON expansion is -42.52 cm, quite close to the value given in Table 5.4.

We next compare the low degree coefficients from several solutions of this paper, and elsewhere, in both the SH and ON representation. The presentation is in Table 5.6 for the SH coefficients and in Table 5.7 for the ON coefficients.

Table 5.6
Low Degree Spherical Harmonic Coefficients of Mean Sea Surface Dynamic Topography. Units are cm.

	Solution				
Coefficient	One† Year	Topex* 4-58	Levitus††	Nerem et al.	Visser et al.
c_{10}	29.9	27.5	13.0	14.5	0.2
c_{11}	-17.3	-16.1	-17.7	-18.7	-8.1
s_{11}	10.5	10.3	3.6	3.3	-0.9
c_{20}	-36.9	-37.8	-28.0	-41.6	-45.4
c_{21}	-5.9	-5.0	-4.5	-7.7	-2.9
s_{21}	13.5	13.7	1.0	4.7	8.7
c_{22}	-4.0	-4.0	2.6	0.1	1.3
s_{22}	2.1	2.0	0.9	2.9	2.0

†Table 5.4; *Table 5.5; ††Table 5.2

The SH coefficients from the one year data solution and the averaging of the 51 SH coefficient sets give very similar results. When these are compared to the values implied by the Levitus data, computed by Engelis, significant differences are noted for the c_{10} and c_{20} coefficients. The values of Nerem et al. (1994) are reasonably close to the solutions of this paper except for the c10

coefficient where the Nerem value agrees with the Levitus implied value. Note the good consistency of the c_{21} coefficient between the Nerem estimate and that of this paper. The Visser et al. (1993) estimates shows a similarity to the other solutions except for the c_{10} term which is considerably smaller than the other estimates. As noted by Denker and Rapp (1990), the c_{10} coefficient is difficult to determine if the altimeter orbits are not precisely known.

Table 5.7
Low Degree Orthonormal Coefficients of Mean Sea Surface Dynamic Topography. Units are cm.

	Solution			
Coefficient	One† Year	Topex* 4-58	Levitus††	Visser et al.
c_{10}	22.4	22.1	18.3	4.1
c_{11}	-19.5	-19.1	-17.9	-10.3
s_{11}	5.8	5.6	4.9	-1.4
c_{20}	-42.7	-42.5	-30.3	-44.9
c_{21}	-2.6	-2.6	-1.6	-2.9
s_{21}	3.2	3.0	2.8	5.6
c_{22}	-1.3	-1.6	-0.2	3.0
s_{22}	3.1	2.9	2.7	2.8

†Table 5.4; *Table 5.5; ††Table 5.2

As with the SH coefficients, the coefficients of the one year SSDT and the average from cycles 4 to 58 agree quite well. We now see, however, a much better agreement between the c10 term of Levitus and of the solution generated here. In the ON representation, the difference for c10 is approximately 4 cm while the difference is about 15 cm when the SH coefficients are compared. The only coefficient for which improved comparisons with Levitus are not obtained is the c20 term. Since we have shown the SH solution (at the lower degrees) is sensitive to the mean removed, it again becomes clear that coefficient comparisons could be better done in ON coefficients.

The magnitude of SSDT was calculated from the ON coefficients to various degrees of the expansion with results given in Table 5.8.

Table 5.8
Magnitude of Sea Surface Topography From ON Coefficients to Degree N.
Units are in cm.

N	Value
10	60.39
13	60.70
15	60.88
20	61.03
24	61.09

The values clearly show the dominant power is at the longer wavelengths.

The spectral characteristics of the coefficient variations was calculated by averaging, over all cycles used, the coefficient standard deviations. Specifically, the degree variance of the temporal variation of SSDT was computed from:

$$\Delta\sigma_n^2 = \frac{1}{n}\sum_{i=1}^{m}\sum_{m=0}^{m}\left[\left(\delta c_{mm}^i\right)^2 + \left(\delta s_{mm}^i\right)^2\right] \qquad (5\text{-}3)$$

where m is the number (51) of cycles averaged and δc^i_{mm} *and* δs^i_{mm} are the residual ON coefficients (i.e. the difference between the coefficients of Topex cycle i and the mean ON coefficient set). Values of $\Delta\sigma_n$ are plotted in Figure 5.1 The value decreases slowly from ±1.6 cm at degree 1 to ±0.4 cm at degree 24. The cumulative variability (i.e. summed from degree 0 to 24) is ±5.2 cm. This value is smaller than other estimates of ocean variability (e.g. ±13 cm, Wang and Rapp (1992)), probably due to the low degree of the series representation used here.

The square root of the degree variances of the mean SSDT (from the ON representation) and its variability are given in Table 5.9 and plotted in Figure 5.1 We feel that this spectrum is more representative of the real spectrum of SSDT than would be found using a regular spherical harmonic expansion with corresponding degree variances. We note that the variability magnitudes are an increasing percentage of the magnitude of the total topography.

Table 5.5
Spherical Harmonic (SH) and Orthonormal (ON) Coefficients of Mean Sea Surface Dynamic Topography and Coefficient Variations. Values are Based on Averaging 51 Sets of SH Coefficients from Topex Cycles 4 to 58. Units are in cm

		SH		ON		ON	
L	M	C	S	C	S	DC	DS
0	0	-0.05	0.00	0.48	0.00	0.51	0.00
1	0	27.50	0.00	22.06	0.00	1.29	0.00
1	1	-16.11	10.28	-19.08	5.63	0.66	0.64
2	0	-37.75	0.00	-42.52	0.00	1.06	0.00
2	1	-4.99	13.70	-2.59	2.95	0.40	0.43
2	2	-4.02	1.97	-1.55	2.94	0.55	0.54
3	0	26.38	0.00	15.67	0.00	1.17	0.00
3	1	-2.80	7.34	-2.85	-4.25	0.43	0.52
3	2	-3.67	-2.05	2.32	-5.55	0.30	0.28
3	3	-3.35	-2.07	-5.38	0.17	0.25	0.45
4	0	-6.63	0.00	-16.10	0.00	0.65	0.00
4	1	0.26	9.33	5.68	1.99	0.52	0.59
4	2	-9.45	-0.09	-2.96	0.40	0.36	0.45
4	3	3.48	-6.10	1.49	-2.48	0.24	0.26
4	4	-0.96	-0.61	-1.81	-2.24	0.32	0.33
5	0	6.44	0.00	3.94	0.00	0.88	0.00
5	1	-1.41	3.24	-2.34	-1.61	0.66	0.57
5	2	-5.65	3.96	2.69	5.05	0.37	0.39
5	3	2.26	-5.90	0.83	1.40	0.27	0.32
5	4	2.70	1.40	-0.36	0.12	0.21	0.29
5	5	-1.31	2.26	-0.42	0.22	0.31	0.29
6	0	9.20	0.00	4.84	0.00	0.45	0.00
6	1	-4.06	1.19	-3.56	2.26	0.59	0.45
6	2	-5.43	5.42	-0.05	3.51	0.40	0.35
6	3	0.21	-8.85	0.42	-2.43	0.39	0.43
6	4	1.00	-0.20	-1.88	0.60	0.25	0.32
6	5	0.19	3.37	1.51	-0.16	0.23	0.23
6	6	-1.57	-0.06	-1.02	-0.73	0.29	0.25
7	0	-6.52	0.00	-0.68	0.00	0.48	0.00
7	1	2.00	-0.36	4.04	3.51	0.48	0.57
7	2	-0.01	1.97	1.25	0.21	0.29	0.35
7	3	-0.29	-2.16	0.13	0.01	0.25	0.62
7	4	1.91	-1.65	0.44	0.00	0.39	0.25
7	5	0.78	2.19	0.58	0.01	0.17	0.21
7	6	0.37	0.61	1.66	1.14	0.16	0.12
7	7	0.21	-1.72	0.41	-0.91	0.16	0.22
8	0	1.56	0.00	1.29	0.00	0.39	0.00

Table 5.5 cont.

8	1	-8.52	-6.86	-6.99	-3.36	0.40	0.42
8	2	-1.71	-1.62	-0.42	-0.06	0.37	0.32
8	3	3.18	0.82	2.53	-0.15	0.22	0.40
8	4	2.96	-0.82	2.75	-0.86	0.32	0.36
8	5	-1.07	2.57	-0.26	1.13	0.19	0.25
8	6	0.62	-0.26	-0.34	0.02	0.17	0.22
8	7	0.61	-0.25	-0.36	0.19	0.18	0.19
8	8	0.47	-0.22	-0.51	0.17	0.17	0.27
9	0	-1.64	0.00	-0.11	0.00	0.37	0.00
9	1	1.25	-0.26	1.30	0.78	0.49	0.36
9	2	-1.98	-2.03	-1.55	-0.99	0.31	0.24
9	3	0.60	2.77	0.38	1.44	0.39	0.33
9	4	-1.12	-0.53	-0.55	0.50	0.21	0.28
9	5	-0.91	1.12	0.38	0.94	0.13	0.28
9	6	0.62	0.91	0.34	0.49	0.20	0.22
9	7	0.62	-2.25	-0.61	-1.47	0.16	0.16
9	8	0.08	0.96	-0.11	0.60	0.20	0.18
9	9	1.07	-0.07	0.19	-0.25	0.22	0.20
10	0	1.10	0.00	1.37	0.00	0.30	0.00
10	1	-0.08	0.10	-2.08	-1.95	0.31	0.26
10	2	-0.27	0.22	-0.59	0.92	0.21	0.24
10	3	-0.75	-0.75	-1.13	-1.07	0.23	0.29
10	4	-0.20	-0.08	0.84	-0.04	0.32	0.17
10	5	-0.62	-1.92	-0.02	-0.52	0.17	0.22
10	6	-0.38	0.32	-0.91	0.41	0.27	0.20
10	7	0.49	-0.60	-0.21	-0.13	0.18	0.14
10	8	-0.66	0.04	-1.07	-0.05	0.19	0.15
10	9	0.01	0.81	-0.68	0.85	0.15	0.17
10	10	0.59	-0.15	-0.05	0.24	0.14	0.18
11	0	-0.61	0.00	-0.55	0.00	0.37	0.00
11	1	0.01	0.46	-0.88	0.77	0.27	0.28
11	2	1.11	-0.51	1.96	-1.36	0.19	0.17
11	3	0.16	0.20	-1.13	0.99	0.24	0.38
11	4	0.95	1.36	1.18	1.43	0.16	0.21
11	5	-0.15	-1.79	-0.65	-0.23	0.20	0.17
11	6	0.13	0.57	-0.93	0.34	0.15	0.15
11	7	0.23	-0.59	-0.58	-1.16	0.20	0.13
11	8	-0.17	0.51	-0.21	0.11	0.16	0.18
11	9	0.30	1.21	0.18	0.40	0.24	0.14
11	10	0.29	0.37	-0.42	-0.48	0.24	0.17
11	11	0.18	-0.36	0.32	-0.06	0.16	0.18
12	0	-0.90	0.00	0.44	0.00	0.22	0.00
12	1	2.89	-0.20	1.61	0.90	0.25	0.17
12	2	0.08	0.32	0.79	-0.41	0.22	0.23
12	3	0.62	0.63	0.47	1.47	0.20	0.24
12	4	1.11	-0.55	1.30	-1.11	0.32	0.32
12	5	0.16	-0.34	0.23	0.96	0.19	0.28
12	6	1.48	0.55	0.70	0.13	0.15	0.24
12	7	-0.29	-0.35	-0.48	0.16	0.19	0.18
12	8	-0.33	-0.13	-0.12	-0.15	0.22	0.12
12	9	0.06	0.63	0.03	0.79	0.17	0.21

Table 5.5 cont.

12	10	1.34	1.37	0.57	0.11	0.13	0.19
12	11	-0.68	0.87	-0.55	0.74	0.14	0.16
12	12	0.01	0.39	0.53	-0.01	0.14	0.17
13	0	1.19	0.00	0.39	0.00	0.26	0.00
13	1	-1.20	-2.88	-0.57	-0.91	0.21	0.28
13	2	-1.44	0.95	0.51	-0.10	0.20	0.15
13	3	0.05	-1.29	0.40	-0.74	0.22	0.15
13	4	-1.12	1.05	0.14	0.46	0.19	0.33
13	5	-0.46	-0.46	-1.06	-0.34	0.17	0.16
13	6	0.31	0.79	-0.17	0.30	0.16	0.13
13	7	-0.21	-1.05	0.37	-0.90	0.15	0.13
13	8	0.02	-0.18	0.77	0.01	0.13	0.12
13	9	-0.13	0.10	0.34	0.32	0.14	0.22
13	10	0.77	0.25	-0.19	0.03	0.14	0.13
13	11	0.77	0.32	0.06	-0.17	0.16	0.15
13	12	-0.47	0.07	-1.02	0.24	0.17	0.14
13	13	0.01	0.52	0.12	-0.52	0.15	0.15
14	0	0.05	0.00	0.04	0.00	0.16	0.00
14	1	0.03	1.55	-0.41	1.31	0.20	0.17
14	2	0.17	-1.10	1.17	-0.46	0.19	0.14
14	3	-2.33	-0.62	-2.26	-0.44	0.19	0.17
14	4	-1.04	0.00	-0.25	-0.51	0.25	0.17
14	5	0.75	0.10	1.53	-0.15	0.21	0.18
14	6	1.02	0.14	0.23	-0.25	0.16	0.16
14	7	-0.78	0.42	0.43	0.32	0.16	0.11
14	8	-0.11	0.05	-0.38	0.29	0.12	0.12
14	9	-1.17	0.18	-0.77	0.16	0.18	0.25
14	10	0.27	1.05	-0.31	0.16	0.12	0.15
14	11	-0.28	-0.19	0.19	-0.46	0.16	0.10
14	12	0.49	0.09	-0.08	0.35	0.17	0.16
14	13	0.41	0.24	0.21	0.16	0.15	0.19
14	14	-0.22	0.38	-0.43	0.17	0.15	0.12
15	0	-0.02	0.00	0.40	0.00	0.21	0.00
15	1	0.85	0.38	0.27	-0.77	0.18	0.16
15	2	-0.19	0.78	-0.17	0.22	0.17	0.14
15	3	0.64	0.27	0.14	0.54	0.15	0.18
15	4	-0.15	-0.68	0.37	-0.87	0.19	0.17
15	5	-2.73	0.25	-1.67	0.12	0.14	0.19
15	6	-0.21	1.09	-0.03	0.52	0.13	0.14
15	7	-1.64	-1.18	-0.55	0.37	0.16	0.12
15	8	0.88	0.10	-0.22	0.34	0.14	0.12
15	9	-0.48	0.33	-0.50	0.79	0.12	0.12
15	10	0.89	0.95	0.43	0.01	0.13	0.11
15	11	-0.37	-0.09	-0.07	-0.69	0.12	0.10
15	12	-0.69	0.05	-0.45	0.65	0.12	0.13
15	13	0.25	-0.07	0.05	-0.26	0.14	0.13
15	14	-0.22	-0.05	-0.10	-0.01	0.16	0.11
15	15	0.26	-0.40	0.03	0.22	0.12	0.13
16	0	-0.13	0.00	0.15	0.00	0.15	0.00
16	1	-0.19	-0.21	-0.50	-0.12	0.24	0.15
16	2	0.45	0.29	0.53	0.82	0.18	0.18

Table 5.5 cont.

16	3	0.53	-0.08	0.05	-0.02	0.12	0.11
16	4	-0.15	-0.42	0.21	0.08	0.11	0.15
16	5	0.12	-0.56	-0.23	0.49	0.18	0.20
16	6	0.23	0.47	-0.66	0.47	0.14	0.21
16	7	-0.17	-0.92	-0.23	0.18	0.11	0.09
16	8	0.49	0.12	-0.32	0.04	0.09	0.11
16	9	-0.01	-0.30	0.04	-0.61	0.14	0.13
16	10	-0.16	-0.05	0.02	0.12	0.15	0.16
16	11	-0.19	0.54	-0.16	0.05	0.12	0.11
16	12	-0.10	-0.05	-0.27	0.58	0.10	0.12
16	13	0.22	0.37	-0.73	0.25	0.17	0.15
16	14	-0.68	0.27	-0.35	0.15	0.13	0.17
16	15	-0.08	-0.67	-0.34	-0.78	0.10	0.14
16	16	-0.20	-0.27	0.09	-0.18	0.15	0.11
17	0	-0.17	0.00	-0.13	0.00	0.22	0.00
17	1	-0.41	0.69	0.03	0.00	0.18	0.17
17	2	0.43	-0.63	0.34	0.08	0.12	0.12
17	3	0.18	-0.40	-0.50	0.26	0.22	0.13
17	4	-0.01	-0.67	0.38	-0.26	0.15	0.11
17	5	0.55	-0.76	0.11	0.35	0.17	0.15
17	6	1.19	-0.29	0.10	-0.43	0.08	0.15
17	7	0.31	-0.38	0.58	0.09	0.12	0.14
17	8	0.50	0.56	-0.48	0.43	0.12	0.12
17	9	0.15	0.80	0.37	0.66	0.10	0.12
17	10	-0.29	-0.92	-0.25	-0.33	0.13	0.14
17	11	0.37	0.61	0.51	-0.24	0.14	0.10
17	12	-0.40	-0.77	-0.46	-0.69	0.15	0.12
17	13	0.05	0.08	-0.19	0.14	0.11	0.11
17	14	0.36	0.13	0.12	-0.36	0.13	0.12
17	15	-0.15	-0.03	-0.52	0.07	0.11	0.14
17	16	0.70	-0.03	0.38	-0.45	0.14	0.16
17	17	-0.56	0.01	-0.35	-0.30	0.10	0.14
18	0	-0.47	0.00	-0.38	0.00	0.14	0.00
18	1	-0.19	-0.22	-0.01	-0.45	0.18	0.12
18	2	-0.58	-0.50	-0.36	-0.35	0.16	0.21
18	3	0.47	0.27	0.11	0.02	0.09	0.10
18	4	0.22	0.36	0.09	0.52	0.17	0.19
18	5	-0.12	-0.22	-0.26	-0.26	0.17	0.13
18	6	-0.34	0.33	0.28	0.43	0.17	0.11
18	7	-0.38	-0.26	0.48	-0.43	0.15	0.08
18	8	0.14	0.16	0.07	0.20	0.12	0.10
18	9	-0.39	-0.88	-0.36	-0.51	0.10	0.09
18	10	0.15	-0.36	-0.25	0.16	0.12	0.10
18	11	0.60	-0.21	-0.19	-0.37	0.08	0.09
18	12	-0.04	0.27	0.10	-0.40	0.11	0.13
18	13	-0.05	0.11	0.30	-0.36	0.11	0.13
18	14	-0.17	0.38	0.13	0.22	0.11	0.14
18	15	0.64	-0.23	0.20	0.02	0.11	0.13
18	16	0.23	0.60	0.04	0.19	0.18	0.10
18	17	-0.31	0.78	-0.12	0.49	0.12	0.12
18	18	0.14	0.25	-0.13	-0.05	0.12	0.11

Table 5.5 cont

19	0	0.34	0.00	0.45	0.00	0.23	0.00
19	1	-0.51	0.02	-0.27	-0.14	0.11	0.18
19	2	-0.12	0.15	-0.08	0.05	0.12	0.11
19	3	-0.36	0.41	0.06	0.44	0.18	0.12
19	4	0.29	-0.08	0.18	-0.20	0.11	0.08
19	5	-0.09	0.38	-0.60	0.53	0.13	0.17
19	6	-0.37	-0.12	0.33	-0.44	0.09	0.14
19	7	-1.00	-0.47	-0.60	-0.28	0.12	0.12
19	8	-0.48	0.40	-0.17	-0.38	0.11	0.09
19	9	-0.16	-0.03	0.04	-0.34	0.10	0.13
19	10	0.40	0.00	0.08	0.52	0.12	0.12
19	11	0.50	-0.24	0.15	-0.31	0.10	0.10
19	12	0.45	0.57	-0.05	0.31	0.10	0.12
19	13	-0.29	-0.24	-0.31	-0.19	0.10	0.09
19	14	-0.48	0.66	-0.14	0.15	0.11	0.12
19	15	0.41	0.26	0.10	-0.05	0.10	0.09
19	16	0.45	0.27	-0.14	-0.04	0.10	0.09
19	17	-0.25	0.35	-0.05	0.56	0.10	0.14
19	18	-0.65	-0.26	-0.40	-0.24	0.12	0.12
19	19	0.10	0.25	0.08	0.15	0.10	0.11
20	0	0.36	0.00	0.08	0.00	0.10	0.00
20	1	0.10	-0.14	0.04	-0.46	0.12	0.08
20	2	-0.18	0.21	0.16	0.09	0.13	0.14
20	3	-0.34	0.13	0.14	-0.11	0.11	0.09
20	4	-0.40	0.27	-0.70	-0.15	0.13	0.10
20	5	0.81	0.38	-0.18	-0.43	0.10	0.11
20	6	-0.44	-0.39	-0.10	-0.24	0.12	0.09
20	7	0.27	-0.17	0.17	0.13	0.09	0.08
20	8	-0.01	0.91	0.11	0.34	0.10	0.11
20	9	-0.43	-0.01	-0.02	-0.06	0.11	0.09
20	10	-0.09	0.30	-0.27	-0.36	0.09	0.15
20	11	-0.72	0.60	-0.57	0.13	0.11	0.09
20	12	0.09	0.01	-0.15	0.10	0.11	0.09
20	13	0.08	-0.27	0.03	-0.12	0.11	0.09
20	14	-0.45	0.55	0.13	0.43	0.10	0.09
20	15	0.10	-0.13	-0.11	-0.35	0.09	0.13
20	16	-0.24	0.50	-0.11	-0.02	0.11	0.13
20	17	0.05	0.28	0.31	-0.12	0.10	0.15
20	18	0.23	-0.27	0.15	0.04	0.13	0.12
20	19	0.19	0.15	0.26	0.09	0.11	0.12
20	20	-0.19	-0.18	0.12	-0.19	0.13	0.09
21	0	-0.09	0.00	-0.31	0.00	0.13	0.00
21	1	0.62	-0.02	-0.03	0.08	0.13	0.13
21	2	0.02	-0.34	-0.39	0.39	0.08	0.09
21	3	-0.37	-0.72	-0.18	-0.36	0.13	0.10
21	4	-0.28	0.33	-0.01	0.27	0.12	0.10
21	5	0.62	0.63	0.63	0.35	0.13	0.16
21	6	-0.05	0.04	-0.07	0.60	0.10	0.11
21	7	0.14	-0.41	0.15	0.42	0.09	0.12
21	8	0.09	-0.61	-0.24	-0.71	0.07	0.07
21	9	-0.47	-0.38	0.30	0.43	0.07	0.10

Table 5.5 cont.

21	10	0.20	0.31	-0.04	0.19	0.09	0.08
21	11	0.11	0.46	0.07	0.37	0.10	0.09
21	12	-0.01	-0.34	0.31	-0.12	0.10	0.08
21	13	0.17	0.06	-0.38	0.24	0.10	0.08
21	14	0.00	-0.45	0.22	-0.52	0.12	0.10
21	15	-0.45	0.36	-0.21	-0.04	0.08	0.12
21	16	-0.08	-0.25	-0.02	-0.40	0.12	0.10
21	17	-0.58	0.11	-0.05	0.26	0.12	0.09
21	18	-0.05	-0.46	0.07	0.01	0.10	0.08
21	19	0.00	-0.14	-0.22	-0.12	0.09	0.13
21	20	-0.14	0.40	0.17	0.22	0.12	0.10
21	21	-0.37	0.07	0.15	0.05	0.10	0.12
22	0	-0.21	0.00	0.00	0.00	0.09	0.00
22	1	-0.12	0.65	0.14	0.19	0.11	0.07
22	2	0.55	-0.11	0.02	-0.23	0.09	0.14
22	3	-0.56	-0.08	-0.04	-0.03	0.09	0.09
22	4	0.43	-0.23	0.21	0.25	0.11	0.10
22	5	-0.43	-0.35	-0.07	-0.05	0.12	0.09
22	6	-0.14	-0.40	-0.19	-0.06	0.09	0.09
22	7	0.58	-0.53	0.32	0.24	0.08	0.09
22	8	0.40	0.49	-0.21	0.61	0.10	0.07
22	9	-0.01	-0.65	0.19	0.07	0.10	0.08
22	10	-0.13	-0.52	0.16	-0.44	0.10	0.08
22	11	-0.24	-0.22	-0.17	0.04	0.12	0.08
22	12	-0.11	-0.56	-0.12	0.04	0.07	0.08
22	13	0.70	-0.03	0.00	-0.06	0.07	0.09
22	14	-0.37	0.21	-0.21	0.03	0.10	0.08
22	15	0.02	0.83	0.02	0.21	0.08	0.08
22	16	-0.13	0.06	0.03	-0.28	0.09	0.13
22	17	-0.83	-0.03	-0.13	0.20	0.10	0.10
22	18	-0.02	-0.13	-0.07	0.38	0.09	0.09
22	19	0.42	-0.16	-0.03	-0.06	0.11	0.09
22	20	0.07	-0.05	-0.07	-0.13	0.10	0.08
22	21	-0.41	-0.17	-0.35	-0.14	0.11	0.11
22	22	-0.38	-0.05	-0.12	0.08	0.09	0.09
23	0	0.46	0.00	0.03	0.00	0.04	0.00
23	1	0.27	-0.26	0.00	-0.01	0.06	0.05
23	2	0.35	0.14	-0.07	-0.14	0.04	0.05
23	3	0.42	-0.09	0.00	-0.02	0.08	0.06
23	4	-0.14	-0.19	0.04	-0.04	0.08	0.07
23	5	-0.32	-0.39	-0.05	-0.24	0.06	0.07
23	6	0.48	0.15	-0.06	0.28	0.07	0.09
23	7	0.32	-0.27	-0.13	-0.35	0.09	0.11
23	8	0.29	-0.09	0.05	-0.17	0.09	0.09
23	9	0.44	-0.60	0.30	-0.28	0.08	0.08
23	10	-0.47	0.05	-0.42	0.08	0.07	0.09
23	11	0.05	0.21	0.13	-0.01	0.13	0.07
23	12	-0.29	-0.52	0.07	-0.06	0.09	0.09
23	13	0.20	0.01	0.00	0.09	0.08	0.07
23	14	-0.15	-0.10	-0.01	-0.18	0.06	0.07
23	15	-0.03	0.04	0.02	-0.08	0.09	0.06

Table 5.5 cont.

23	16	-0.25	0.22	-0.21	-0.15	0.07	0.10
23	17	-0.36	-0.22	-0.15	-0.21	0.09	0.10
23	18	-0.02	-0.41	0.01	-0.09	0.11	0.08
23	19	0.03	-0.39	-0.12	-0.42	0.08	0.07
23	20	-0.04	0.24	0.12	0.05	0.07	0.10
23	21	0.00	0.07	0.10	0.06	0.09	0.09
23	22	0.30	-0.21	0.35	0.05	0.08	0.08
23	23	-0.11	-0.28	-0.15	-0.15	0.10	0.09
24	0	-0.45	0.00	0.01	0.00	0.02	0.00
24	1	-0.29	-0.13	-0.02	-0.05	0.03	0.03
24	2	-0.08	0.73	-0.01	0.10	0.04	0.04
24	3	0.12	0.35	-0.02	0.10	0.03	0.03
24	4	0.28	-0.11	-0.10	0.08	0.05	0.05
24	5	0.22	0.61	0.12	0.15	0.05	0.05
24	6	0.31	-0.38	0.02	-0.17	0.04	0.06
24	7	0.36	0.43	-0.01	0.18	0.05	0.05
24	8	0.38	0.64	0.20	0.18	0.04	0.08
24	9	-0.03	-0.22	0.08	-0.11	0.04	0.06
24	10	-0.05	-0.08	-0.05	-0.03	0.06	0.07
24	11	0.16	0.13	0.28	-0.01	0.05	0.06
24	12	-0.31	-0.49	-0.11	-0.17	0.05	0.06
24	13	0.05	-0.02	0.01	0.02	0.08	0.06
24	14	-0.17	-0.10	0.09	-0.04	0.05	0.08
24	15	-0.19	-0.21	-0.13	0.11	0.06	0.06
24	16	0.31	0.00	0.14	0.04	0.05	0.07
24	17	0.06	0.09	0.08	0.18	0.06	0.06
24	18	0.27	-0.09	-0.04	0.02	0.07	0.07
24	19	0.47	0.40	0.23	0.30	0.09	0.07
24	20	0.12	-0.05	0.06	-0.12	0.08	0.08
24	21	-0.28	0.21	-0.19	0.07	0.07	0.06
24	22	-0.04	0.21	0.01	0.15	0.06	0.08
24	23	-0.10	-0.17	-0.07	-0.07	0.07	0.07
24	24	0.13	-0.02	0.08	-0.01	0.07	0.06

Table 5.9
Square Root of Degree Variances of Mean Sea Surface Dynamic Topography and Its Variability, by Degree and Cumulatively, from TOPEX Cycles 4 to 58, Using Orthonormal Coefficients. Units are in cm.

	By Degree		Cumulatively	
Degree	SSDT	VAR PART	SSDT	VAR PART
0	0.02	0.51	0.02	0.51
1	29.70	1.58	29.71	1.66
2	42.83	1.44	52.12	2.20
3	18.35	1.50	55.26	2.66
4	17.92	1.31	58.09	2.97
5	7.70	1.52	58.60	3.33
6	8.21	1.34	59.17	3.59
7	6.03	1.36	59.48	3.84
8	8.87	1.23	60.14	4.03
9	3.58	1.20	60.24	4.21
10	4.25	1.01	60.39	4.33
11	4.12	1.03	60.53	4.45
12	3.68	1.04	60.64	4.57
13	2.66	0.94	60.70	4.67
14	3.67	0.90	60.81	4.75
15	2.84	0.81	60.88	4.82
16	2.19	0.84	60.92	4.89
17	2.13	0.82	60.96	4.96
18	1.79	0.80	60.98	5.02
19	1.87	0.76	61.01	5.08
20	1.57	0.70	61.03	5.13
21	1.95	0.69	61.06	5.18
22	1.31	0.64	61.08	5.21
23	1.14	0.56	61.09	5.24
24	0.83	0.42	61.09	5.26

Also plotted in Figure 5.1 are the square root of the geoid undulation error (Nerem et al., 1994b) implied by the JGM-2 potential coefficient model used in our determination of SSDT. These errors were computed to reflect the uncertainty in the ocean areas. The figure shows that the magnitude of geoid undulation error approaches the magnitude of the SSDT signal between degree 13 to 15. This is a suggestion that SSDT estimates may not be reliable beyond these degrees. This issue will be addressed again in the next section.

Figure 5.2 shows the square root of the cumulative degree variances of the mean SSDT, the variability components, and the JGM-2 geoid undulation error. We note again (see Table 5.6) that most of the mean SSDT signal is contained in the lower degrees of the ON expansion.

Finally, we note (Table 5.5) the small (±5.1 mm) variation of the degree zero term of the ON expansion. This variation is associated with mean sea level variations, annual and semi-annual variations, drift of the altimeter bias, and variations that can be associated with environmental and geophysical corrections. To study this further, the degree zero term of the ON expansion is plotted in Figure 5.3 from Topex cycle 4 to 58. A straight line was fitted to these values (from cycles 4 to 58) and the slope found was 4.2 (±1.6) mm/yr which is in close agreement with the value of 4.8 mm/yr given in Table 3.1. The difference may relate to the influence of the annual and semi-annual terms that have not been included in the analysis that led to the zero degree terms plotted in Figure 5.3.

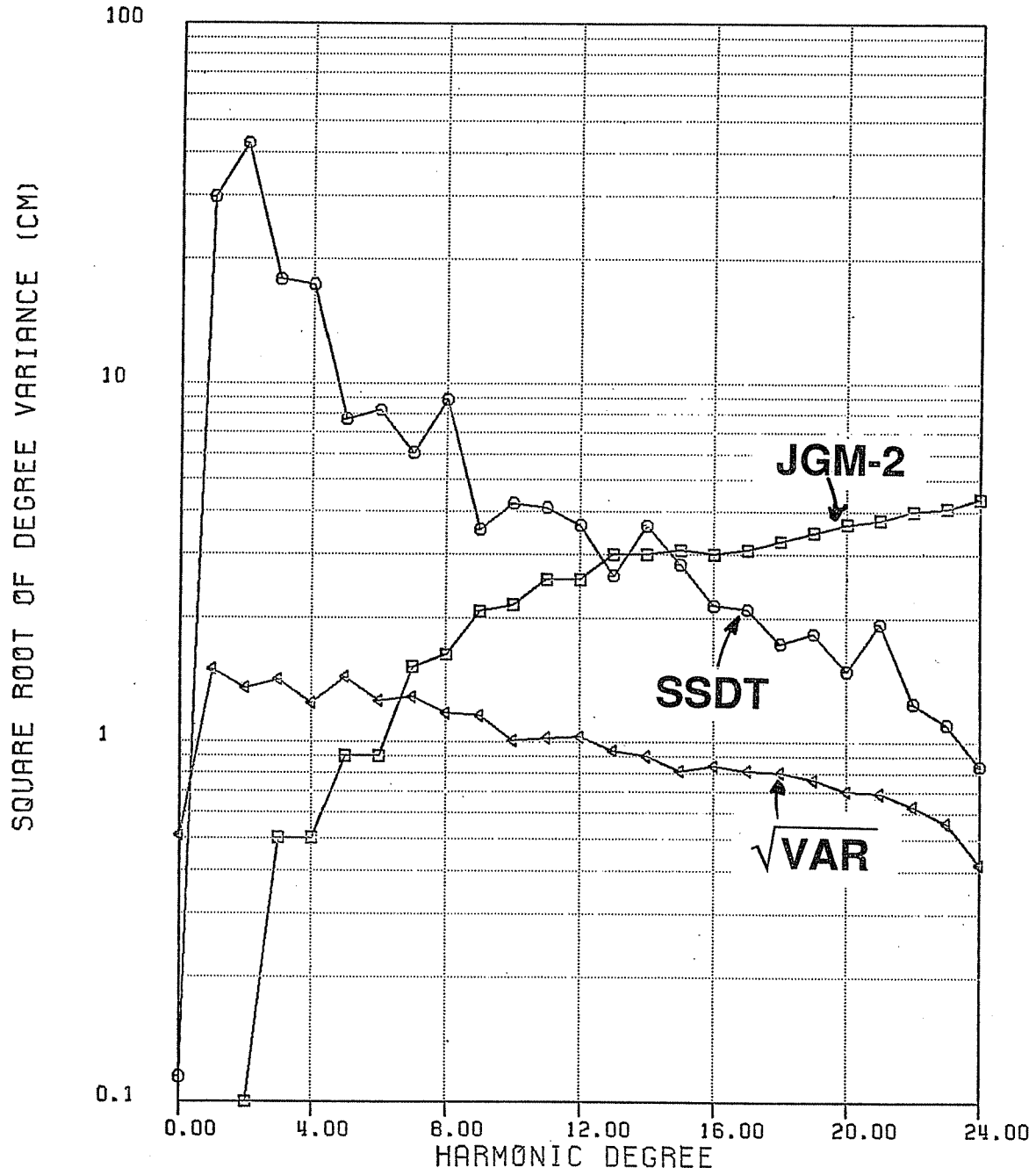

Figure 5.1 Square Root of Degree Variance of the ON Expansion of Mean Sea Surface Dynamic Topography, Its Time Variation, and the Geoid Undulation Accuracy in Ocean Areas Based on the JGM-2 Potential Coefficient Model

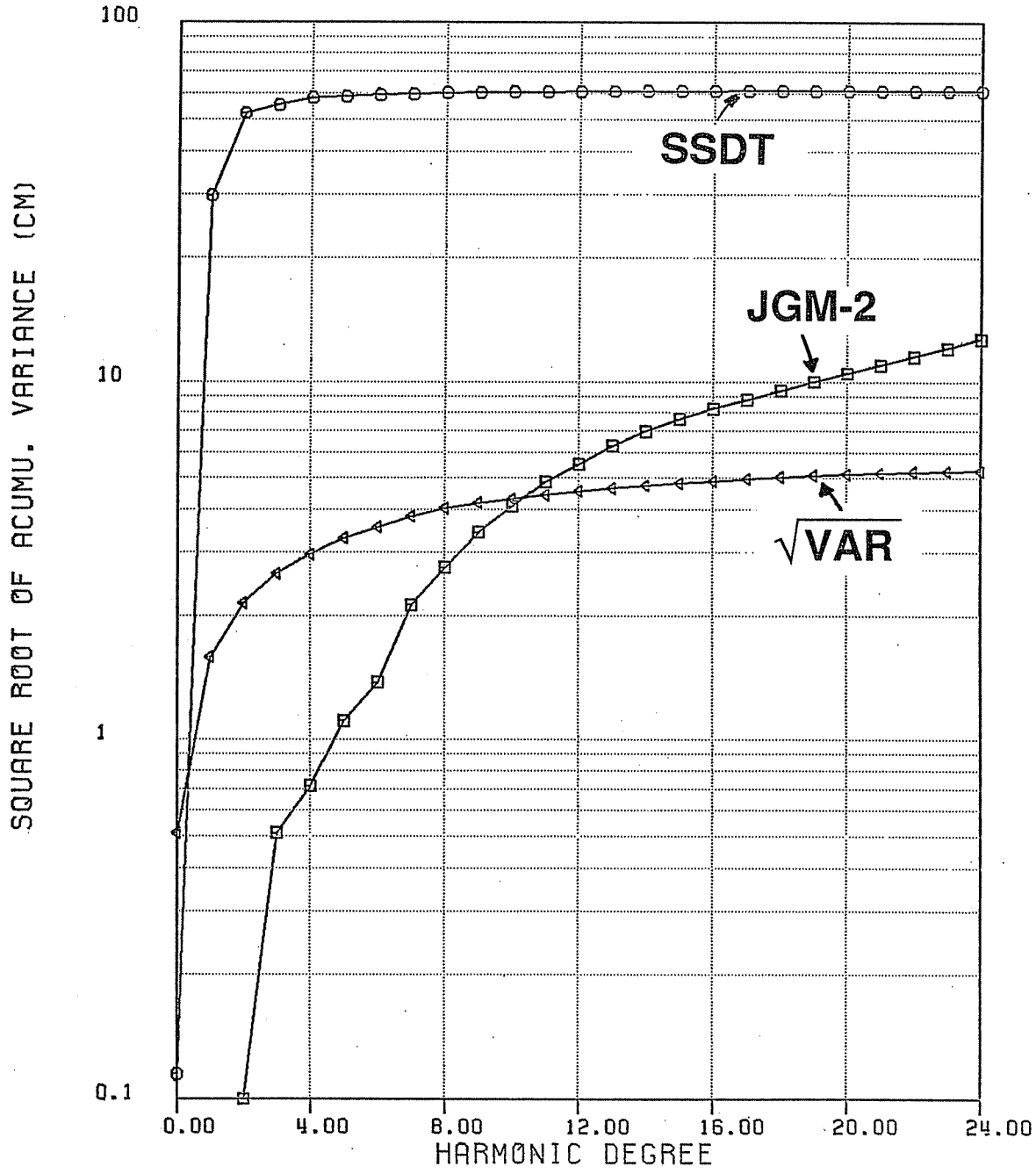

Figure 5.2 Square Root of Cumulative Degree Variances of the Mean Sea Surface Dynamic Topography, Its Time Variation, and the JGM-2 Geoid Undulation Accuracy in Ocean Areas

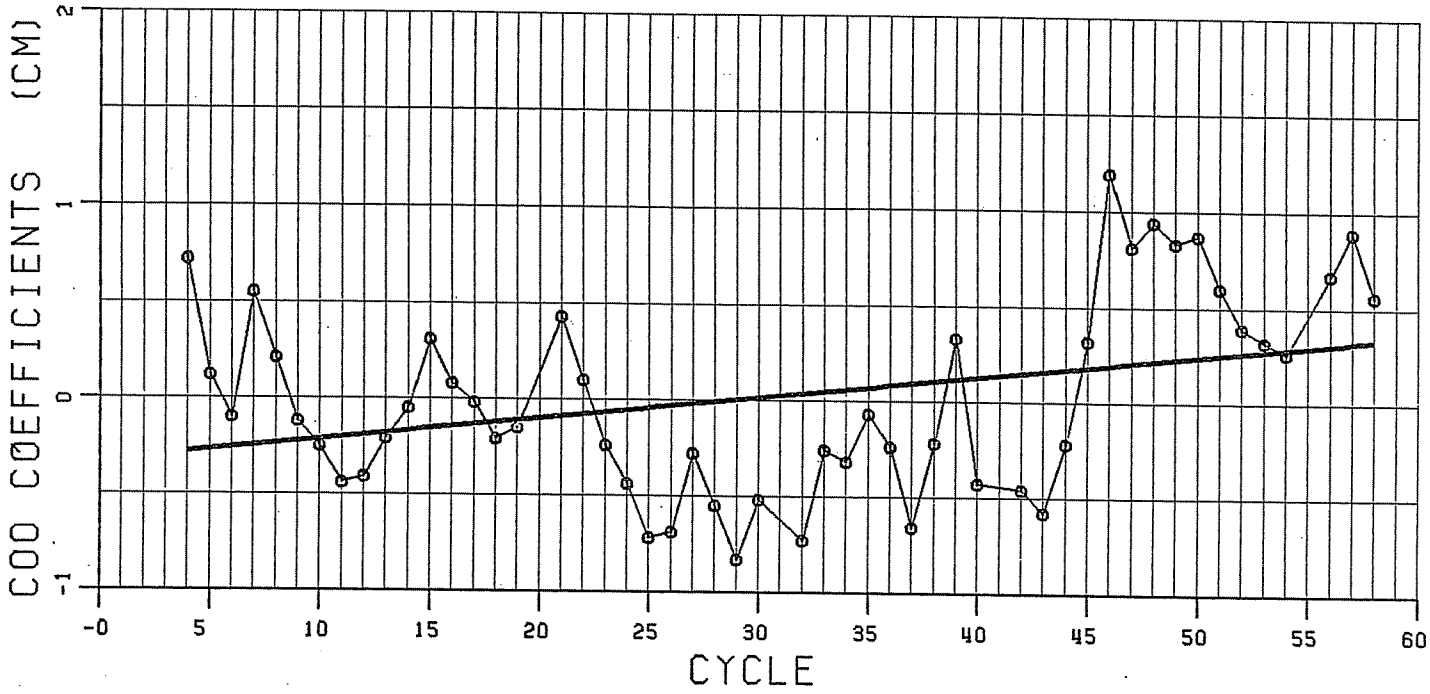

Figure 5.3. Value of the Zero Degree Coefficient of the ON Expansions of Sea Surface Dynamic Topography from Cycle 4 to Cycle 58

Using the altimeter drift estimate of 2.0 mm/yr noted in Section 3.3.3, the net change is 2.2 (± 1.6) mm/yr which is quite comparable to the 2.8 mm/yr found by a very different procedure. Although the two values are quite close, the two procedures used are not independent verification of the change, since the same data set and correction terms are used.

Considering Figure 5.3, one sees that the bias rate would be dependent on the time (or cycle) span used. Since no annual or semi-annual corrections were applied to the sea surface topography analysis in this section, it could be dangerous to calculate a bias rate from a time span shorter than a year. Continued monitoring of this c_{00} term, as well as continued analysis directly solving for the bias rate as described in Section 3.3.3, is needed.

5.5 Construction of Geostrophic Currents Maps from Orthonormal and Spherical Harmonic Coefficients

The geostrophic velocity can be calculated from the sea surface dynamic topography by (Engelis, 1985; Apel, 1990, p. 292):

$$u = -\frac{g}{fR}\frac{\partial \zeta}{\partial \phi}$$
$$v = \frac{g}{fR\cos\phi}\frac{\partial \zeta}{\partial \lambda} \qquad (5\text{-}4)$$

where g is gravity, f is the Coriolis force coefficient, u and v are the components of the geostrophic velocity in the meridian (north-south) and parallel (east-west) direction. The value of f is $2\omega\sin\phi$ where ω is the rotation rate of the Earth. In a spherical approximation g (gravity) and R (Earth radius) are constant. In the calculations carried out for this report using program TS0548.LIB.HWANG#OCCUR, g and R varied based on an ellipsoid model for the Earth.

Denote the components of the slope of the SSDT:

$$\xi = -\frac{\partial \zeta}{R\partial \phi}$$
$$\eta = -\frac{1}{R\cos\phi}\frac{\partial \zeta}{\partial \lambda} \qquad (5\text{-}5)$$

so that equation (5-1) can be written as:

$$u = \frac{g}{f}\xi$$
$$v = -\frac{g}{f}\eta \qquad (5\text{-}6)$$

The components ξ and η can be computed easily from given spherical harmonic coefficients (Rapp, 1982) at a given location since ξ and η are similar to deflections of the vertical. If the sea surface dynamic topography is represented by a set of orthonormal coefficients, u and v are computed by first transforming the orthonormal coefficients into spherical harmonic coefficients by using eq. (4-16), then ξ and η are computed from the transformed spherical harmonic coefficients.

Finally (5-6) is used to calculate u and v at the given location. The geostrophic velocity can also be represented by its magnitude and direction (Engelis, 1985):

$$A = \sqrt{u^2 + v^2}$$
$$z = \tan^{-1}\frac{u}{v} \qquad (5\text{-}7)$$

where A is the magnitude and z is the azimuth of the geostrophic velocity. In this study, we are more interested in the ocean circulation pattern rather than the strength (magnitude) of the geostrophic velocity. Therefore, the azimuth z is calculated on a 5°x5° grid globally, and then plotted over the oceans. Note the unit length of the geostrophic velocity is used for all geostrophic velocity maps shown in this report.

First we consider the representation of the mean SSDT based on the SH coefficients given in Table 5.5. Three plots have been prepared showing the results for a maximum degree of 24 (Figure 5.4); 13 (Figure 5.5); and 10 (Figure 5.6). The general patterns between the plots remain the same as expected because the dominant signal is at the lower degrees. However, there are a few regions in which unrealistic high frequency gradients are present in the degree 24 solution. One specific location is the Gulf of Carpentaria, just north of Australia. Although special data editing was applied here, the mean SSDT value appears to be contaminated by errors that are likely due to unmodeled high frequency tide errors and/or geoid undulation error. Other areas showing larger than expected gradients in the degree 24 solution, are in the Mediterranean Sea; northern part of the Arabian Sea and the Sea of Okhotsk ($\phi = 55°$, $\lambda = 148°$).

As the lower degree expansions are considered some of the gradients in the regions noted previously are significantly reduced. Based on the spectrum signal/noise ratio discussed in Section 5.4, we feel that the most accurate representation of the mean SSDT is the one to degree 13 (Figure 5.5). But this would not preclude good information in expansions to higher degree. However, one must be careful in such expansions to recognize that the values can be easily contaminated by geoid undulation errors, with the contamination increasing as the degree of expansion increases.

We next calculated the flow vector directions based on the SH expansion to degree 24 (Figure 5.7); to degree 13 (Figure 5.8); and to degree 10 (Figure 5.9). The values were computed on a 5°x5° grid using the program referenced at the start of Section 5.5.

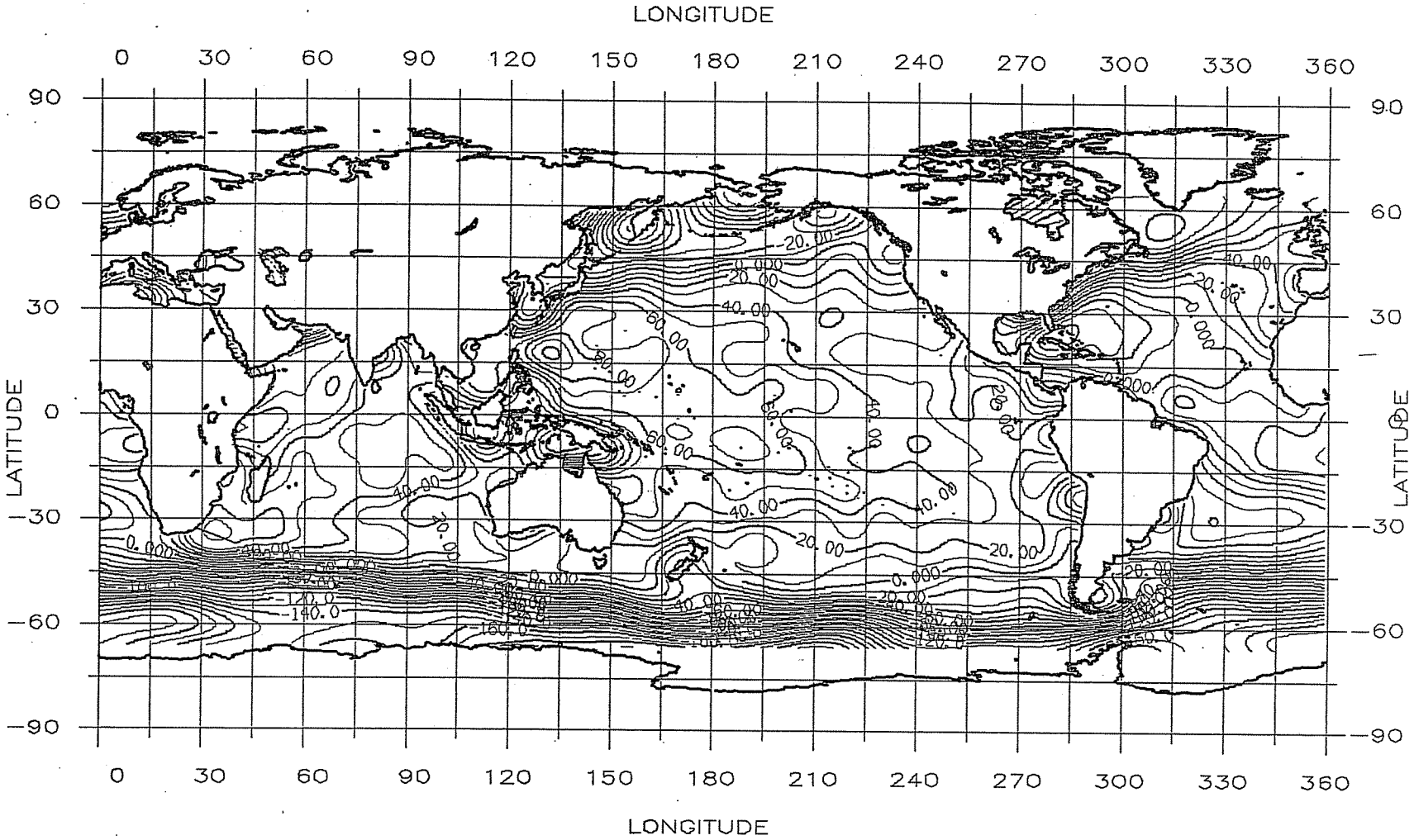

Figure 5.4. Mean Sea Surface Dynamic Topography from Topex Cycles 4 to 58 Based on a Spherical Harmonic Expansion to Degree 24. Contour interval is 10 cm.

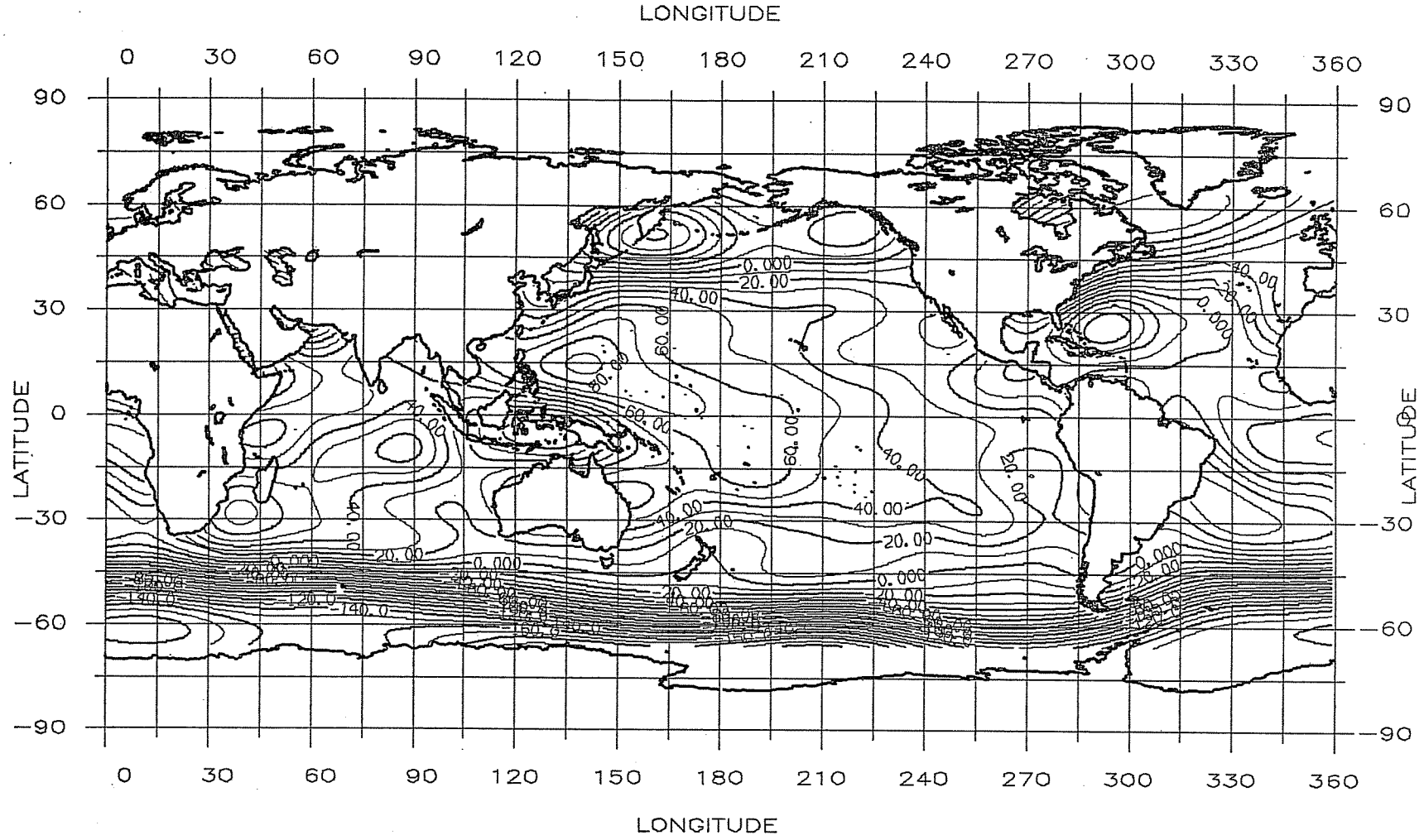

Figure 5.5. Mean Sea Surface Dynamic Topography from Topex Cycles 4 to 58 Based on a Spherical Harmonic Expansion to Degree 13. Contour interval is 10 cm.

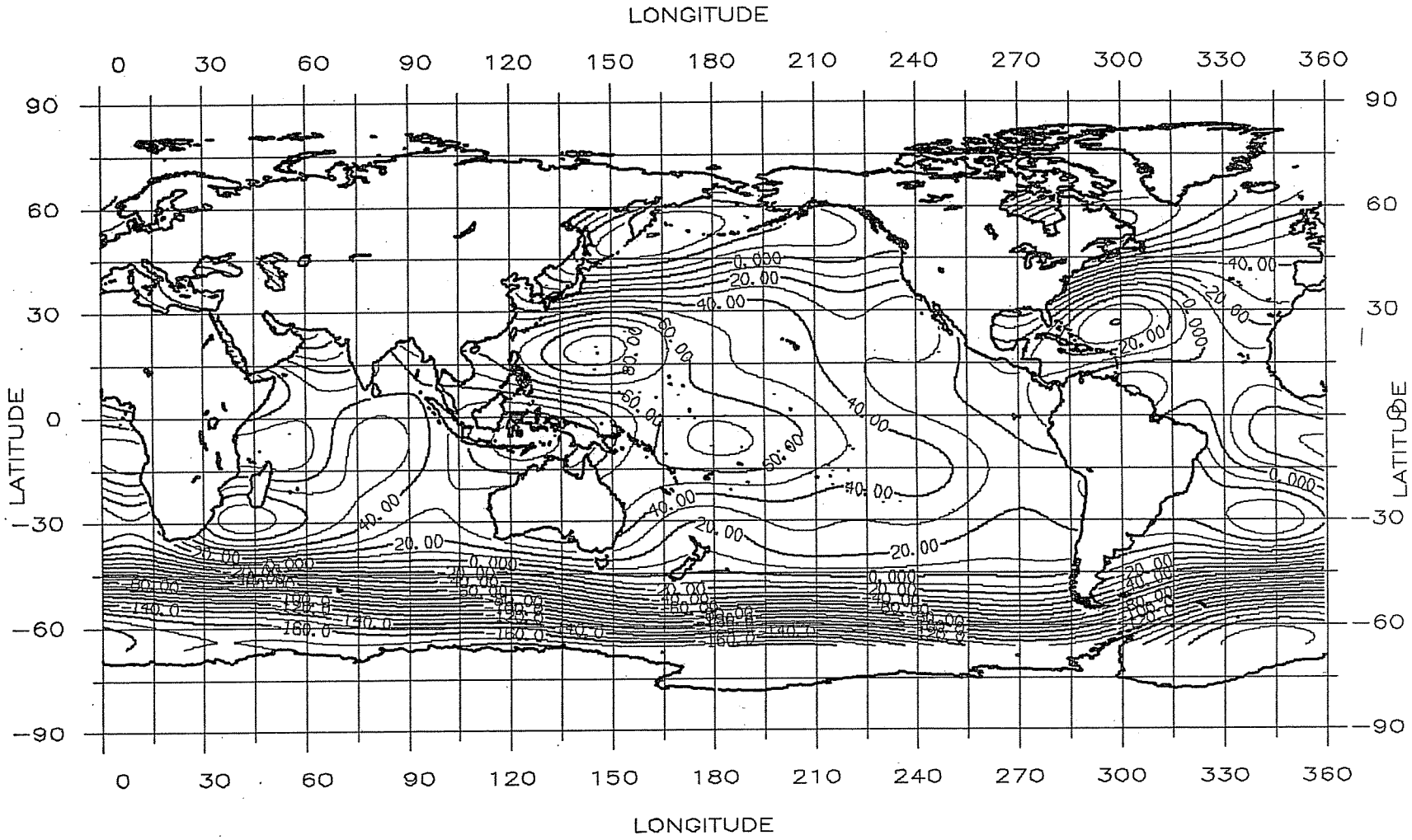

Figure 5.6. Mean Sea Surface Dynamic Topography from Topex Cycles 4 to 58 Based on a Spherical Harmonic Expansion to Degree 10. Contour interval is 10 cm.

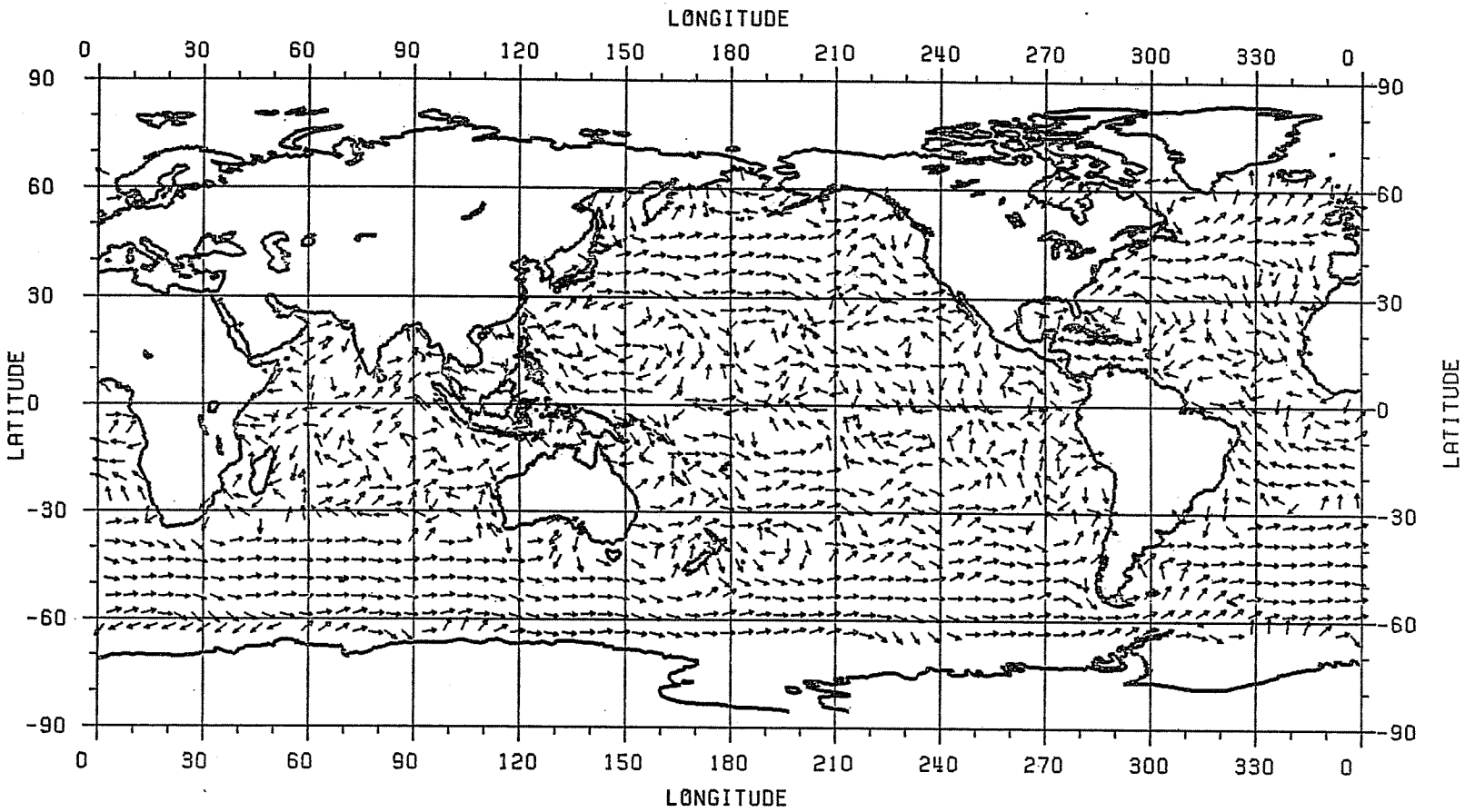

Figure 5.7. Geostrophic Flow Vectors Implied by the Mean Sea Surface Topography SH Expansion to Degree 24

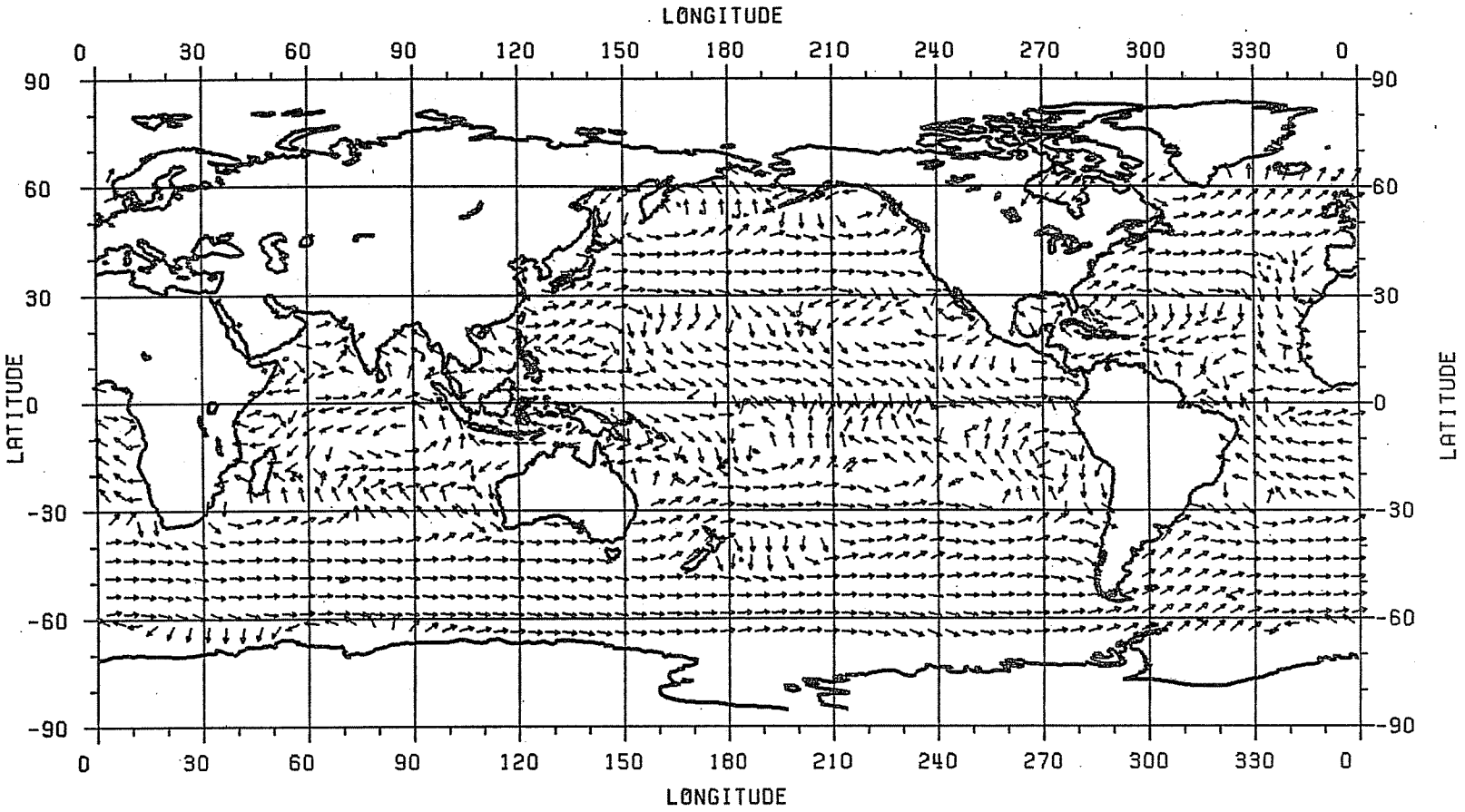

Figure 5.8. Geostrophic Flow Vectors Implied by the Mean Sea Surface Topography SH Expansion to Degree 13

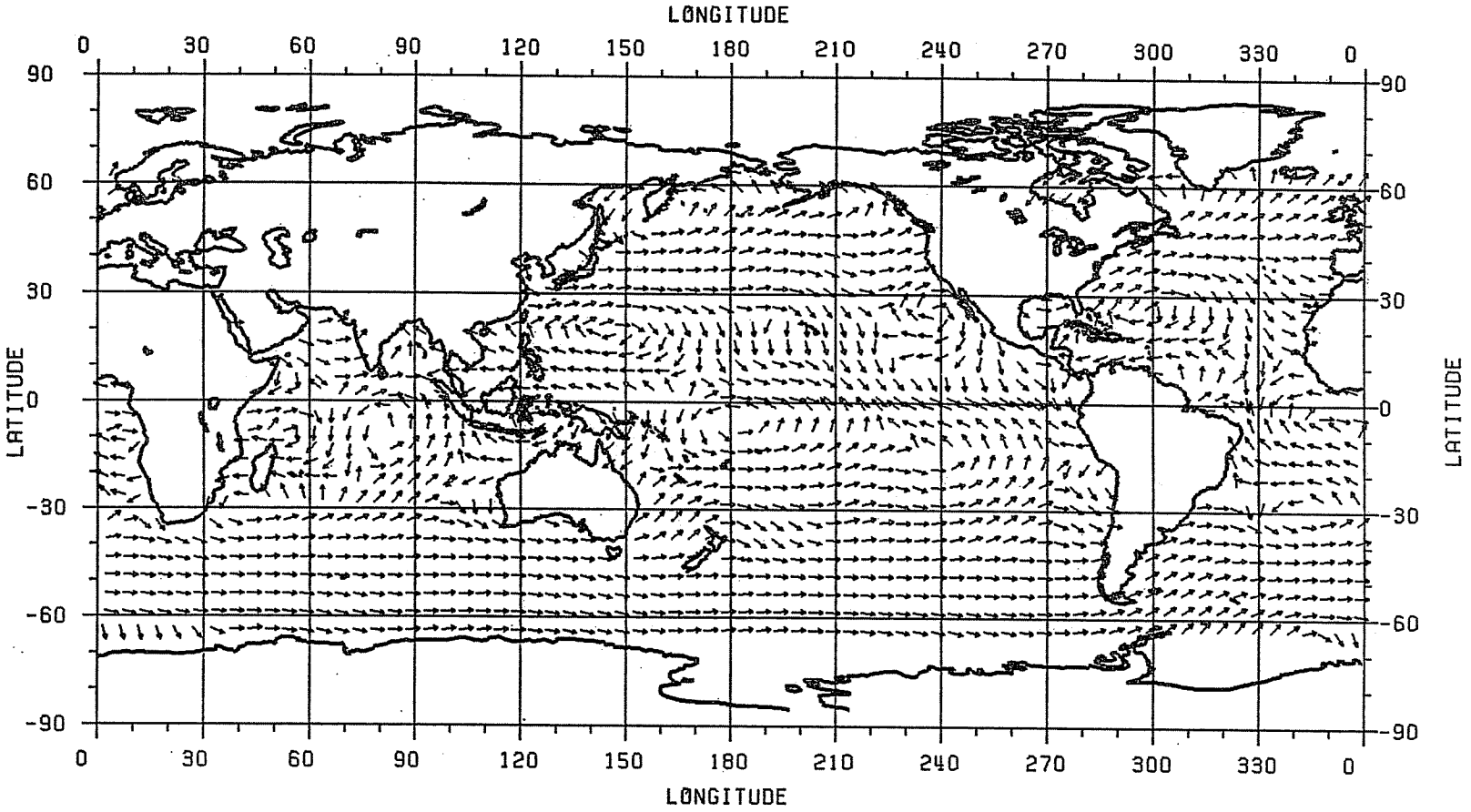

Figure 5.9. Geostrophic Flow Vectors Implied by the Mean Sea Surface Topography SH Expansion to Degree 10

The flow patterns shown in the three figures represents a mean pattern since the SSDT has been based on Topex cycles 4 to 58. Consequently the standard comparisons with the major current pattern is appropriate. To do this we start from a general circulation map such as Fig. 14.1 in Neumann and Pierson (1966). Although this figure is for the current situation for Northern Hemisphere winter, we will interpret the flows for an average, non-seasonal case. (As more Topex data is analyzed seasonal current patterns can easily be studied.) In Table 5.10 we list 16 major currents and indicate the degree in which the current can be seen in the circulation figures constructed from the Topex data. Although listed in the table, some of the currents may (or could) be too narrow to be represented by the low degree harmonic expansion of the report. They are retained here for continuity with higher degree expansions that may be done later. The codes have been designed purely on the basis of visual comparison with Figure 14.1 in Neumann and Pierson.

Table 5.10
Appearance of Major Circulation Patterns in Flow Maps
Computed From Topex Altimeter Data

	Degree of Solution		
Current	24	13	10
North Equatorial C.	0	0	0
South Equatorial C.	0	00	0
Gulf Stream	X	X	X
North Atlantic C.	X	X	X
Guiana C.	X	00	X
Brazil C.	00	00	00
Falkland C.	X	X	X
Antarctic Circumpolar C.	XX	XX	XX
Kuroshio C.	X	X	0
North Pacific C.	XX	XX	XX
California C.	X	0	0
Peru C.	0	00	00
East Australian C.	00	00	00
West Australian C.	00	00	00
Mozambique C.	00	0	0
Agulhas C.	0	0	0

Notation:
- 00 conflicting results
- 0 no evidence
- X some structure apparent
- XX clear structure

Some of the major current patterns are seen in each figure. These include the North Atlantic and North Pacific C., the Falkland C. and the Antarctic Circumpolar C. The Gulf Stream and the Kuroshio C., both western boundary currents can be vaguely recognized in the plots. Some currents (e.g. Agulhas) are not seen at all while some currents (e.g Brazil, East and West Australian C.) have directions opposite to that generally expected.

The flow vectors from the degree 24 solution are more "inconsistent" than from the lower degree solutions. This inconsistency can be seen from nearby flow vectors that have widely different (or even opposite) directions. This is most probably caused by the errors in the potential coefficient model used to define the geoid undulation used in this calculation. The flow vector from the degree 13 and degree 10 solutions are more consistent (as would be expected) than the degree 24 solution. A goal of this type of analysis is to achieve the highest resolution consistent with the accuracy of the data. As discussed in Section 5.4, the highest degree, that currently

appears reasonable, for which the expansions shjould be taken is degree 13. This appears to be partially borne out by the flow pattern seen with the degree 24 solution.

The results presented in this section are only partially encouraging. More direct correlation with existing circulation knowledge is desirable. Additional study is needed on seasonal variations in the flow pattern. And clearly improvement is needed in the geoid undulation accuracy for the methods to show improved accuracy.

6. SUMMARY AND CONCLUSIONS

The analysis described in this report uses Topex satellite altimeter data to estimate improved tide models, dynamic sea surface topography and ocean circulation patterns. Data for several time spans were used to develop the procedures for the calculation of the final models using data from cycles 4 to 58. The following sections very briefly review the methods and main conclusions of the main research sections of this report.

6.1. Mathematical Model Development

The basic modeling procedures were developed in this section. The fundamental observation to study was the sea surface dynamic topography and its time variations with respect to a mean sea surface height along the Topex track. The time variations of the residual sea surface topography were due to tide errors in the Cartright/Ray model; annual and semi-annual effects; and bias and bias rate terms. Each of the quantities was represented by a spherical harmonic expansion. The tide constituents represented were M_2, S_2, O_1, and K_1. A new data weighting algorithm was implemented to reduce the impact of the higher data density at high latitudes. This algorithm will be used in most of the computations (both adjustment and residual computations) carried out for this report.

6.2. Parameter Estimates

This section first developed the procedures for normal point computations and data editing. Initial tests were made to degree 8 using data from Topex cycles 4 to 54. The first tests examined the impact of an OSU or JPL edit, and the minimum number of cycles at a point on the reference track. We found that a solution using the OSU edit with a minimum number of 5 cycles per reference track point was reasonable.

The most comprehensive solution for this report was a solution to degree 15 using Topex data from cycles 4 to 58. The solution used 321,302 normal points to estimate 3572 harmonic coefficients. The coefficients were used to construct maps of the amplitude and phase of the annual and semi-annual terms. The largest amplitude (±10 cm) of the annual variation was associated with the usual western boundary currents (e.g. Gulf Stream, Falkland Current, Kurshio Current). The root mean square magnitudes of the ocean annual regional was ±4.0 cm. The amplitude (±4.5 cm) in the Northern Hemisphere was slightly larger (±3.5 cm) than in the Southern Hemisphere. A study of the phase plots showed the maximum amplitudes occuring with the heating and cooling cycle.

The tide model corrections were calculated at each of the normal points. The largest values were associated with the M_2 components where the largest correction was -12 cm with a RMS correction of ±2.9 cm. The new tide model (N34) was verified at the 104 tide gauge set provided by C. G. Provost and the 95 station subset used by other investigators of tide model evaluations. For the M_2 component, the RMS tide gauge amplitude difference for the M_2 component was ±3.3 cm for the Cartright/Ray model and ±2.2 cm for the new model of this paper.

A final result relates to the bias rate which was found to average, over all normal points, 4.8 mm/yr. Considering recent estimates of altimeter drift of 2.0 mm/yr (cycles 4 to 58) the net slope is 2.8 mm/yr. More data is needed to examine the stability of the slope.

6.3. Sea Surface Dynamic Topography Analysis

The representation of the SSDT in terms of a spherical harmonic expansion and an orthromal expansion was studied. The estimation of both types of coefficients was discussed as well as the transformation between the coefficient sets. For numerical tests the ocean was defined

as the region between latitude ±70° with a depth greater than zero meters. Selected regions (e.g. Caspian Sea and Black Sea) were excluded from the general region. Seven test expansions were made of SSDT using Topex cycle 17 data. The various tests involved data editing was well as the use of a priori SSDT information in near shore land areas.

The SSDT expansions were generally made to degree 24. We found that spherical harmonic coefficients (SH) transformed from orthonormal coefficients (ON) could be quite large with symptoms of instability caused by lack of SSDT data (and definition) in land areas. Although the SSDT representation, in the ocean areas, is quite comparable (±5 cm) the SH coefficients, computed from the ON coefficients, were unrealistic. However the use of ON coefficients for spectral analysis purposes seemed quite reasonable and is to be recommended. The final recommendation from the test solutions was to estimate the spherical harmonic representation of SSDT and transform this representation to the ON representation when such representation is needed for spectral analysis studies.

6.4. SSDT Representations from Multiple Topex Cycles

The estimation of the SH coefficients of SSDT was next carried out for multiple Topex cycles. This was done after a modified OSU edit criteria was adopted where normal points were deleted if the magnitude of SSDT exceeded 1 m in two defined geographic regions. The regions are such that tide and geoid evaluation error could be significant. Preliminary analysis was made with 10 cycles of Topex data to determine improved a priori degree variance information.

Several tests were carried out to understand the impact of the bias term applied to the original SSDT. The bias exists because of an inaccurate equational radius to which the Topex data was referred and a bias in the altimeter data itself. We found that the low degree SH coefficients were quite dependent on the bias term applied to the data and the a priori weight that could be applied to the degree 0 term. When however, a SH expansion was transformed to the ON expansion the low degree ON coefficients were quite stable except for the degree zero term which was directly dependent on the bias term used.

Tests were carried out with one year of Topex data (cycles 17 to 53) to determine the bias that would make the degree zero term of the ON expansion effectively zero. This bias of 55 cm, was then used in all additional analyses. This bias value was also used to infer a new equational radius of 6378136.71 m based on an altimeter bias of -14 cm. This new radius is 11 cm larger than the new radius estimated, in a much different way, by Rapp, Yi, and Wang (1994).

The production calculations first determined the SH coefficients to degree 24 for Topex cycles 4 to 58. The data used in these computations was corrected for the tides implied by the N34 model and a bias of 55 cm. These computations were used to determine 51 SH coefficient sets which were averaged to form a representative mean SSDT SH expansion. The degree 2,0 term, -37.8 cm, is similar to that found by other investigators. The mean SH representation was correlated to the equivalent ON expansion. Based on these coefficients the rms magnitude of SSDT was found to be ±61 cm. The ON coefficients were used to calculate the degree variances of SSDT and plotted with the ocean geoid undulation error reported by Nerem et al. (1994). This error equaled the SSDT signal near degree 13 indicating that the SSDT determinations may not be reliable above this degree.

The degree zero terms of the 51 ON expansions (transformed from the SH expansions) were examined to find a small change with the coefficient increasing in time. The slope of the line fitting the degree zero terms was 4.2 mm/yr, similar to the 4.8 mm/yr found in the simultaneous solutions with tides, and annual semi-annual times. Considering an altimeter drift estimate of 2.0 mm/yr the net bias rate is 2.2 (±1.6) mm/yr.

Plots were made of the SSDT and the direction of the geostraphic flow vectors implied by the mean coefficient representation to degrees 24, 13, and 10. The flow vectors from each plot were compared to generally accepted average circulation patterns. The agreement could best be characterized as fair. The degree 24 solutions showed the most problems as flow vectors lacked coherent behavior in some regions. This behavior is consistent with the previous result that SSDT above degree 13 could be unreliable. The flow vectors from the lower degree solutions showed more consistency but less detail as is expected. The general flow patterns implied by the lower degree expansions did resemble the generally expected pattern but significant conflicts remained. Such conflicts could simply relate to the resolution of the SSDT representation.

6.5. Future Work

This report has extended numerous prior studies to the analysis of Topex data from cycles 4 to 58. The analysis with new Topex data can continue to improve the current results. Clearly the continued monitoring of the bias rate question is important. Processing of two years of data will enable a more reliable mean SSDT determination. We will thus be able to check the consistency of the annual and semi-annual variations in the ocean surface. The cycle to cycle variations in SSDT can be studied through the SH expansions through the construction of a time interpolation process.

Much remains to be learned about the ocean surface and its variations from the analyses of the Topex data.

REFERENCES

Andersen, O.B., P.L. Woodworth, and R.H. Flather, Intercomparison of Recent Ocean Tide Models, Draft Report, August 9, 1994.

Apel, J., Principles of Ocean Physics, Academic Press, New York, 1987.

Callahan, P., GDR Users Handbook, JPL D-8944, Rev. A, Pasadena, CA, 1993.

Cartwright, D.E. and R.D. Ray, Oceanic Tides From Geosat Altimetry, J. Geophys. Res., Vol. 95, C3, 3069-3090, 1990.

Cartwright, D.E., R.D. Ray and B.V. Sanchez, Oceanic Tide Maps and Spherical Harmonic Coefficients From Geosat Altimetry, NASA Technical Memorandum 104544, Goddard Space Flight Center, Greenbelt, MD, 1991.

Christensen, E.J. et al., Calibration of TOPEX/POSEIDON at Platform Harvest, J. Geophys. Res. - Oceans, in press, 1994.

Denker, H. and R.H. Rapp, Geodetic and Oceanographic Results from the Analysis of 1 Year of Geosat Data, J. Geophys. Res., 95, 13,151-13.168, 1990.

Engelis, T., Global Circulation From SEASAT Altimeter Data, Marine Geodesy, Vol. 9, No. 1, 45-69, 1985.

Engelis, T., Spherical Harmonic Expansion of the Levitus Sea Surface Topography, Report No. 385, Dept. of Geodetic Science and Surveying, The Ohio State University, Columbus, October 1987.

Hwang, C., Orthogonal Functions Over the Oceans and Applications to the Determination of Orbit Error, Geoid and Sea Surface Topography From Satellite Altimetry, Report No. 414, Dept. of Geodetic Science and Surveying, The Ohio State University, Columbus, December 1991.

Hwang, C., Fast Algorithm for the Formation of Normal Equations in a Least Squares Harmonic Analysis by FFT, manuscripta geodaetica, 18, 46-52, 1993a.

Hwang, C., Spectral Analysis Using Orthonormal Functions With a Case Study on the Sea Surface Topography, Geophys. J. Int., 115, 1148-1160, 1993b.

Ichikawa, K. and S. Imawaki, Life History of a Cyclonic Ring Detached From the Kuroshio Extension as Seen by the Geosat Altimeter, J. Geophys. Res., Vol. 99, C8, 15,953-15,966, 1994.

Jacobs, G.A., G.H. Born, M.E. Parke, and P.C. Allen, The Global Structure of the Annual and Semi-Annual Sea Surface Height Variability From Geosat Altimeter Data, J. Geophys. Res., 97(C11), 17813-17828, 1992.

Kim, J-H, and R.H. Rapp, Major Data Sets and Files in the Area of Gravimetric and Altimetric Research, internal report, Dept. of Geodetic Science and Surveying, The Ohio State University, Columbus, August 1990.

Knudsen, P., Global Low Harmonic Degree Models of the Seasonal Variability and Residual Ocean Tides From Topex/Poseidon Altimeter Data, J. Geophys. Res. - Oceans, in press, 1994.

Koblinsky, G.J., R.S. Nerem, R.G. Williamson, and S.M. Klosko, Global Scale Variations in Sea Surface Topography Determination From Satellite Altimetry, in Sea Level Changes: Determination and Effects, Geophysical Monograph 69, IUGG, Vol. II, Amer. Geophys. Union, 1992.

LeProvost, M.L. Genco, F. Lyard, P. Vincent, and P. Canceil, Spectroscopy of the World Ocean Tides From a Hydrodynamic Finite Element Model, J. Geophys. Res. - Oceans, Topex/Poseidon special issue, in press, 1994.

Maul, G., Guest Editorial, Special Issue: Pacific Ocean Sea Level Variability, Marine Geodesy, Vol. 12, pp. 229-233, 1988.

Nerem, .R.S., E.J. Schrama, C.J. Koblinsky, and B.D. Beckley, A Preliminary Evaluation of Ocean Topography From the TOPEX/POSEIDON Mission, J. Geophys. Res. - Oceans, in press, 1994a.

Nerem, R.S. et al., Gravity Model Development for TOPEX/POSEIDON: Joint Gravity Models 1 and 2, J. Geophys. Res., in press, 1994b.

Neumann, G., and W. Pierson, Jr., Principles of Physical Oceanography, Prentice-Hall, 1966.

Parke, M., R. Stewart, and D. Forbes, On the Choice of Orbits for an Altimetric Satellite to Study Ocean Circulation and Tides, J. Geophys. Res., 92(C11), 11,693-11,707, 1987.

Perigaud, C. and P. Delecluse, Annual Sea Level Variations in the Southern Tropical Indian Ocean From Geosat and Shallow-Water Simulations, J. Geophys. Res., 97, C12, 20,169-20,178, 1992.

Rapp, R.H., A Fortran Program for the Computation of Gravimetric Quantities From High Degree Spherical Harmonic Expansions, Report No. 334, Dept. of Geodetic Science and Surveying, The Ohio State University, Columbus, 1982.

Rapp, R.H., R.S. Nerem, C-K Shum, S.M. Klosko, and R.G. Williamson, Consideration of Permanent Tidal Deformation in the Orbit Determination and Data Analysis for the Topex/Poseidon Mission, NASA Tech. Memo. 100775, January 1991.

Rapp, R.H., Y.M. Wang, and N.K. Pavlis, The Ohio State 1991 Geopotential and Sea Surface Topography Harmonic Coefficient Models, Report No. 410, Dept of Geodetic Science and Surveying, The Ohio State University, Columbus, 1991

Rapp, R.H. and Y.M. Wang, Dynamic Topography Estimates Using Geostat Data and a Gravimetric Geoid in the Gulf Stream Region, Geophys. J. Int., 117, p.511-528, 1994

Rapp, R.H. and Y. Yi, TOPEX/POSEIDON Reference Ground Track, in TOPEX/POSEIDON Research News, Issue 2, p. 15-17, March 1994.

Rapp, R.H., Y. Yi, and Y.M. Wang, Mean Sea Surface and Geoid Gradient Comparisons With Topex Altimeter Data, Journal of Geophysical Research - Oceans, in press, 1994.

Rapp, R.H., Y.M. Wang, and Y. Yi, Global Sea Level Change Implied by Topex Altimeter Data, presented at the 1994 Spring Meeting, American Geophysical Union, Baltimore, May 1994.

Rapp, R.H. and D.A. Smith, Preliminary Estimates of Gulf Stream Characteristics From Topex Data and a Precise Gravimetric Geoid, J. Geophys. Res. - Oceans, Topex/Poseidon special issue, in press, 1994.

Ray, R.D. and B.V. Sanchez, Radial Deformation of the Earth by Oceanic Loading, NASA Technical Memorandum 100743, Goddard Space Flight Center, Greenbelt, MD, July 1989.

Sanchez, B.V. and D. Morrow, Normal Modes of the World's Oceans - A Numerical Investigation Using Proudman Functions, NASA Technical Memorandum 104587, Goddard Space Flight Center, Greenbelt, MD, 1993.

Schrama, E.J.O., and R. Ray, A Preliminary Tidal Analysis of Topex/Posiedon Altimetry, J. Geophys. Res-Oceans, Topex/Poseidon Special Issue, December 1994.

Tsimplis, M.N., and P.L. Woodworth, The Global Distribution of the Seasonal Sea Level Cycle Calculated from Coastal Tide Gauge Data, J. Geophys. Res., 99(C8), 16,031 - 16,040, 1994.

Visser, P.N.A.M., K.F. Wakker, B.A.C. Ambrosius, Dynamic Sea Surface Topography from GEOSAT Altimetry, Marine Geodesy, 16, 215-229, 1993.

Wang, Y.M. and R.H. Rapp, The Determination of a One Year Mean Sea Surface Height Track From Geosat Altimeter Data and Ocean Variability Implications, Bulletin Geodesique, 66: 336-345, 1992.